NONLINEAR FINITE ELEMENT ANALYSIS OF REINFORCED CONCRETE DEEP BEAMS WITH OPENINGS

A Thesis

Submitted to the College of Engineering
of the University of Babylon in Partial
Fulfillment of the Requirements
for the Degree of Master
of Science in Civil
Engineering
(Structural Engineering)

By

KHAMAIL ABDUL-MAHDI MOSHEER

(B.Sc.)

SUPERVISOR

Assist. Prof. Dr. Ammar Y. Ali Assist. Prof. Dr. Nameer A. Alwash

2005

Π

{قَالُوا سُبْحَانَكَ لا عِلْمَ لَنَا إِلاَّ مَا عَلَّمْتَنَا إِنَّكَ أَنْتَ الْعَلِيمُ الْحَكِيمُ}

صدق الله العظيم

سورة البقرة

الآية (32)

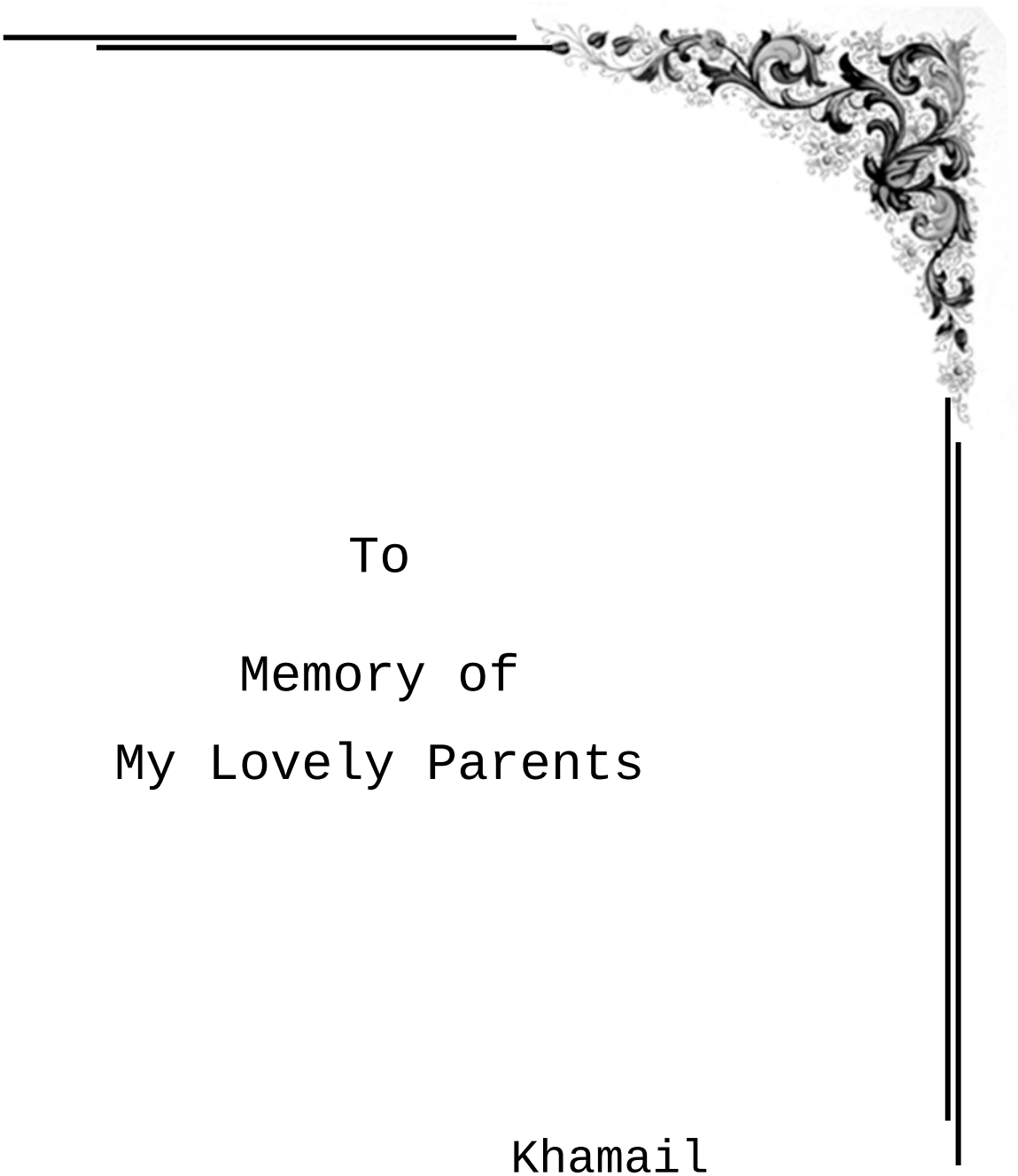

To

Memory of

My Lovely Parents

Khamail

ACNOWLEDGMENT

*Firstly, all thanks and praise be to **God** for enabling me to achieve this research work.*

*I would like to express my deepest gratitude and gratefulness to **Dr. Ammar Y. Ali** and **Dr. Nameer A. Alwash,** the supervisors of this study for their guidance, encouragement, and constructive suggestions.*

*Special thanks to my grandfather **Mr. Ja'fer Al-Husseni**, my brother **Samir**, and my dear sister **Sara** for their support.*

Acknowledgments to the staff of the Civil Engineering Department, College of Engineering, and the staff of the Research Unit, for all the facilities made available for me.

*A word of thank to **Mrs. Azhar Hamza** and all my friends for their support.*

Finally, I would like to express my deepest gratitude to all who gave me helpful hand through this study.

CERTIFICATION

We certify that this thesis, titled **"Nonlinear Finite Element Analysis of Reinforced Concrete Deep Beam with Openings",** was prepared by **Khamail Abdul-Mahdi Mosheer** under our supervision at the University of Babylon in fulfillment of partial requirements for the degree of Master of Science in Civil Engineering (Structural Engineering).

Signature:
Name: Asst. Prof. Dr. Ammar Y. Ali
(Supervisor)
Date: / / 2005

Signature:
Name: Asst. Prof. Dr. Nameer A. Alwash
(Supervisor)
Date: / / 2005

CERTIFICATION

We certify that we have read this thesis, titled **"Nonlinear Finite Element Analysis of Reinforced Concrete Deep Beam with Openings",** and as examining committee examined the student **Khamail Abdul-Mahdi Mosheer** in its contents and in what is connected with it, and that in our opinion it meets the standard of a thesis for the degree of Master of Science in Civil Engineering (Structural Engineering).

Signature:
Name: Lecturer Dr. Ali N. Attiyah
(Member)
Date: / / 2005

Signature:
Name: Asst. Prof. Dr. Haitham H. AL-Daami
(Member)
Date: / /2005

Signature:
Name: Prof. Dr. Husain M. Husain
(Chairman)
Date: / / 2005

Signature:
Name: Asst. Prof. Dr. Ammar Y. Ali
(Supervisor)
Date: / / 2005

Signature:
Name: Asst. Prof. Dr. Nameer A. Alwash
(Supervisor)
Date: / / 2005

Approval of the Civil Engineering Department
Head of the Civil Engineering Department

Signature:
Name: Asst. Prof. Dr. Ammar Y. Ali
Date: / / 2005

Approval of the Deanery of the College of Engineering

Signature:
Name: Asst. Prof. Dr. Haroun A. K.
Date: / / 2005
Dean of the College of Engineering
University of Babylon
Date: / / 2005

ABSTRACT

This research deals with nonlinar analysis of reinforced concrete deep beams with and without openings by three dimensional finite element method under static load. The constitutive models of the material nonlinearity are adopted to take into account the nonlinear stress-strain relationships of concrete and steel, cracking and crushing of concrete, and yielding of reinforcement. A twenty-noded isoparametric brick element with sixty degrees of freedom is employed to model the concrete while the reinforceing bars are modeled as axial members embedded through the brick element with perfect bond.

The results of the finite element method and those available from experiments and analysis of simply supported and continuous deep beams have shown good agreement with difference about (6%) as average for the ultimate load and about (9%) as average for deflection.

Parametric study is considered to deal with the effect of some selected parameters such as opening location, web reinforcement, depth to span ratio, compressive strength, and boundary condition on the overall behavior and ultimate strength of deep beams. It was found that providing an opening at the shear zone causes sharp decrease in ultimate load by about (31%-56%) for simply supported deep beams and about (8%-30%) for continuous deep beams. The more safe location is found to be within the flexural zone.

On the other hand, a comparative study was carried for analysis of reinforced concrete continuous deep beams by various methods: finite element method, ACI-Code, and strut-tie model. It was concluded that mechanism of tied-arch action is present in continuous deep beams as in simply supported deep beams, while the ACI-Code provision does not recommend this concept.

LIST OF CONTENTS

SUBJECT **PAGE**

Acknowledgment……..…….…… I
Abstract…….……...…… II
List of Content…….……..……. III
List of Tables……...…….…….…… VI
List of Figures……..…….…… VII
Notations……..……..…….. XI

CHAPTER ONE: INTRODUCTION

1.1 General……. 1
1.2 Shear and Flexural Behavior of deep beams…….. ……. 1
1.3 Scope and Aims……. ……... 4
1.4 Thesis Layout …...…… 4

CHAPTER TWO: REVIEW OF LITERATURE

2.1 Introduction…… 5
2.2 Experimental Studies …….…… 5
2.3 Theoretical and Analytical Studies …….……. 9
2.4 Present Study……..…… … 13

CHAPTER THREE: FINITE ELEMENT ANALYSIS

3.1 Introduction……..... 14
3.2 Three-Dimensional Brick Element…….……. 15
3.2.1 Shape Functions …….…… 16
3.2.2 Strain and Stress Fields …….…… 18
3.2.3 Element Stiffness Matrix …….…….. 21
3.3 Reinforcement Idealization ……...…….…..... 21
a) Distributed Representation……. 21
b) Discrete Representation…….…… 22
c) Embedded Representation…… 22

SUBJECT **PAGE**

3.4 Numerical Integration…… 24
3.5 Uniaxial and Multi-Axial Behavior of concrete…….... 27
3.6 Stress-Strain Models…….. …… 30
3.7 Modeling of Concrete Fracture……..... 31
3.7.1 Cracking Models ……..…….…..... 31
3.7.1.1 Smeared Cracking Models……..……..…..... 32
3.7.1.2 Discrete Cracking Models ……..…..... 34
3.7.2 Post-Cracking Models…….……..…..... 34
3.7.3 Shear Transfer Across the Cracks…….....… 35
3.8 Concrete Model Adopted in The Analysis …….. 36
3.8.1 Modeling of Concrete in Compression……..……...……. 37
3.8.1.1 The Yield Criterion…….…….……. 37
3.8.1.2 Hardening Rule …….……...……..... 39
3.8.1.3 Flow Rule…….……..… 43
3.8.1.4 The Incremental Stress-Strain Relationship…….…...…… 43
3.8.1.5 Crushing Condition……... ……..…… 46
3.8.2 Modeling of Concrete in Tension……...…… 46
3.8.2.1 Cracking Criterion…….……...……..… 46
3.8.2.2 Post-Cracking Model……..…….……. 49
3.8.2.2.1 Tension-Stiffening Model……..……....…..... 49
3.8.2.2.2 Shear Retention Model……..…….…… 50
3.8.2.3 Modeling of the Compressive Strength Reduction
Due to Orthogonal Cracks……..…..……...…….. 52
3.9 Modeling of Reinforcement…….……...…….. 54

CHAPTER FOUR: SOLUTION ALGORITHM OF NONLINEAR PROBLEM AND COMPUTER PROGRAM

Introduction……..…….....…….…… 55
4.2 Solution Techniques for Nonlinear Problems...……..……..…… 55
4.2.1 Linear-Incremental Techniques……...……....…..... 55
4.2.2 Iterative Techniques…….……....…… 56
4.2.2.1 Conventional Newten-Raphson Method……..……. 57
4.2.2.2 Modified Newton-Raphson Method……..…..…… 59
4.2.2.3 Combined Newton-Raphson Method…….……. 59

SUBJECT **PAGE**

4.2.3 Incremental-IterativeTechniques……..…… 60
4.3 Convergence Criterion…….… 61
4.4 Analysis Termination Criterion…….……... 61
4.5 Outline of Computer program…….…..……... 62

CHAPTER FIVE: APPLCATION AND DISCUSSION

5.1 General ……..…..…..…..... 63
5.2 Simply Supported Reinforced Concrete Deep Beams….. ……..…..…. 64
5.3 Continuous Reinforced Concrete Deep Beam……..……..…… 72
5.4 Simply Supported Reinforced Concrete Deep
Beams with Openings…..... 76
5.5 Parametric study of Simply Supported Reinforced Concrete
Deep Beams with Openings……...…….... 81
5.5.1 Effect of Opening Location along the Beam
Span and the Depth..…..……....……..... 84
.2 Effect of Web Reinforcement……....…….…… 88
5.5.3 Effect of Span-Depth ratio……...…...…… 90
5.5.4 Effect of Compressive Strength …….…….……. 91
5.5.5 Effect of Boundary Condition …….……..…….…….. 92
5.6 Continuous Reinforced Concrete Deep Beam with Openings…….…….. 93
5.7 Estimation of Shear Strength of Continuous Reinforced Concrete
Deep Beams by Various Methods……..…….…..... 98
.1 ACI-Code Method.....…..….... ... . ……..... 98
! Strut-and-Tie Method……..…….…..… 99
7.3 Finite Element Method…….…..…… 100
5.7.4 Discussion of the Result..……...……..…..…….. 103

CHAPTER SIX: CONCLUSIONS AND RECOMMENDATIONS

6.1 Conclusions……..……..... 104
6.2 Recommendations……..…… 105
REFRENCES……....……... 106
APPENDIX A……...……..……..…..... A-1
APPENDIX B…….…… B-1

LIST OF TABLES

TABLE NO.	TITLE	PAGE
3.1	Shape Function of the Quadratic 20-Node Brick Element…..…	17
5.1	Material Properties and Additional Parameters of Deep Beams…..……	68
5.2	Comparision Shear Strength for Deep Beams……..…..	71
5.3	Material Properties and Additional Parameters of Continuous Deep Beam……. …...….	74
5.4	Material Properties and Additional Parameter of Simply Supported Deep Beam with Openings……..…	78
5.5	Measured and Computed Ultimate Loads…….…….	79
5.6	Opening Notations……	82
5.7	Material Properties and Additional Parameters of Simply Supported Deep Beams with Openings…….…...……	85
5.8	Shear Strength of Simply Supported Deep Beams with openings……...	87
5.9	Opening Notations…….....	94
5.10	Material Properties and Additional Parameters of Continuous Deep Beams with Openings…….……..…..…	96
5.11	Material Properties and Additional Parameters of Continuous Deep Beams ……...……	102
5.12	Predicted and actual ultimate Shear Strength in Continuous Deep beams with Single Point Load per Span…..……..…..…	102

LIST OF FIGURES

FIG. NO.	TITLE	PAGE
1.1	Distribution of Flexural Stresses in homogeneous Simply Supported Deep Beam……..	3
2.1	Eccentric Load ……	6
2.2	Kong's Equation notation……	7
3.1	Linear and Quadratic Isoperimetric Solid Element…..……...	15
3.2	Local Coordinate System……..……..	16
3.3	Distribution of Sampling Points over the Element in 15 Gaussian point integration Rule ……	26
3.4	Typical Uniaxial Stress –Strain Curve for Concrete in Compression……..……..	27
3.5	Biaxial Strength of Concrete……..…..…..……	29
3.6	Triaxial Strength Envelope of Concrete ……..…….……	29
3.7	Cracking of Concrete……..…...	32
3.8	Smeared Crack Model…….…….....	33
3.9	Discrete Crack Model…….	34
3.10	Uniaxial Stress-Strain Curve, Pre-and Post Failure Regime…..…	37
3.11	Uniaxial Stress-Strain Curve for Concrete……...…. ..	42
3.12	Post Cracking Model for Concrete…….	50

FIG. NO.	TITLE	PAGE
3.13	Shear Retention for Concrete……	51
3.14	Uniaxial Compressive Stress-Strain Relationship for Cracked Concrete……..	53
3.15	Stress-Strain Relationship of Steel Bars Used in the Analysis……...	54
4.1	Linear Incremental Method……	56
4.2	Conventional Newton – Raphson Method…….…….	57
4.3	Modified Newton – Raphson Method…….. ..	59
4.4	Combined Newton – Raphson Method……	60
4.5	Incremental - Iterative Technique ……..……...	60
5.1	Simply Supported Deep Beams/ Geometry, Loading arrangement , and Reinfocement Details……..…….....	66
5.2	Finite Element Idealization of Half of the Simply Supported Deep Beams...…...…….……..	67
5.3	Load-Deflection Curve at Mid-Span for (A_4) Deep Beam ….....	68
5.4	Load-Deflection Curve at Mid-Span for (K_2) Deep Beam……	69
5.5	Load-Deflection Curve at Mid-Span for (K_1) Deep Beam ……..	69
5.6	Load-Deflection Curve at Mid-Span for (A_4) Deep Beam (Comparison with previous studies).....……..	70
5.7	Load-Deflection Curve at Mid-Span for (K_2) Deep Beam (Comparison with previous studies).....…..…...	70

FIG. NO.	TITLE	PAGE
5.8	Cracking Patterns of Simply Supported Deep Beams.....…....	71
5.9	Continuous Deep Beam Geometry and Reinforcement Details....	73
5.10	Finite Element Idealization of One Span of Continuous Deep Beam ……..…….	73
5.11	Load-Deflection Curve at Mid-Span for Continuous Deep Beam …….……	74
5.12	Load-Deflection Curve at Mid-Span for Continuous Deep Beam (Comparison with previous studies)….....……....	75
5.13	Crack Patterns of Continuous Deep Beam at Failure for One Span…...……...…….……	75
5.14	Simply Supported Deep Beams with Opening……..	77
5.15	Finite Element Idealization of Beam (M-0.4/5)…….……...	78
5.16	Influence of Opening Location through Depth of the Beam……...……..……	79
5.17	Cracking Patterns of Simply Supported Deep Beam (M0.4/5)……	80
5.18	Simply Supported Deep Beams with opening /Geometry, Loading arrangement, and Reinforcemt Details……..…	82
5.19	Finite Element idealization of B0 and B2…….….	83
5.20	Load-Deflection Curve at Mid-Span for Deep Beams (B0, B1, B2, and B3)…….……..…...…	85
5.21	Load-Deflection Curve at Mid-Span for Deep Beams (B0, B4, and Bm5)…….…..…….....…	86
5.22	Load-Deflection Curve at Mid-Span for Deep Beams (B0, B6, B7, and B8)…… …….....….....	86

FIG. NO.	TITLE	PAGE
5.23	Load-Deflection Curve at Mid-Span for Deep Beams (B0, B6, B9, and B10)……..…….……..…..…..…...	87
5.24	Load-Deflection curve for Beam B0 with Effect of Web Reinforcement……...….	88
5.25	Load-Deflection Curve at Mid-Span for Beam B2 with Effect of Web Reinforcement……...……	89
5.26	Load-Deflection Curve at Mid-Span for Beam B2 with Different Span–Depth Ratio…..……..…..……..……	90
5.27	Load-Deflection Curve at Mid-Span for Beam B2 with Different Compressive Strength …..……..	91
5.28	Load-Deflection Curve at Mid-Span for Beam B0 with Different of Boundary Conditions……..…...	92
5.29	Continuous Deep Beams with Opening/ Geometry, Loading arrangement, and Reinforceme Details…..……	94
5.30	Finite Element Mesh of Half Bc0 and Bc1 Beams……..……..	95
5.31	Load -Deflection Curve at Mid-Span for Bc0 and Bc1…....…	96
5.32	Load -Deflection Curve at Mid-Span for Bc0 and Bc2.....	97
5.33	Load -Deflection Curve at Mid-Span for Bc0 and Bc3…….....	97
5.34	Deep Beam…….……..……..…….	99
5.35	Continuous Deep Beam……...……..…	101
5.36	Actual and Predicted Strength for Continuous Deep Beams…..	103

LIST OF TABLES

TABLE NO.	TITLE	PAGE
3.1	Shape Function of the Quadratic 20-Node Brick Element…..…	17
5.1	Material Properties and Additional Parameters of Deep Beams…..…….	68
5.2	Comparision Shear Strength for Deep Beams……..……..	71
5.3	Material Properties and Additional Parameters of Continuous Deep Beam……. …...….	74
5.4	Material Properties and Additional Parameter of Simply Supported Deep Beam with Openings……..…	78
5.5	Measured and Computed Ultimate Loads…….…….	79
5.6	Opening Notations……	82
5.7	Material Properties and Additional Parameters of Simply Supported Deep Beams with Openings……..……	85
5.8	Shear Strength of Simply Supported Deep Beams with openings……...……...	87
5.9	Opening Notations…….....	94
5.10	Material Properties and Additional Parameters of Continuous Deep Beams with Openings…….…..…..…	96
5.11	Material Properties and Additional Parameters of Continuous Deep Beams ……..…….	102
5.12	Predicted and actual ultimate Shear Strength in Continuous Deep beams with Single Point Load per pan…..……..…	102

LIST OF FIGURES

FIG. NO.	TITLE	PAGE
1.1	Distribution of Flexural Stresses in homogeneous Simply Supported Deep Beam……..	3
2.1	Eccentric Load ……	6
2.2	Kong's Equation notation……	7
3.1	Linear and Quadratic Isoperimetric Solid Element…..……...	15
3.2	Local Coordinate System……..……..	16
3.3	Distribution of Sampling Points over the Element in 15 Gaussian point integration Rule ……	26
3.4	Typical Uniaxial Stress –Strain Curve for Concrete in Compression……..……..	27
3.5	Biaxial Strength of Concrete……..…..…..……	29
3.6	Triaxial Strength Envelope of Concrete ……...…..……	29
3.7	Cracking of Concrete……..……	32
3.8	Smeared Crack Model…….…….....	33
3.9	Discrete Crack Model…….	34
3.10	Uniaxial Stress-Strain Curve, Pre-and Post Failure Regime…..….	37
3.11	Uniaxial Stress-Strain Curve for Concrete……...…. ..	42
3.12	Post Cracking Model for Concrete…….	50
3.13	Shear Retention for Concrete…….……	51

]FIG. NO.	TITLE	PAGE
3.14	Uniaxial Compressive Stress-Strain Relationship for Cracked Concrete……..	53
3.15	Stress-Strain Relationship of Steel Bars Used in the Analysis……...	54
4.1	Linear Incremental Method……	56
4.2	Conventional Newton – Raphson Method…….…….	57
4.3	Modified Newton – Raphson Method…….. ..	59
4.4	Combined Newton – Raphson Method……	60
4.5	Incremental - Iterative Technique ……..……...	60
5.1	Simply Supported Deep Beams/ Geometry, Loading arrangement , and Reinfocement Details……..…….....	66
5.2	Finite Element Idealization of Half of the Simply Supported Deep Beams...…...…….……..	67
5.3	Load-Deflection Curve at Mid-Span for (A4) Deep Beam ….....	68
5.4	Load-Deflection Curve at Mid-Span for (K2) Deep Beam…..…	69
5.5	Load-Deflection Curve at Mid-Span for (K1) Deep Beam …….69	
5.6	Load-Deflection Curve at Mid-Span for (A4) Deep Beam (Comparison with previous studies).....……..	70
5.7	Load-Deflection Curve at Mid-Span for (K2) Deep Beam (Comparison with previous studies).....…...…..	70
5.8	Cracking Patterns of Simply Supported Deep Beams.....…..	71
5.9	Continuous Deep Beam Geometry and Reinforcement Details….	73
5.10	Finite Element Idealization of One Span of Continuous Deep Beam ……..…….	73

FIG. NO.	TITLE	PAGE
5.11	Load-Deflection Curve at Mid-Span for Continuous Deep Beam ……	74
5.12	Load-Deflection Curve at Mid-Span for Continuous Deep Beam (Comparison with previous studies)…..……....	75
5.13	Crack Patterns of Continuous Deep Beam at Failure for One Span…...……...……	75
5.14	Simply Supported Deep Beams with Opening……..	77
5.15	Finite Element Idealization of Beam (M-0.4/5)…..……....	78
5.16	Influence of Opening Location through Depth of the Beam……...……..……	79
5.17	Cracking Patterns of Simply Supported Deep Beam (M0.4/5)……..……	80
5.18	Simply Supported Deep Beams with opening /Geometry, Loading arrangement, and Reinforcemt Details…..……..…	82
5.19	Finite Element idealization of B0 and B2……..…...……..	83
5.20	Load-Deflection Curve at Mid-Span for Deep Beams (B0, B1, B2, and B3)……..……..…...…	85
5.21	Load-Deflection Curve at Mid-Span for Deep Beams (B0, B4, and Bm5)……..…….....…	86
	Load-Deflection Curve at Mid-Span for Deep Beams (B0, B6, B7, and B8)…… …….....….....	86
5.23	Load-Deflection Curve at Mid-Span for Deep Beams (B0, B6, B9, and B10)……..…….…….....…...…..	87
5.24	Load-Deflection curve for Beam B0 with Effect of Web Reinforcement……...….	88

FIG. NO.	TITLE	PAGE
5.26	Load-Deflection Curve at Mid-Span for Beam B2 with Different Span–Depth Ratio…..……...…...……...…….……	90
5.27	Load-Deflection Curve at Mid-Span for Beam B2 with Different Compressive Strength …..…….……..	91
5.28	Load-Deflection Curve at Mid-Span for Beam B0 with Different of Boundary Conditions…….....….....	92
5.29	Continuous Deep Beams with Opening/ Geometry, Loading arrangement, and Reinforceme Details….……	94
5.30	Finite Element Mesh of Half Bc0 and Bc1 Beams……...……..	95
5.31	Load -Deflection Curve at Mid-Span for Bc0 and Bc1…....…	96
5.32	Load -Deflection Curve at Mid-Span for Bc0 and Bc2.....	97
5.33	Load -Deflection Curve at Mid-Span for Bc0 and Bc3…….....	97
5.34	Deep Beam…….……..……..…….	99
5.35	Continuous Deep Beam……...…….…	101
5.36	Actual and Predicted Strength for Continuous Deep Beams…..	103

NOTATIONS

ACI	American concrete Institute
ξ, η, ζ	Natural coordinate system
u, v, w	Displacement components in x, y and z – direction respectively
N_i	Shape function at the ith node
u_i, v_i, w_I	Nodal displacement
x, y, z	Global or cartisian coordinates
x_i, y_i, z_I	Global coordinates of ith node
$\{\varepsilon\}$	Strain vector
ε	Strain
[B]	Strain – displacement matrix
$\{a\}^e$	Nodal displacements
[J]	Jacobian matrix
$\{\sigma\}$	Stress vector
σ	Stress
[D]	Constitutive matrix
$\{\varepsilon'\}$	Strain vector of bar element
[B′]	Strain–displacement matrix of the bar element
[D′]	Constitutive matrix of the bar element
As	Cross–sectional area of the bar
[k′]	Stiffness matrix of the bar element
W_i	Weight of the sampling point
I_1	First stress invariant

J_2	Second deviatoric stress invariant
α, β	Material parameters
σ_o	Equivalent effective stress at the onset of plastic deformation
C_p	Plasticity coefficient
f'c	Ultimate compressive strength of concrete
$\{\varepsilon_p\}$	Effective accumulated plastic strain vector
$\bar{\sigma}$	Equivalent uniaxial stress
ε'_o	Total strain corresponding to the parabolic part of the curve
ε_c	Total effective strain of concrete
ε_e	Elastic component of total effective strain of concrete
ε_p	Plastic component of total effective strain of concrete
H'	Hardening parameter
λ	Compression reduction factor
K	Hardening parameter which governs the expansion of the yield surface
$\lambda_1, \lambda_2, \lambda_3$	Participation factors
$\bar{I}_1$	First strain invariant
$\bar{J}_1$	Second deviatoric strain
ε_{cu}	Ultimate concrete strain
σ_{cr}	Cracking stress of concrete
E_1	Reduced modulus of elasticity
β_1	Reduction factor

G	Shear modulus of elasticity
D_{cr}	Cracked material stiffness in the local axis
l, m, n	Directional cosines in the x, y, z directions respectively
ε_{cr}	Cracking strain
σ_n	Stress normal to the cracked plane
ε_n	Strain normal to the cracked plane
α_1	The rate of stress release as the crack widens
α_2	Sudden loss of stress at instant of cracking
γ_1	Rate of decay of shear stiffness as the crack widens
γ_2	Sudden loss in shear stiffness at the instant of cracking
γ_3	Residual shear stiffness due to the dowel action
f_t	Maximum tensile strength of concrete
F.E.	Finite element

Chapter One

INTRODUCTION

1.1 General

The classical definition of a deep beam is the member which has a depth much greater than the normal in relation to its span, while the thickness in the perpendicular direction is much smaller than either the span or the depth. Deep beams occur in engineering structures such as in bunkers and water tanks where the walls act as vertical beams spanning between column supports [Khalaf,(1986), Mahmoud,(1992)]. In some multistory buildings, it is often desirable to have the lower floors free of columns, therefore; these beams may be designed as beams spanning across the column free space. Almost, these structures may include elements in the form of deep beams provided with openings for electrical cables, mechanical ducts and water and sewerage pipes (EL-Hashimy et al (1989)).

ACI-building code (2002) classified deep beams as those with span to depth ratio about (4) or less, or a shear span less than about twice the depth.

1.2 Shear and Flexural behavior of Deep Beam

The previous studies showed that reinforced concrete deep beams have behavior more complex and differ from that of shallow beams in many items:

1. In deep beams the transverse sections which are plane before bending do not remain plane after bending (Winter and Nilson,(1978)).
2. The neutral axis does not usually lie at mid-depth and moves away from the loaded face of the member as the span to depth ratio decreases as shown in Fig. (1.1) (ACI-Code,(1995)).
3. Flexural stresses and strains are not linearly distributed across the beam depth (Winter and Nilson,(1978)).

The flexural strength can be predicted with sufficient accuracy using the classical methods employed for beams of normal proportions. The equivalent rectangular stress block and associated parameters can be employed without change. Experimental studies showed that shear strength of deep beams may be as much as (2-3) times greater than that predicted by using the expression for normal members (Winter and Nilson,(1978)). It is well known that shear transfer of diagonally cracked concrete beams of normal proportions takes place by four mechanisms:

1.Direct transfer in the uncracked concrete compression zone.
2. Aggregate interlocking.
3.Dowel action of the flexural main reinforcement.
4.Direct tension of the web reinforcement.

For deep beams, however in addition to the items above, a significant amount of load is carried to the supports by compression thrust joining the load and the reaction (Sanad and Saka (2001)). Diagonal cracks, which form roughly in a direction parallel to a line from load to support, isolate a compression strut, which acts with the horizontal compression in the concrete and the tensile force in the main reinforcement as a truss to equilibrate the loads (Winter and Nilson,(1978)).

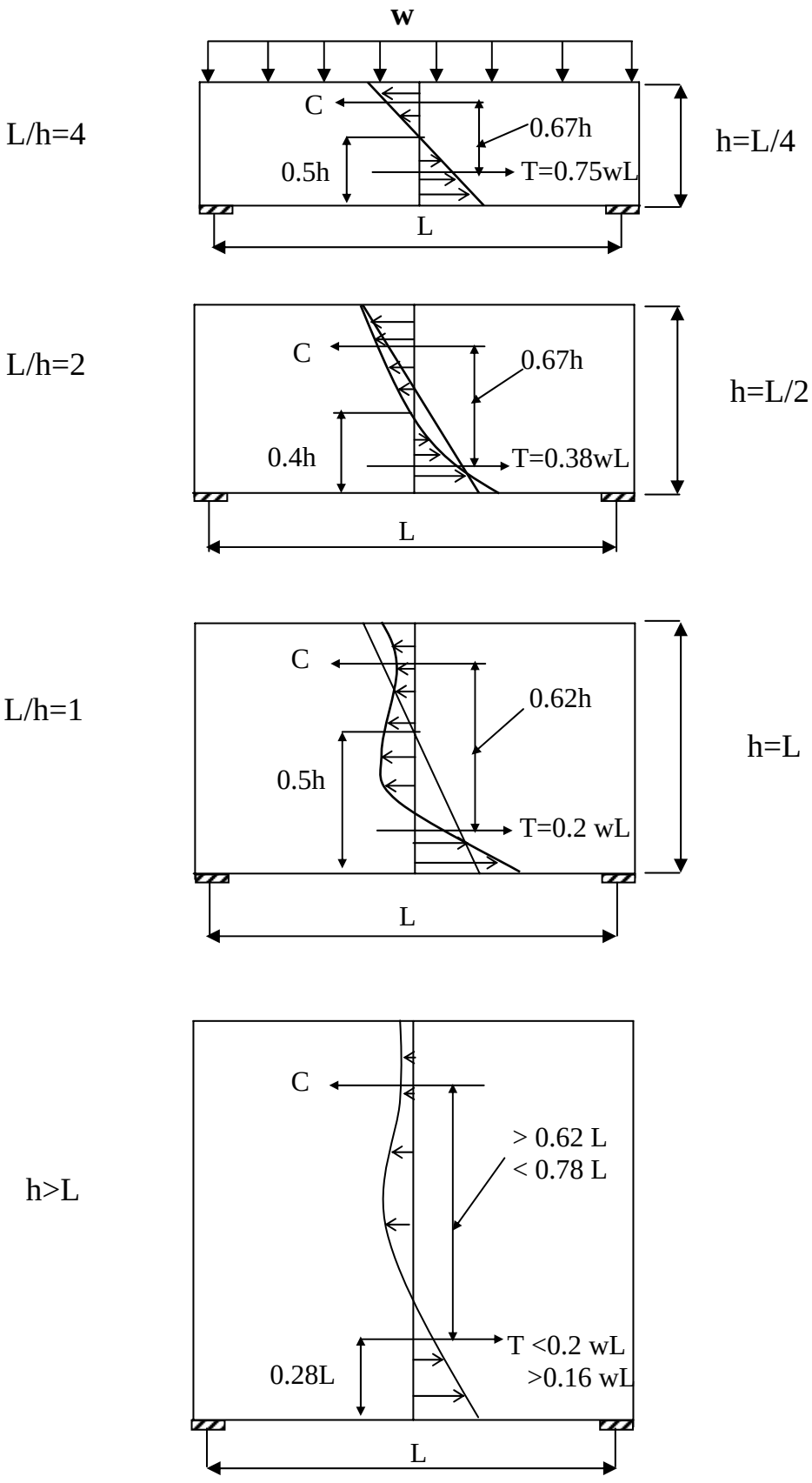

Figure (1.1): Distribution of Flexural Stresses in Homogeneous Simply Supported Deep Beam (ACI-Code,(1995)).

1.3 Scope and Aims

The basic objective of the work is to study the effect of openings on strength and the overall behavior of simply supported and continuous reinforced concrete deep beams under static loads.

The presence of openings in the reinforced concrete deep beams in addition to nonhomogeneites of reinforced concrete, material nonlinearity and cracking patterns makes the problem more complex. Three-dimensional finite element method will be used to predict the overall behavior, stresses and strains components, at various stages of loading and to predict the cracking initiation and the failure load. Material nonlinearities due to cracking of the concrete, plastic flow or crushing of concrete and yield condition of reinforcement are considered. The maximum tensile strength of concrete is used as a criterion for cracking initiation. The tension stiffening of concrete will be used to describe post-cracking behavior of the concrete. The aggregate interlocking effect and the dowel action are incorporated in the model.

1.4 Thesis Layout

This thesis is organized in six chapters. The present introductory Chapter is being the first. Chapter two is devoted to the review of literature. Chapter three is concerned with the constitutive relations for reinforced concrete materials. Chapter four presents the numerical algorithm used for solution of the nonlinear reinforced concrete problem. In chapter five several numerical examples are presented and verified with previous analytical and experimental studies. Chapter seven gives the conclusions and suggestions for future research.

Chapter Two

REVIEW OF LITERATURE

2.1 Introduction

Accurate prediction of the ultimate strength of reinforced concrete deep beams is of prime importance for developing a reliable method for their design. For this purpose many experiments have been carried out to investigate the behavior of such beams. The data collected from these experiments constitute the basis of some of the expressions available in the literature for analytically predicting the behavior of these beams (Sanad and Saka (2001)). In this Chapter a literature survey is divided into two scopes.

1. Experimental studies
2. Theoretical and analytical studies

2.2 Experimental studies

In this item, the most important tests in this field will be reviewed.

Ramakrishnan and **Ananthanarayana** (**1968)** tested twenty six simply supported reinforced concrete deep beams. The beams had span to depth ratio ranging from 0.94 to 2.1. Other variables studied were the type of loading , percentage of tensile steel and effect of shrinkage mesh reinforcement , which at the same time would act as web reinforcement. Seventeen beams faild in shear , four in flexure-shear and five beams in flexure . Their approach to the problem starts from the definition of diagonal

tension crack for which they assumed it to be essential because of shear failure in deep beams. Adopting this definition , they used the procedure of the indirect tension test to evaluate the ultimate load of deep beams failing in shear as:

$P = ß\ k\ f_t\ b\ H$ ……..*(2.1)*

where:

P = ultimate load

ß = shear span coefficient equal to 2 for central concentrated load, symmetrical two-point load and uniformly distributed load

= (1+ tanθ cotø) for eccentric load

θ and ø = angles as indicated in Fig. (2.1)

k = coefficient equal to 1.57 for a cylinder split test and equal to 1.36 for a diagonal cube split test

f_t = tensile strength of concrete from corresponding test (Psi)

b = thickness of the beam (in)

H = total depth of the beam (in)

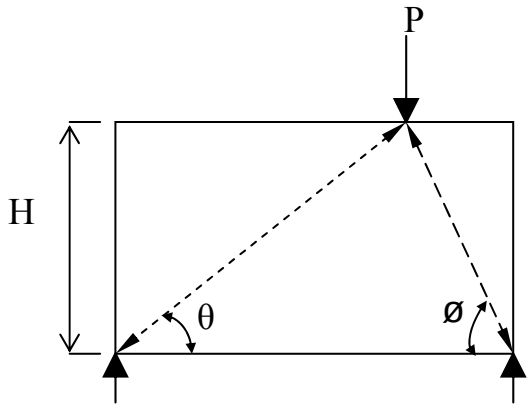

Fig. (2.1): Eccentric Load (Ramakrishnan and Ananthanarayana (1968))

Kong and **Sharp (1973)** tested twenty four simply supported reinforced concrete deep beams to study the effects of openings on load and cracking.

This study presented an empirical formula to evaluate the ultimate shear capacity (Q_{ult}) of reinforced concrete deep beams with openings located at critical shear zone. This equation was put for beams subjected to two concentrated loads, applied symmetrically about mid–span as shown in Fig.(2.2). Kong's equation determines the ultimate capacity (Q_{ult})of such beam as follows:

$$Q_{ult} = c_1\left[1 - 0.35\frac{k_1.x}{k_2.D}\right] ft\ D\ k_2\ b + c_2 \sum A \frac{y}{D}\sin\alpha \qquad .....(2.2)$$

where:

c_1 = coefficient equal 1.35

c_2 = coefficient equal 300 N/mm^2 for deformed bars and 130 N/mm^2 for plain bars

k_1 and k_2 = coefficients defining the opening position

x = clear shear span (mm)

D,b = beam depth and width respectively (mm)

f_t = cylinder splitting tensile strength (N/mm^2)

A = area of web bar

α = angle of intersection between a typical web bar and load path

y = depth at which typical web bar intersects the load path (mm)

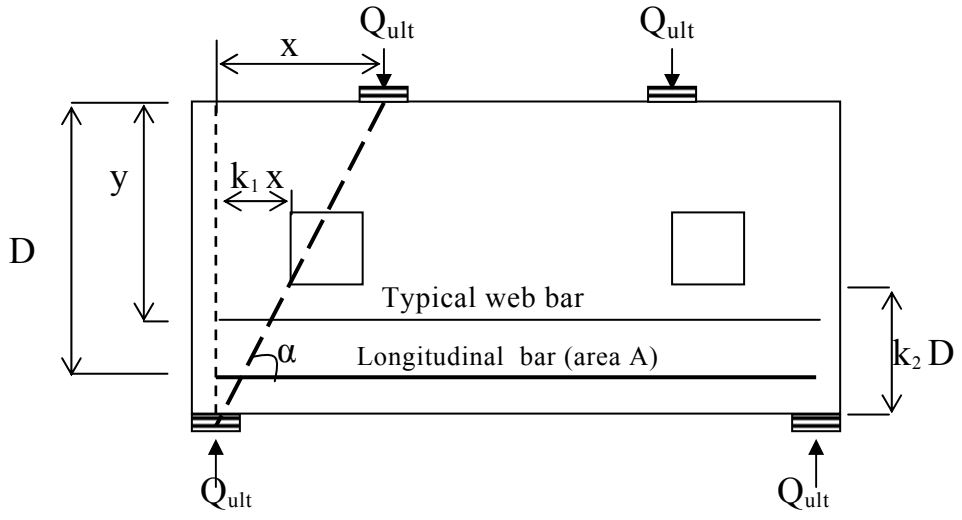

Fig.(2.2): Kong's equation notation (Kong and Sharp,(1973))

Besser and **Cusens** (**1985**) , tested seven simply supported reinforcrd concrete deep beam panels with depth to span ratio in the range of 1 to 4. They concluded that service load capacity, as determined by initial diagonal cracking, increases significantly for depth to span ratio less than 3. In terms of ultimate load, bearing was a primary factor in five of the seven tests, diagonal cracking and buckling provided the failure modes of the other panels. A beam panel of span to depth equal to one failed in shear with a diagonal fracture line joining the load and support points. While specimens with depth to span ratios larger than 1 failed by crushing of bearing zones. This was the most common mode of failure among these members and was exhibited by panels with depth to span ratios between 1.5 to 3.5. The largest specimen tested, having a depth to span ratio equal 4, failed by lateral buckling.

The complete load-deformation response of fiber reinforced concrete deep beams was investigated both analytically and experimentally by **Mansur** and **Ong (1991)**. The softened truss model theory for nonfibrous concrete had been modified by using a new stress-strain relationship for fiber concrete, and a series of tests was carried out to generate relevant information. The major parameters of the study were the span to depth ratio,volume fraction of fibers, and ratios of longitudinal and transverse reinforcement. A comparison of test results with theoretical predictions of the load-deflection response showed very good agreement.

Roberto et al (1999) studied the behavior of three lightly reinforced and three unreinforced deep beams. Four specimens were tested after a single thermal cycle (T = 250 or 400ºC) and two specimens were tested in the state (T =20ºC), in order (1) to measure the complete load-displacement response in three-point bending, and (2) to study crack formation. The

results showed that the ultimate capacity decreases markedly in the unreinforced specimens.. The ultimate capacity of the lightly reinforced beams was little affected by concrete decay (after a cycle at 400ºC), owing to the negligible sensitivity of the steel to a thermal cycle up to 500ºC.

2.3 Theoretical and Analytical Studies

There are many researchers who deal with deep beams by theoretical and analytical studies:

Khalaf (**1986**) presented a nonlinear analysis of reinforced concrete deep beams by using the finite element method under static load. Concrete was represented by a quadrilateral element. The main reinforcement was represented by either simple truss elements or constant strain traingular elements connected to the concrete by spring linkage element at nodes with proper stiffness to simulate bond and dowel action. The secondary steel was represented by truss element connected perfectly to the concrete nodes. The behaviour of concrete in compression was idealized by nonlinear elasticity based model. In tension, the behavior of concrete was idealized by smeared cracking model in which the cracked concrete was assumed to remain as a continuum. The analytical results obtained, such as deflection, crack pattern and ultimate loads showed reasonable agreement with experimental results.

Cervera et al (1987) used a three dimensional analysis to study plates, shells and deep beams. He adopted the 20-noded isoparametric element and the effect of shear and normal stresses were included in this analysis. In concrete, the nonlinear behavior and crushing were considerded in compression. In tension, cracking and tension stiffening were considered.

The results obtained from this study showed good agrement with the exptrimental results.

EL-Hashimy et al (1989) investigated the cracking load of reinforced concrete deep beams with openings by two dimensional finite element method. The study includes beams subjected to uinform and concentreted loads. Concrete and main steel reinforcement were simulated by rectangular plane stress elements which behave as elastic materials.

A parametric study was presented including the influence of both openings properties and opening location along the beam span and through the depth. They suggested coefficints to be used with Kong's equation to calculate the cracking load of deep beams with openings subjected to concentrated loads. The suggested equation gave agreement about (20%) of maximum difference with the finite element results for the case of span to depth ratio ranging between 1.0 and 1.5 and opening located at critical shear zone below the beam mid-hight.

Mahmoud (1992) Presented nonlinear analysis of reinforced concrete deep beams under static load by using the finite element method. Concrete was represented by 8-noded plane stress isoparametric elemenl for two dimensional analysis and 20-noded brick element for three dimensional analysis. Bar elements were used to represent the reinforcement in this analysis. Perfect bond between the concrete and reinforcement was assumed. An elastic-perfectly plastic model was used for plane stress analysis, and a strain hardening model was used in the three dimensional finite element analysis. The effect of support boundary conditions were studied. The results obtained from this study showed good agreement with the experimental results.

Siao (1995) used the strut-tie approach for the analysis of shear strength of simply supported and continuous reinforced concrete deep beams. This approach can be applied to deep beam with high depth to span ratio. In this analysis he illustrated that there was no difference in shear behavior of single and double span deep beams.

Husain and **Ali** (**1995**) extended the original Timoshenko deep beam theory to inculde the effects of externally distributed moments. Full expression of the governing equations for deep beams including these effects were obtained both in coupled and uncoupled forms. As an application to the distributed moment generations, the problems of deep beams resting on elastic foundations with both compressional and frictional restraints were investigated in detail. In the solution of the governing equations of deep beams resting on elastic foundation, the coupled form was used to retain all terms of loadings in the expressions. Extensive finite difference and finite element formulations were developed to solve various problems. The results from these different methods were plotted together to compare and check the accuracy of the solutions. Good agreement was found in these methods, which indicated the efficiency of these methods.

AL-Taan and Ali (1998) presented a nonlinear finite element analysis of fibrous concrete deep beams with conventional reinforcement under static load. The constitutive models of nonlinear materials behavior were presented to take into account the nonlinear stress-strain relationship of concrete, cracking, pullout of the steel fibres, yielding of the reinforcement, and post-cracking shear transferred by aggregate interlock. An incremental iterative procedure was employed for the nonlinear solution. The computed results of the various examples showed good agreement with the published

experimental results which inculded deflection, strain, cracking patterns and ultimate loads.

Daniel and **Patrick (1999)** presented a general framework aimed for dealing with the failure analysis of reinforced concrete deep beams. A versatile numerical method was aimed for providing a reliable solution. It was based on the yield design theory which estimates the ultimate load-carrying capacity of reinforced concrete structures. The concrete material was treated as a classical two-dimensional continuum, whereas the longitudinal reinforcement was regarded as bar elements. In particular, it was shown that the shear span to depth ratio with the amount of longitudinal reinforcement, plays a crucial role in the transition from flexural to shear failure modes of the beam.

Ashour (2000) carried out a mechanism analysis of shear failure of simply supported reinforced concrete deep beams. Concrete and steel reinforcement were modeled as rigid perfectly plastic materials. The failure modes were idealized as an assemblage of rigid blocks separated by yield line. Comparison of the predicted shear capacity of numerous deep beams showed good agreement with the results obtained from experiments. A parametric study of main variables affecting shear strength of deep beams was conducted. The presented model showed that the shear span to depth ratio has more influence on the shear capacity than the span to depth ratio and as the former increases, the shear strength decreases.

Tan et al. (2001) This study deal with the analysis of prestressed concrete deep beams by strut-tie model. The model can be used for both pre and post-tensioned deep beams. A comparison showed that the predictions

were in good agreement with the experimental results of four case studies of thirty nine deep beams.

2.3 Present Study

The present study deals with the case of simply supported and continuous reinforced concrete deep beam with opening at flexural and shear zones by using the three dimension nonlinear finite element analysis. A 20-node brick element with 60 degrees of freedom is imployed to model the concrete. Steel reinforcement is represnted by embedded bar through the brick element with perfect bond between concrete and steel.

Chapter Three

FINITE ELEMENT ANALYSIS OF REINFORCED CONCRETE

3.1 Introduction

Finite element technique has been used for nonlinear analysis of reinforced concrete structures through more than forty years. Attention was first focused on two-dimensional and axisymmetrical models, but it was soon widened to include plate, shell and beam systems. In spite that two-dimensional analysis gives an adequate and more economical model in many problems, but it is insufficient to represent the behavior of reinforced concrete when including three-dimensional effects of the applied forces. So, it is believed that the use of three-dimensional analysis provides a better representation of material nonlinearity and cracking of the reinforced concrete members [12, s15], as well as it involves a large number of degrees of freedom for a given discretization than the two-dimensional analysis [Cervera et al, (1987), Coenen,(1980)]

Nowadays, the three-dimensional finite element method has been extensively used for the nonlinear analysis of reinforced concrete members because it yields a wide range of information for a single computer analysis. The information includes displacements, strains, distribution of normal and shear stresses in concrete, cracking pattern at different stages of loading and forces in longitudinal steel bars and stirrups (Chen 1982).

In the present study, the 20-node isoparametric brick element is used for the idealization of concrete, while the steel reinforcement is formulated by using bar elements embedded inside the concrete with the assumption of perfect bond between the two types of elements.

3.2 Three–Dimensional Brick Element

The quadratic 20-node brick element shown in Fig. (3.1) is adopted to represent concrete. This type of element is popular due to its superior performance. A major advantage of the quadratic 20–node brick element over the 8–node brick element, when studying complex cases, is that less number of elements can be used, as well as it may have curved sides and therefore provides a better fit to curved sides of an actual structure [Cook,(1974), Moaveni,(1999)].

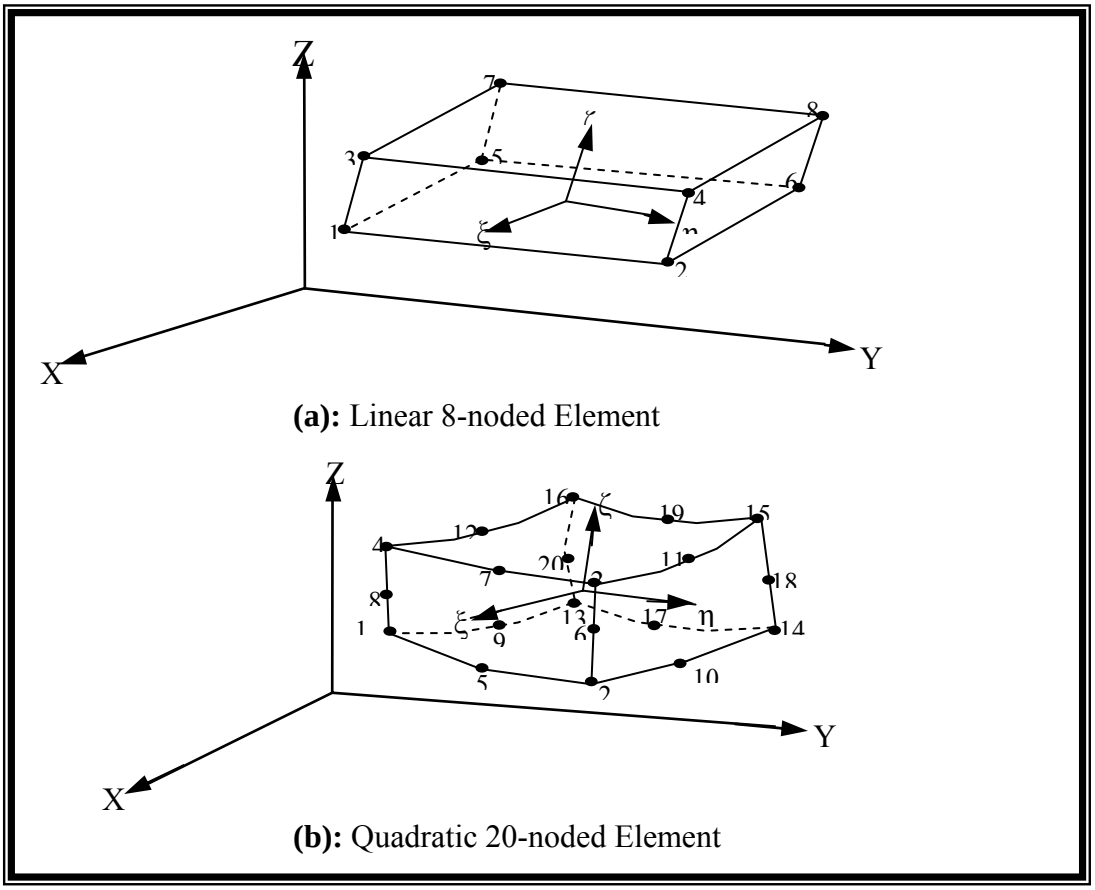

(a): Linear 8-noded Element

(b): Quadratic 20-noded Element

Figure (3.1): Linear and Quadratic Isoparamatric Solid Element

3.2.1 Shape Functions

The natural local coordinates system is used to describe the displacement components of a point p(ξ, η, ζ) within the element. These local coordinates (ξ, η, ζ) are scattered in the center of the brick element where the origin point is located as shown in the Fig. (3.2)

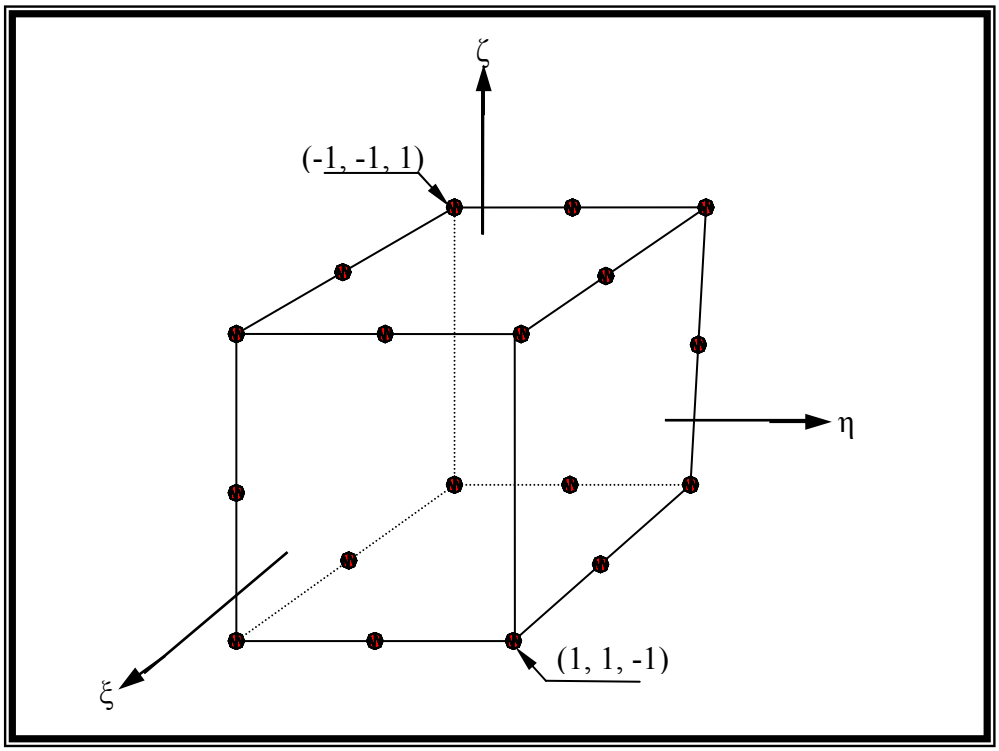

Figure (3.2): Local Coordinate System

The element has 20 nodes and 60 degrees of freedom and bounded by planes with ξ, η, and ζ = ± 1 in ξ, η, ζ space. The starting point for the stiffness matrix derivation is the element displacement field. The isoparametric definition of displacement components is:

$$\left.\begin{aligned} u(\xi,\eta,\zeta) &= \sum_{i=1}^{n} Ni\ (\xi,\eta,\zeta)ui \\ v(\xi,\eta,\zeta) &= \sum_{i=1}^{n} Ni\ (\xi,\eta,\zeta)vi \\ w(\xi,\eta,\zeta) &= \sum_{i=1}^{n} Ni(\xi,\eta,\zeta)wi \end{aligned}\right\} \quad \ldots(3.1)$$

where N_i (ξ, η, ζ) is the shape function at the i-th node and u_i, v_i and w_i are the corresponding nodal displacements with respect to global x, y, and z coordinates. The shape functions of the quadratic 20-node brick element are shown in Table (3.1)

Table (3.1): Shape Functions of the Quadratic 20-Node Brick Element (Cook,(1974))

Location	ξ	η	ζ	Ni (ξ, η, ζ)
Corner nodes	±1	±1	±1	$(1+\xi\,\xi_i)(1+\eta\,\eta_i)(1+\zeta\zeta_i)\,(\xi\,\xi_i+\eta\,\eta_i+\zeta\,\zeta_i-2)/8$
mid – side nodes	0	±1	±1	$(1-\xi^2)(1+\eta\,\eta_i)(1+\zeta\,\zeta_i)/4$
mid – side nodes	±1	0	±1	$(1-\eta^2)(1+\xi\,\xi_i)(1+\zeta\,\zeta_i)/4$
mid – side nodes	±1	±1	0	$(1-\zeta^2)(1+\xi\,\xi_i)(1+\eta\,\eta_i)/4$

To check the above mathematical model, each of its 20 shape functions has a value of unity at its specified node and a value of zero at any of the other 19 nodes. Also the sum at any point in the element is 1.

In the isoparametric group of elements, the interpolation shape functions are also used to define the geometry of the element and the global

coordinates of any point p(x, y, z) in the terms of the natural local coordinates by using the relations:

$$\left.\begin{aligned} x(\xi,\eta,\zeta) &= \sum_{i=1}^{20} Ni\,(\xi,\eta,\zeta)\,xi \\ y(\xi,\eta,\zeta) &= \sum_{i=1}^{20} Ni\,(\xi,\eta,\zeta)\,y_i \\ z(\xi,\eta,\zeta) &= \sum_{i=1}^{20} Ni\,(\xi,\eta,\zeta)\,zi \end{aligned}\right\} \qquad \ldots(3.2)$$

where x_i , y_i and z_i are the global coordinates of the node i .

3.2.2 Strain and Stress Fields

Since the geometrical nonlinearities are not considered in the present work, displacement gradients remain small throughout the loading process and hence the engineering components of strain can be expressed in terms of the first partial derivatives of the displacement components. Therefore, the linearized strain–displacement relationships may be written as:

$$\{\varepsilon\} = \begin{Bmatrix} \varepsilon_x \\ \varepsilon_y \\ \varepsilon_z \\ \gamma_{xy} \\ \gamma_{yz} \\ \gamma_{zx} \end{Bmatrix} = \begin{Bmatrix} \frac{\partial u}{\partial x} \\ \frac{\partial v}{\partial y} \\ \frac{\partial w}{\partial z} \\ \frac{\partial u}{\partial y} + \frac{\partial v}{\partial x} \\ \frac{\partial v}{\partial z} + \frac{\partial w}{\partial y} \\ \frac{\partial w}{\partial x} + \frac{\partial u}{\partial z} \end{Bmatrix} = \sum_{i=1}^{20} \underbrace{\begin{bmatrix} \frac{\partial Ni}{\partial x} & 0 & 0 \\ 0 & \frac{\partial Ni}{\partial y} & 0 \\ 0 & 0 & \frac{\partial Ni}{\partial z} \\ \frac{\partial Ni}{\partial y} & \frac{\partial Ni}{\partial x} & 0 \\ 0 & \frac{\partial Ni}{\partial z} & \frac{\partial Ni}{\partial y} \\ \frac{\partial Ni}{\partial x} & 0 & \frac{\partial Ni}{\partial z} \end{bmatrix}}_{[B]} \cdot \underbrace{\begin{Bmatrix} u_i \\ v_i \\ w_i \end{Bmatrix}}_{\{a\}^e} \qquad \ldots(3.3)$$

Since the shape functions N_i are functions of the local coordinates rather than Cartesian coordinates, a relationship needs to be established between the derivatives in the two coordinates systems. By using the chain rule, the partial differential relation can be expressed in matrix form as:

$$\begin{bmatrix} \frac{\partial Ni}{\partial \xi} \\ \frac{\partial Ni}{\partial \eta} \\ \frac{\partial Ni}{\partial \zeta} \end{bmatrix} = \underbrace{\begin{bmatrix} \frac{\partial x}{\partial \xi} & \frac{\partial y}{\partial \xi} & \frac{\partial z}{\partial \xi} \\ \frac{\partial x}{\partial \eta} & \frac{\partial y}{\partial \eta} & \frac{\partial z}{\partial \eta} \\ \frac{\partial x}{\partial \zeta} & \frac{\partial y}{\partial \zeta} & \frac{\partial z}{\partial \zeta} \end{bmatrix}}_{[J]} \cdot \begin{bmatrix} \frac{\partial Ni}{\partial x} \\ \frac{\partial Ni}{\partial y} \\ \frac{\partial Ni}{\partial z} \end{bmatrix} \qquad \text{…. } (3.4)$$

where [J] is the Jacobian matrix and the elements of this matrix can be obtained by differentiation of equation (3.2). The Jacobian matrix can be expressed as:

$$[J] = \begin{bmatrix} \sum \frac{\partial Ni}{\partial \xi} x_i & \sum \frac{\partial Ni}{\partial \xi} y_i & \sum \frac{\partial Ni}{\partial \xi} z_i \\ \sum \frac{\partial Ni}{\partial \eta} x_i & \sum \frac{\partial Ni}{\partial \eta} y_i & \sum \frac{\partial Ni}{\partial \eta} z_i \\ \sum \frac{\partial Ni}{\partial \zeta} x_i & \sum \frac{\partial Ni}{\partial \zeta} y_i & \sum \frac{\partial Ni}{\partial \zeta} z_i \end{bmatrix} \qquad \text{…. } (3.5)$$

Then, the derivatives of the shape function with respect to Cartesian coordinates can obtain as:

$$\begin{bmatrix} \frac{\partial Ni}{\partial x} \\ \frac{\partial Ni}{\partial y} \\ \frac{\partial Ni}{\partial z} \end{bmatrix} = [J]^{-1} \cdot \begin{bmatrix} \frac{\partial Ni}{\partial \xi} \\ \frac{\partial Ni}{\partial \eta} \\ \frac{\partial Ni}{\partial \zeta} \end{bmatrix} \qquad \text{…. (3.6)}$$

where $[J]^{-1}$ is the inverse of Jacobian matrix given by:

$$[J]^{-1} = \begin{bmatrix} \frac{\partial \xi}{\partial x} & \frac{\partial \eta}{\partial x} & \frac{\partial \zeta}{\partial x} \\ \frac{\partial \xi}{\partial y} & \frac{\partial \eta}{\partial y} & \frac{\partial \zeta}{\partial y} \\ \frac{\partial \xi}{\partial z} & \frac{\partial \eta}{\partial z} & \frac{\partial \zeta}{\partial z} \end{bmatrix} \qquad \text{…. (3.7)}$$

As $[J].[J]^{-1} = [J]^{-1}.[J] = [I]$ (unit matrix)

The vector of stresses is given by:

$$\{\sigma\} = \begin{Bmatrix} \sigma_x \\ \sigma_y \\ \sigma_z \\ \tau_{xy} \\ \tau_{yz} \\ \tau_{zx} \end{Bmatrix} \qquad \text{….(3.8)}$$

and the stress – strain relationship is represented as:

$$\{\sigma\} = [D].\{\varepsilon\} \qquad \text{…. } (3.9)$$

where [D] is the constitutive matrix.

3.2.3 Element Stiffness Matrix

The tangential stiffness matrix of the three-dimensional isoparametric solid element is given by:

$$[K]^e = \int_{v^e} [B]^T.[D].[B]\ dv^e \qquad \text{….. } (3.10)$$

By using the transformation product rule, the stiffness matrix becomes:

$$[K]^e = \int_{-1}^{+1}\int_{-1}^{+1}\int_{-1}^{+1} [B]^T [D][B]|J|d\xi d\eta d\zeta \qquad \text{….(3.11)}$$

3.3 Reinforcement Idealization

In developing a finite element model for reinforced concrete members, at least three alternative representations of reinforcement have been used:

a) Distributed Representation

The steel bars are assumed to be distributed into an equivalent layer within the concrete element with axial properties in the direction of the bars only [Cervenka and Gerstle,(1971), Cervera et al,(1987)]. A composite concrete-reinforcement constitutive relation is used. Perfect bond is usually assumed between the concrete and the steel.

b) Discrete Representation

A discrete representation of the reinforcement by using independent one–dimensional elements has been widely used. Axial force members, or bar links, may be used and they are assumed to be pin connected with two–degrees of freedom at the nodal points. Beam elements may also be used, and assumed to be capable of resisting axial force, shear, and bending, with three degrees of freedom assigned at each node. In either case, the one–dimensional reinforcement elements are easily superimposed on the multi–dimensional finite element mesh representing the concrete. A significant advantage of the discrete representation is that it can account for possible displacement of the reinforcement with respect to the surrounding concrete (Cook,(1974)).

c) Embedded Representation

This representation assumes that the reinforcement bar is considered to be an axial member built into the isoparametric concrete element such that its displacements are consistent with those of the element.

Perfect bond between the steel and the concrete has been assumed in this case (Owen and Hinton,(1980)). The embedded representation is adopted in the present work.

For particular types of problems, a combination of representations may be used. As an example, discrete beam elements may be used for main reinforcement in beams while axial bar elements for stirrups. On the other hand, a distributed model can be used for the steel throughout the surface of the curved shell and discrete bar or beam elements for special reinforcements along the edge.

A derivation is presented in this section for a bar parallel to the local coordinate axis ξ. A similar derivation can be used for bars paralleled to η and ζ axes (Phillips and Zienkiewcz,(1976)).

For a bar lying inside a hexahedral brick element and parallel to the local coordinate axis ξ, with $\eta = \eta_c$ and $\zeta = \zeta_c$, the displacement representations are:

$$\left.\begin{aligned} u &= \sum_{i=1}^{n} N_i(\xi)u_1 \\ v &= \sum_{i=1}^{n} N_i(\xi)v_1 \\ w &= \sum_{i=1}^{n} N_i(\xi)w_1 \end{aligned}\right\} \quad \text{....(3.12)}$$

The strain-displacement relationship can be expressed in the local coordinate system as:

$$\varepsilon' = \sum_{i=1}^{n}\left[\frac{1}{h^2}\begin{bmatrix} c_1 & c_2 & c_3 \\ c_2 & c_4 & c_5 \\ c_3 & c_5 & c_6 \end{bmatrix}\begin{bmatrix} \frac{\partial N_i}{\partial x} \\ \frac{\partial N_i}{\partial y} \\ \frac{\partial N_i}{\partial z} \end{bmatrix}\right].\begin{bmatrix} u_i \\ v_i \\ w_i \end{bmatrix} \quad \text{....(3.13)}$$

where:

$$C_1 = (\partial x/\partial\xi)^2,$$
$$C_2 = (\partial x/\partial\xi)(\partial y/\partial\xi),$$
$$C3 = (\partial x/\partial\xi)(\partial z/\partial\xi)$$
$$C_4 = (\partial y/\partial\xi)^2,$$
$$C_5 = (\partial y/\partial\xi)(\partial z/\partial\xi),$$
$$C_6 = (\partial z/\partial\xi)^2$$

and

$$h = \sqrt{C_1^2 + C_4^2 + C_6^2} \qquad \text{….(3.14)}$$

Eq. (3.13) is expressed in a compact form as:

$$\{\varepsilon'\}=[B']\{a\}^e \qquad \text{....(3.15)}$$

where [B′] is the strain-displacement matrix of the bar element. Then the stiffness matrix of an axially loaded bar element may be expressed as:

$$[K]^e = \int_{v^e} [B]^T .[D].[B]\ dv^e \qquad \text{…. (3.16)}$$

The constitutive matrix [D′] represents the modulus of elasticity of the steel bar for the case of one-dimensional bar element lying in the direction parallel to the natural coordinate lineξ, and the volume differential dv^e can be written as:

$$dv^e = As.dx' = As.h.d\xi \qquad \text{....(3.17)}$$

where ***As*** is the cross-sectional area of the bar. By substitution of Eq. (3.17) into Eq. (3.16), the stiffness matrix of the embedded bar can be expressed as:

$$[K']^e = As \int_{-1}^{+1} [B]^T [D'] [B']h\, d\xi \qquad \text{....(3.18)}$$

3.4 Numerical Integration

To perform the integration required to set up the element stiffness matrix, suitable scheme of numerical integration has to be made. In finite element work, the Gauss-Legendre quadrature scheme has been found to be

accurate and efficient. The finite integral of the element stiffness matrix given in Eq. (3.11), can be expressed in the form (Irons,(1971)).

$$I = \int_{-1}^{1}\int_{-1}^{1}\int_{-1}^{1} F(\xi,\eta,\zeta)\,d\xi\,d\eta\,d\zeta \qquad \text{....(3.19)}$$

which may be rewritten numerically as:

$$I = \sum_{i=1}^{ni}\sum_{j=1}^{nj}\sum_{k=1}^{nk} Wi.Wj.Wk\,F(\xi_i,\eta_j,\zeta_k) \qquad \text{….(3.20)}$$

where ***ni, nj, nk*** are the number of Gaussian points in the ξ_i,η_j,ζ_k direction respectively. The function $F(\xi_i,\eta_j,\zeta_k)$ represents the matrix multiplication $([B]^T.[D].[B].\det[J])$ at sampling points ξ_i,η_j,ζ_k.

In a similar manner, the integral of the stiffness matrix of the embedded reinforcement can be written as:

$$I = \sum_{i=1}^{ni} Wi\,F(\xi_i) \qquad \text{….(3.21)}$$

The application of the three-dimensional finite element analysis in connection with the nonlinear behavior of reinforced concrete structures needs a large amount of computation time, due to the frequent evaluation of the stiffness matrix. Therefore, it is necessary to choose a suitable integration rule that minimizes the computation time with sufficient accuracy. Several types of integration rules can be used such as the eight (2 *x* 2 *x* 2), and the twenty-seven (3 *x* 3 *x* 3). Gaussian rules are used to integrate the stiffness matrix of eight node linear and twenty node quadratic

brick elements [Hinton,(1988), Irons,(1971)]. The integration rules, which exist in this program, are the 27 (3 *x* 3 *x* 3) point Gauss quadrature and the 15 point type integration rule. The weights and abscissa of the sampling points are listed in Appendix (A) .The relative distribution of the Gaussian points over the element is given in Fig. (3.3).

In the present study, 15 Gauss points are used for the numerical integration, because a reduced integration rule is found to be accurate and computationally efficient than the other types of integration rules. This is due to the fact that the reduced integration rule can significantly reduce the effect of shear locking which may occur in plate analysis when the full integration rule has been used (AL-Shaarbaf and Mohammed,(1999)).

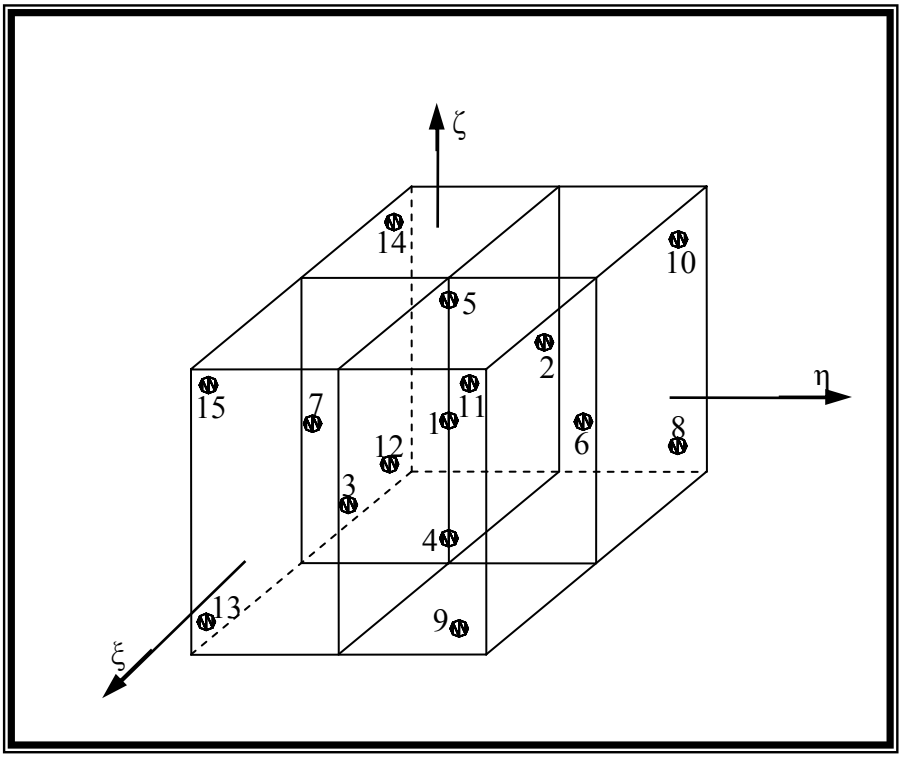

Figure (3.3): Distribution of Sampling Points over the Element in 15 Gaussian point integration Rule (Cervera et al,(1987))

3.5 Uniaxial and Multi-Axial Behavior of Concrete

A typical stress-strain relationship for concrete in compression is shown in Fig. (3.4). It can be seen that the stress-strain curve has a nearly linear elastic behavior up to about 30 percent of its maximum compressive strength ***(f′c)***. For the stress above this point, the curve shows a gradual increase in curvature up to about ***(0.75 f′c - 0.90 f′c)***, beyond which it bends more sharply and approaches the peak point at ***(f′c)***. Beyond this point, the stress-strain curve has a descending part until crushing failure occurs at some ultimate strain ε_u (Chen,(1982)).

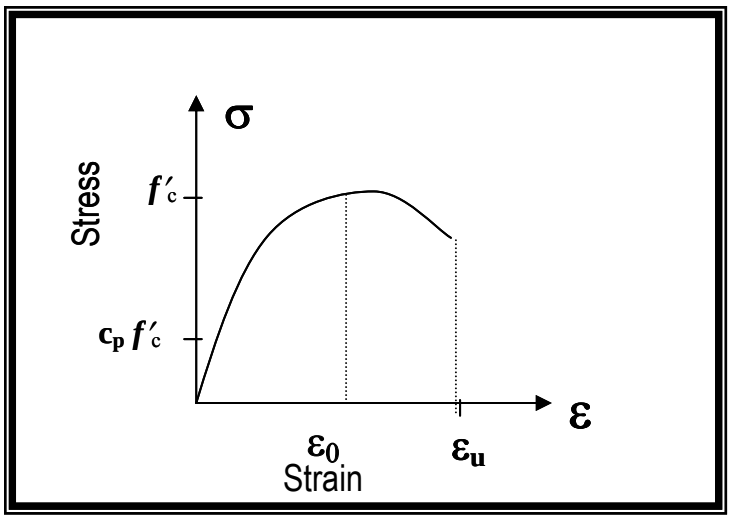

Figure (3.4): Typical Uniaxial Stress –Strain Curve for Concrete in Compression (Chen,(1982))

Poisson ratio ***(ν)*** which is defined as the ratio of lateral strain to the principal compressive strain has been observed in the experiments to be constant up to a stress level of ***(80%)*** of f′c and ranges between ***0.15*** and ***0.22*** (Chen,(1982)).

Under tensile stresses, the shape of the stress-strain curve for concrete shows many similarities to the uniaxial compression curves. However,

some differences exist, that the uniaxial tension state of stress tends to arrest the crack much less frequently than the compressive state of stress. Therefore, it can be expected that the interval of stable crack propagation is relatively short. It has been found that the ratio between the uniaxial tensile and compressive strength may vary considerably but usually ranges from ***0.05*** to ***0.1***. The modulus of elasticity under uniaxial tension is somewhat higher and Poisson ratio somewhat lower than in compression (Metha,(1986)).

The behavior of concrete under multi-axial stress condition is very complex if it is compared with that under uniaxial stress condition and has not yet been assessed experimentally in a complete manner. Various material models with considerable simplifying assumptions have been proposed in literature. A typical biaxial strength envelope is shown in Fig. (3.5) (Kupfer et al,(1969)). It has been seen that the maximum compressive strength increases for biaxial compression state. A maximum strength increase of approximately ***25*** percent is achieved at a stress ratio of $(\sigma_2 / \sigma_1 = 0.5)$, and this is reduced to about ***16*** percent at an equal biaxial compressive state $(\sigma_2 / \sigma_1 = 1)$. Under biaxial compression–tension state of stress, the compressive strength decreases almost linearly as the applied tensile stress is increased (Chen,(1982)).

Experiments indicate that concrete in triaxial stresses has a fairly consistent failure surface which is a function of the three principal stresses, Fig. (3.6). This failure surface can be represented by three-stress invariants. These invariants are the first invariant of the stress tensor (I), and the second and the third invariant of the stress deviatoric tensor (J2) and (J3).

Under biaxial tension, the strength is almost the same as that of uniaxial tensile strength. When subjected to triaxial compressive stresses, concrete exhibits strength, which increases with increasing the confining pressure.

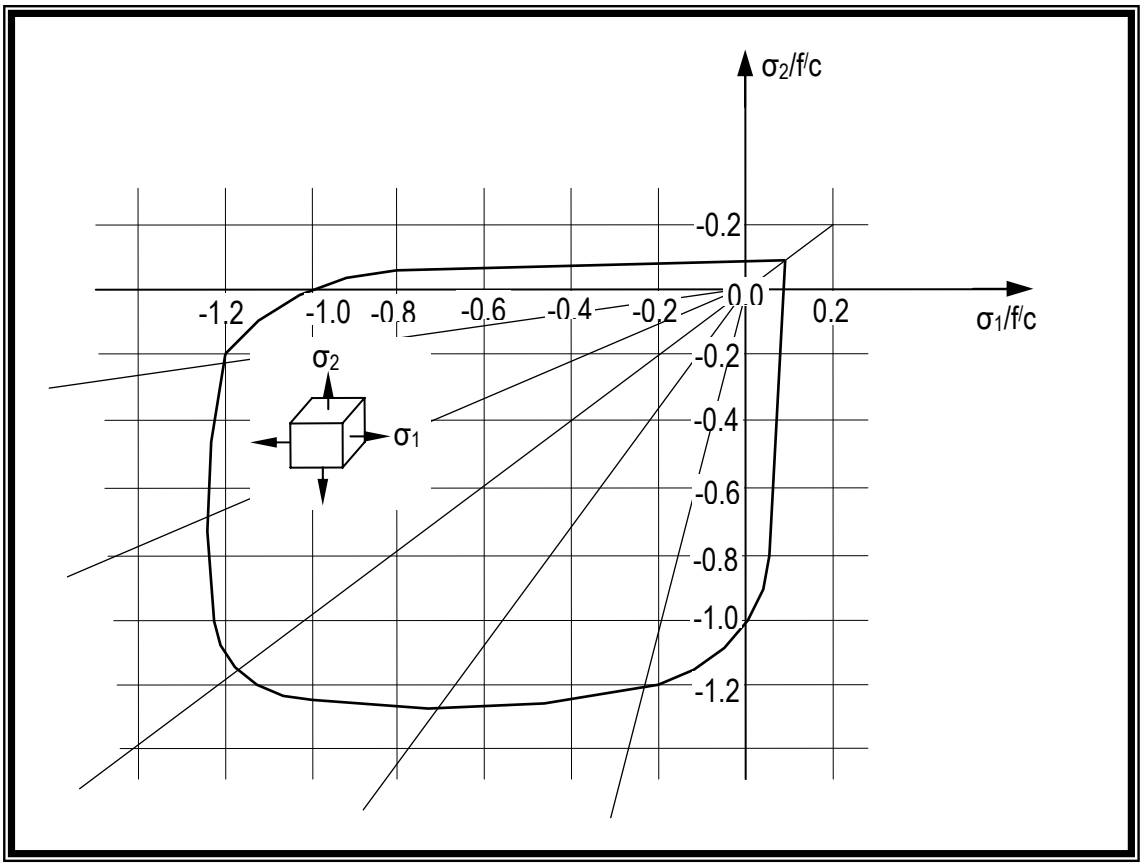

Figure (3.5): Biaxial Strength of Concrete (Kupfer et al,(1969)).

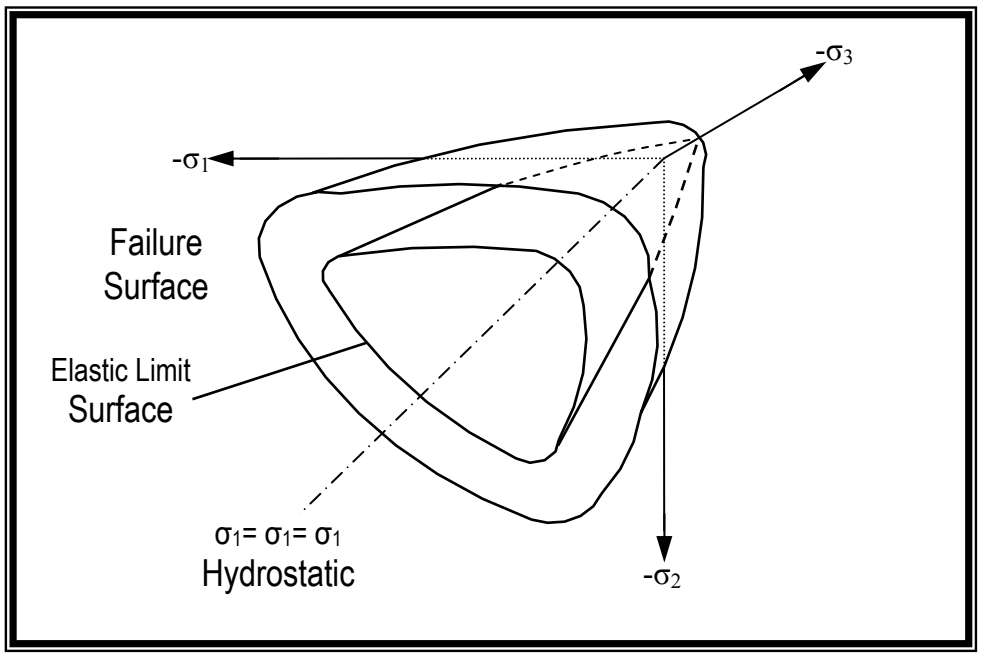

Figure(3.6): Triaxial Strength Envelope of Concrete (Chen,(1982)).

3.6 Stress-Strain Models

Several approaches for describing the complicated stress-strain relationship of concrete under various stress-strain states have been usually used. These approaches can be generally divided into:

-Elasticity based models.
-Plasticity based models.

Elasticity based models may be linear or nonlinear elastic models. In the former, the stress-strain relation for uncracked and cracked concrete is developed depending on the theory of linear elasticity. These models are adequate when the failure condition is the tensile cracking of concrete. However, these models fail to identify the inelastic deformation. This disadvantage becomes obvious when the material experiences unloading. This can be improved by introducing nonlinear elastic models.

Nonlinear elastic models are based on two approaches, the total and the incremental stress-strain formulation. With the total stress-strain model, the current state of stress is assumed to be uniquely expressed as the function of the current state of strain. This type of model is reversible and path independent, which is generally not true for concrete. Also, it suffers from inability to predict the inelastic deformation. For the incremental formulation, the state of stress is dependent on the current state of strain and on the stress path followed to reach such a state (this type of formulation is incrementally reversible and path dependent). This formulation gives a good representation for concrete behavior as compared with the total stress formulation.

Plasticity based models, have been used extensively in recent years for concrete modeling in compression. It is known that under triaxial compression, concrete can flow as a ductile material on the yield surface

before reaching the crushing strain. To account for this property, various plasticity models have been introduced. In these models, concrete may be defined as an elastic-perfect plastic material or as a strain hardening material. The prediction of the overall behavior by using the plasticity based models gives a good agreement with experimental results. So, this type of modeling is adopted in the present work.

3.7 Modeling of Concrete Fracture

Generally, concrete fracture may be either a compression fracture (i.e crushing of concrete) or a tension fracture (i.e cracking of concrete).

The crushing failure occurs when the material can resist no further compressive loading while the tension failure of concrete is characterized by a gradual growth of cracks that are joined together and eventually disconnect larger parts of the structure. It is a usual assumption that formation of cracks is a brittle process and that the strength in the tension-loading direction abruptly goes to zero after such cracks have formed, Fig. (3.7a). But when the reinforcement bars bridge the concrete cracks, the strength mechanism becomes more complex and the carrying strength of concrete between cracks can be safely exploited (Chen,(1982)).

3.7.1 Cracking Models

In general, the models, which have been developed to represent cracking in connection with the finite element analysis of reinforced concrete members, are composed of three basic components, a criterion for crack initiation, a method of crack representation and a method for cracking propagation.

Two fracture criteria are commonly used, the maximum principal stress criterion and the maximum principal strain criterion. When a principal stress or strain exceeds its limiting value a crack is assumed to occur in a plane normal to the direction of the offending principal stress or strain (Chen,(1982)), Fig.(3.7b).

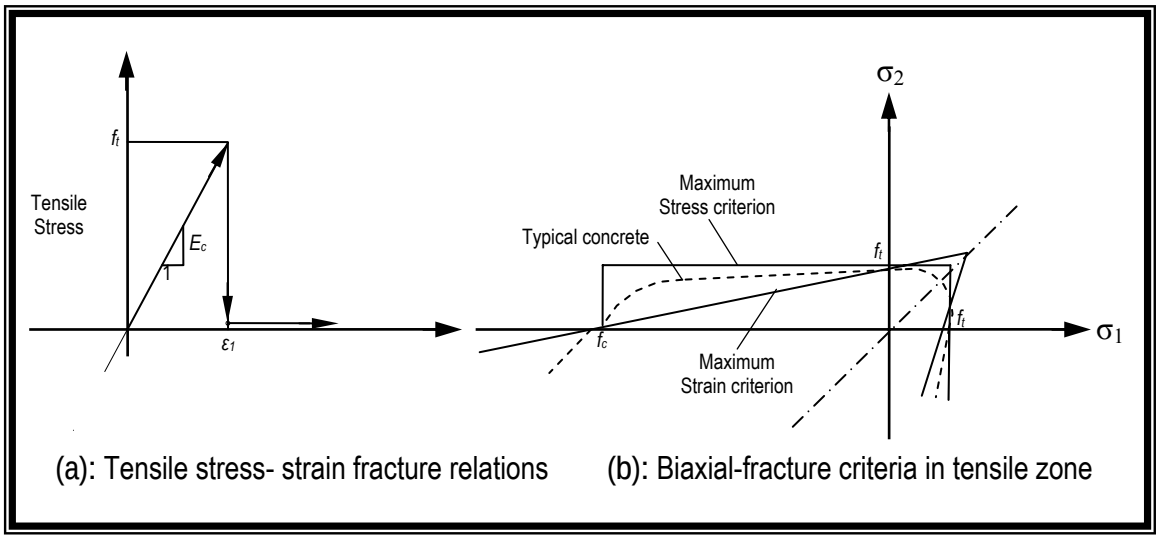

Figure (3.7): Cracking of Concrete (Chen,(1982))

In the finite element analysis of concrete structures, two approaches have been employed for crack modeling, these are the smeared cracking and the discrete cracking models (Hinton,(1988)). The particular cracking model to be selected depends upon the purpose of the analysis. If overall load-deflection behavior is desired, without regard to completely realistic crack patterns and local stresses, the smeared crack model is probably the best choice, while if detailed local behavior is of interest; adoption of the discrete cracking model is useful. The two approaches will be discussed in the following sections.

3.7.1.1 Smeared cracking model

In this approach, the cracked concrete is assumed to remain a continuum, i.e., the cracks are smeared out in a continuous fashion. It is assumed that

the concrete becomes orthotropic or transversely isotropic after the first cracking has occurred, one of the material axis being oriented along the direction of cracking. In the smeared cracking model, a crack is not discrete but implies an infinite number of parallel fissures across that part of the finite element, Fig. (3.8) [Bathe and Ramaswamy, (1979),Chen,(1982)]

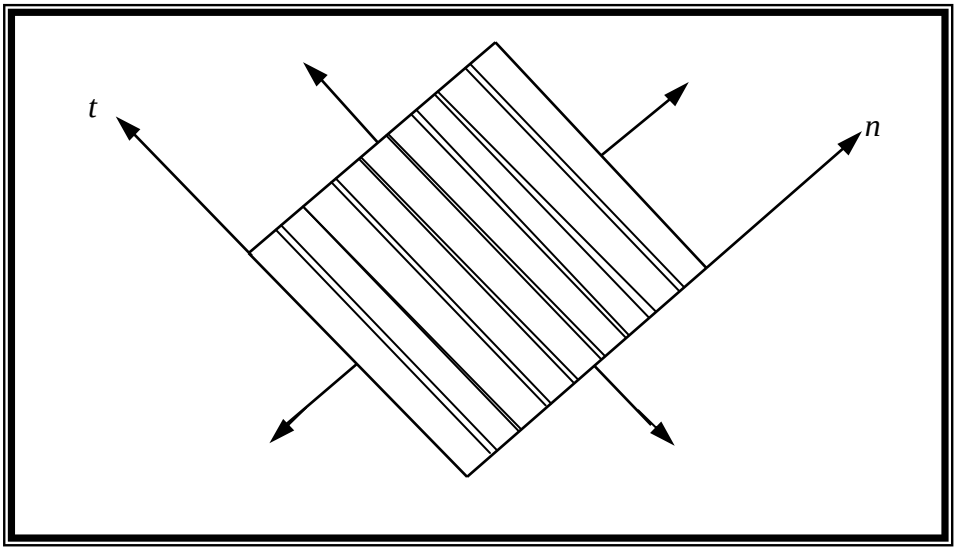

Figure (3-8): Smeared Cracke Model (Chen,(1982))

Two different models are used for defining the crack direction. The first is the fixed orthogonal crack. In this approach, the direction of the crack is fixed normal to the direction of the first principal tensile stress that exceeds the cracking stress. By fixing the direction of the cracks, the subsequent rotation of the principal stress is ignored. The second model is the rotating or swinging crack model. In this approach, the crack direction is assumed to be normal to the principal tensile strain direction when the tensile strains reach a specified limiting value. With further loading and changing of the principal strain direction, the crack is assumed to rotate and the orthotropic material axes are set in the new crack direction.

3.7.1.2 Discrete cracking model

An alternative to the continuous smeared cracking model is the introduction of discrete crack model. This is normally done by disconnecting the displacement at nodal points of adjoining elements by the cracks as shown in Fig. (3.9). One obvious difficulty in such an approach is that the location and orientation of the cracks are not known in advance. Thus, geometrical restriction imposed by the preselected finite element mesh can hardly be avoided. This can be rectified to some extent by redefinition of element nodes. Such techniques are unfortunately extremely complex and time consuming (Chen,(1982)).

In the present study, the smeared fixed–crack model has been adopted.

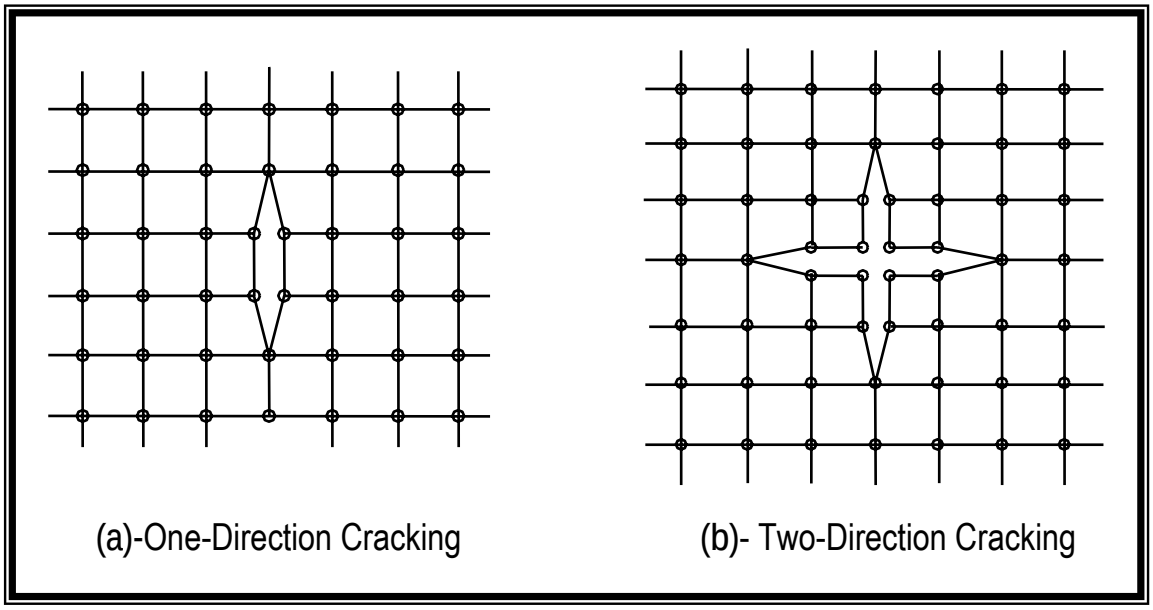

Figure (3.9): Discrete Crack Model (Chen,(1982))

3.7.2 Post-Cracking Models

In the plain and reinforced concrete structures, cracking is not a perfectly brittle phenomenon and experimental evidence shows that the tensile stresses normal to a cracking plane are gradually released as the crack width increases. This type of response is usually modeled in the finite element analysis by using either the tension stiffening or the strain softening concepts.

For reinforced concrete structures where the behavior is characterized by the formation of closely spaced cracks, the first concept seems to be more suitable than the latter. The latter is found to be useful for analyzing plain concrete structures where the behavior is governed by the formation of a single micro-crack or a few dominant cracks (Chen,(1982)).

In the case where reinforcement exists, the nature of the stress release is further complicated by the restraining effect of the reinforcing steel. After cracking, the concrete stresses drop to zero and the steel carries the full load. The concrete between cracks, however, still carries some tensile stresses. This tensile stress drops as the load increases and the drop is associated primarily with bond deterioration between steel and concrete. This ability of concrete to share the tensile load with the reinforcement is termed as ***tension stiffening*** phenomenon (Chen,(1982)).

The tension stiffening effect of concrete has been studied in finite element analysis by using two procedures. First, the tension portion of the concrete stress-strain curve has been given a descending branch. Descending branches of many different shapes have been employed, Linear, bilinear and curved shapes. The second is to increase the steel stiffness. The additional stress in the steel represents the total tensile force carried by both the steel and the concrete between the cracks (Chen,(1982)).

3.7.3 Shear Transfer across the Cracks

Several mechanisms exist by which shear is transferred across reinforced concrete sections. Among these mechanisms are the shear stiffness of uncracked portion of concrete, aggregate interlock in the crack surface (or interface shear transfer), dowel in the reinforcement bars action and the combined effect of tension in reinforcement and arching action.

For the shear transfer across the cracked concrete planes crossed by reinforcement, the two major mechanisms are the dowel action and the

aggregate interlock. Shear transfer by these two mechanisms is accompanied by slippage or relative movement of crack faces. In the dowel action, shear forces are partially resisted by the stiffness of reinforcing bars because slippage imposes bearing forces of opposite direction on the bars. The aggregate interlock mechanism is of frictional nature. Slippage causes the irregular faces of the crack to separate slightly. Tensile stresses created in the steel bars by the separation of crack faces in turn develop same shear resistance (AL-Shaarbaf,(1990)).

3.8 Concrete Model Adopted in the Analysis

In this study, a plasticity-based model is adopted for the nonlinear analysis of three-dimensional reinforced concrete structures under static loads. In compression, the behavior of concrete is simulated by an elastic-plastic work hardening model followed by a perfectly plastic response, which is terminated at the onset of crushing. The plasticity model in compression state of stress requires the following characteristics:

1. yield criterion
2. hardening rule
3. flow rule
4. crushing condition

In tension, linear elastic behavior prior to cracking is assumed. A smeared crack model with fixed orthogonal cracks is adopted to represent the cracked concrete. The model will be described in terms of the following:

1. cracking criterion
2. post-cracking formulation
3. shear retention model

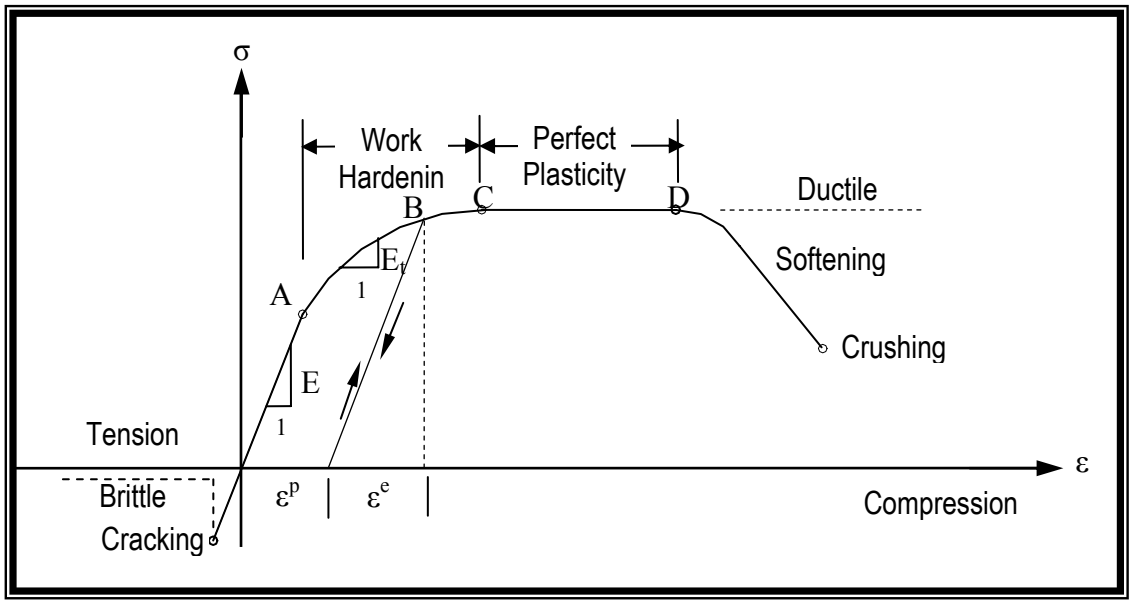

Figure (3.10): Uniaxial Stress-Strain Curve, Pre-and Post Failure Regime (Chen,(1982)).

3.8.1 Modeling of Concrete in Compression

3.8.1.1 The yield criterion

Under a triaxial state of stress, the yield criterion for concrete is generally assumed to be dependent on the three stress invariants. However, a yield criterion dependent on two stress invariants only has been proved to be adequate for most practical situations. The yield criterion incorporated in the present model is of such type and it has been successfully used in research. It can be expressed as (Cervera et al,(1987)):

$$f(\sigma) = f(I_1, J_2) = (\alpha I_1 + 3\beta J_2)^{1/2} = \sigma_o \qquad \ldots(3.22)$$

where (α) and (β) are material parameters, (I_1) is the first stress invariant given by:

$$I_1 = \sigma_x + \sigma_y + \sigma_z \quad \ldots(3.23)$$

J_2 is the second deviatoric stress invariant given by:

$$J_2 = \frac{1}{3}\{(\sigma_x^2 + \sigma_y^2 + \sigma_z^2) - (\sigma_x\sigma_y + \sigma_y\sigma_z + \sigma_z\sigma_x)\} + \tau_{xy}^2 + \tau_{yz}^2 + \tau_{xz}^2 \quad \ldots(3.24)$$

and $\sigma_o \geq 0$ is the equivalent effective stress at the onset of plastic deformation, this σ_o can be determined from the uniaxial compression test as:

$$\sigma_o = C_p \cdot f'_c \quad \ldots(3.25)$$

where $0 \leq Cp \leq 1.0$ is the plasticity coefficient, which is used to mark the initiation of the plastic deformation.

The parameters (α) and (β) are determined by using the uniaxial and biaxial compression tests. Then for a uniaxial compression state, the yield stress is given by:

$$\sigma_x = -\sigma_o \quad \ldots(3.26)$$

and for the equal biaxial compression state, the yield stress is given by:

$$\sigma_x = \sigma_y = -\gamma\sigma_o \quad \ldots(3.27)$$

If the results obtained by Kupfer et al for the failure envelope is employed for initial yield, the value of the constant (γ) is equal to (1.16). From Eq. (3.22)

through Eq. (3.27), the material constants can be found to be:

$\alpha = 0.35468\sigma_o$ and $\beta = 1.35468$ …*(3.28)*

writing $C = \dfrac{\alpha}{(2\sigma o)} = 0.17734$

Therefore Eq. (3.22) can be written as:

$$f(\sigma) = (2C\sigma_o I_1 + 3\beta J_2)^{1/2} = \sigma_o \quad \text{…(3.29)}$$

This can be solved for σ_o as:

$$f(\sigma) = C.I_1 + \{(C.I_1)^2 + 3\beta J_2\}^{1/2} = \sigma_o \quad \text{…(3.30)}$$

3.8.1.2 Hardening rule

The concept of plastic flow in work hardening materials extends to the notion of perfectly plastic solids for which the yield or failure surface remains fixed in stress space. The hardening rule defines the motion of the subsequent loading surfaces during plastic loading. A number of hardening rules has been proposed to describe the growth of subsequent loading surface for work-hardening materials. Some of these rules are; isotropic hardening, kinematic hardening and mixed hardening. The isotropic model applies mainly to proportional loading. For cyclic and reversed types of loading, kinematic hardening rule is more appropriate. Combinations of isotropic and kinematic hardening are called mixed hardening rules (Chen,(1982)).

An isotropic hardening rule is used in the present study. Therefore, from Eq. (3.30), the subsequent loading surface may be expressed as:

$$f(\sigma) = C.I_1 + \{(C - I_1)^2 + 3\beta J_2\}^{1/2} = \bar{\sigma} \qquad \ldots(3.31)$$

where $\bar{\sigma}$ represents the stress level at which further plastic deformation will occur and this is termed as the effective stress or equivalent uniaxial stress.

The incremental theory of plasticity implies a relationship between the effective stress and the effective plastic strain. The effective plastic strain increment $\delta\varepsilon_p$ that results from an incremental plastic work dw_p, may be determined by using the work-hardening hypothesis as:

$$d\varepsilon_p = \frac{dw_p}{\bar{\sigma}} = \frac{\{\sigma\} d\{\varepsilon_p\}}{\bar{\sigma}} \qquad \ldots(3.32)$$

where $d\varepsilon_p$ represents the effective accumulated plastic strain increment, along the strain path.

The effective plastic strain can be written as:

$$\varepsilon_p = \int d\varepsilon_p \qquad \ldots(3.33)$$

In the present model, a parabolic stress-strain curve is used for the equivalent uniaxial stress-strain relationship beyond the limit of elasticity, ($C_p f'_c$). This relationship represents the work-hardening stage of behavior. When the peak compressive stress is reached, a perfectly plastic response is assumed to occur. Figure (3.11) shows the equivalent uniaxial stress-strain curve in the various stages of behavior. These are given by:

(a) During the elastic stage, when $\bar{\sigma} \le C_p . f'_c$

$$\bar{\sigma} = E . \varepsilon_c \qquad \ldots(3.34)$$

(b) After the initial yielding and up to the ultimate concrete compressive strength, when:- $C_p . f'_c \le \bar{\sigma} \le f'_c$

$$\bar{\sigma} = C_p f'c + E[\varepsilon_c - \frac{C_p . f'c}{E}] - [\frac{E}{2\varepsilon'_o}][\varepsilon_c - \frac{C_p f'c}{E}]^2 \qquad \ldots(3.35)$$

c) for $\varepsilon_c \ge (2 - C_p) f'c / E$

$$\bar{\sigma} = f'c \qquad \ldots(3.36)$$

where ε'_o represents the total strain corresponding to the parabolic part of the curve that can be calculated from:

$$\bar{\varepsilon}_o = \frac{2(1 - C_p)}{E} f'_c \qquad \ldots(3.37)$$

A value of ***0.3*** is assumed for the plasticity coefficient ***(Cp)*** in the present study and hence plastic yielding begins at a stress level equal to ***(0.3 f′c).***

The total effective strain ε_c is composed of two parts, elastic and plastic components:

$$\varepsilon_c = \varepsilon_e + \varepsilon_p \qquad \ldots(3.38)$$

The elastic strain $\boldsymbol{\varepsilon_p}$ is given by:

$$\varepsilon_e = \frac{\bar{\sigma}}{E} \qquad \ldots(3.39)$$

By substituting Eq. (3.38) and Eq. (3.39) into Eq. (3.35), the effective stress-plastic strain relation can be expressed as:

$$\bar{\sigma} = C_p f'_c - E \varepsilon_p + (2E^2 . \varepsilon'_o \varepsilon_p)^{1/2} \qquad \ldots(3.40)$$

Differentiation of Eq. (3.40) with respect to the plastic strain leads to the slope of the tangent of the effective stress-plastic strain curve, which represents the hardening coefficient, H, that is needed in the formulation of the incremental stress-strain relation:

$$\bar{H} = \frac{d\bar{\sigma}}{d\varepsilon_p} = E\left(\sqrt{\frac{\varepsilon_0}{2\varepsilon_p}} - 1\right) \qquad \ldots(3.41)$$

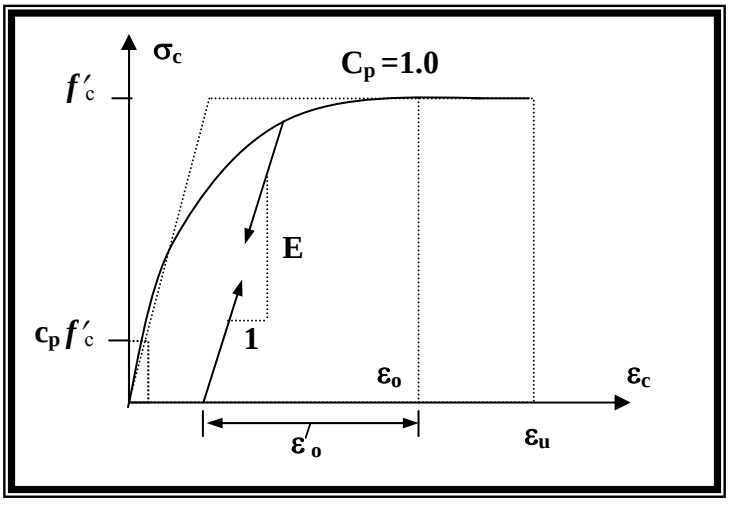

Figure (3.11): Uniaxial Stress-Strain Curve for Concrete

3.8.1.3 Flow rule

In plasticity theory, a flow rule must be defined so that the plastic strain increment can be determined for a given stress increment. The associated flow rule has been widely used for concrete models mainly because of its simplicity. This approach is adopted in the current model. The plastic strain increment is expressed as [Cervera et al,(1987)):

$$\mathrm{d}(\varepsilon_{\mathrm{p}}) = \mathrm{d}\lambda \ \frac{\partial \mathrm{f}(\sigma)}{\partial \sigma} \qquad \ldots(3.42)$$

The normal to the current loading surface $\frac{\partial f(\sigma)}{\partial \sigma}$ is termed as the flow vector, The yield function derivatives with respect to the stress components define the flow vector **{a}** as:

$$\{\mathrm{a}\} = \left[\frac{\partial \mathrm{f}}{\partial \sigma_{\mathrm{x}}}, \frac{\partial \mathrm{f}}{\partial \sigma_{\mathrm{y}}}, \frac{\partial \mathrm{f}}{\partial \sigma_{\mathrm{z}}}, \frac{\partial \mathrm{f}}{\partial \tau_{\mathrm{xy}}}, \frac{\partial \mathrm{f}}{\partial \tau_{\mathrm{yz}}}, \frac{\partial \mathrm{f}}{\partial \tau_{\mathrm{zx}}} \right]^{\mathrm{T}} \qquad \ldots(3.43)$$

These derivatives are given in Appendix (B):

3.8.1.4 The incremental stress-strain relationship

During the plastic loading, both of the initial yield and the subsequent stress states must satisfy the yield condition. $\boldsymbol{F(\sigma, K) = 0}$. The yield function defined in Eq. (3.35) can be rewritten as,

$$\mathrm{F}(\sigma, \mathrm{K}) = \mathrm{f}(\sigma) + \mathrm{f}(\mathrm{k}) = 0 \qquad \ldots(3.44)$$

where k is the hardening parameter, which governs the expansion of the yield-surface. By differentiating Eq. (3.44), then

$$dF = \frac{\partial F}{\partial \sigma} d\sigma + \frac{\partial F}{\partial K} dK = 0 \qquad \ldots(3.45)$$

or

$$a^T d\sigma - A\, d\lambda = 0 \qquad \ldots(3.46)$$

where

$$A = -\frac{1}{d\lambda}\frac{\partial F}{\partial K} dK \qquad \ldots(3.47)$$

The total incremental strain vector can be rewritten as:

$$d\{\varepsilon)\} = d\{\varepsilon_e\} + d\,\lambda \frac{\partial F}{\partial \sigma} \qquad \ldots(3.48)$$

The elastic strain increment is related to the stress increment by the elastic constitutive relation which is given in:

$$d\{\sigma\} = [D] d\{\varepsilon_e\} \qquad \ldots(3.49)$$

where [D] is the elastic constitutive matrix given by

$$[D] = \frac{E}{(1+\nu)(1-2\nu)} \begin{bmatrix} 1-\nu & \nu & \nu & 0 & 0 & 0 \\ \nu & 1-\nu & \nu & 0 & 0 & 0 \\ \nu & \nu & 1-\nu & 0 & 0 & 0 \\ 0 & 0 & 0 & (1-2\nu)/2 & 0 & 0 \\ 0 & 0 & 0 & 0 & (1-2\nu)/2 & 0 \\ 0 & 0 & 0 & 0 & 0 & (1-2\nu)/2 \end{bmatrix} \qquad \ldots(3.50)$$

Substitution of Eq. (3.49) into Eq. (3.48) yields

$$d\varepsilon = [D]^{-1} d\sigma + d\lambda\{a\} \qquad \ldots(3.51)$$

Pre-multiplying both sides of Eq. (3.51) by $\{a\}^T [D]$ and eliminating $a^T . d\sigma$ by making use of Eq. (3.46), the following expression for the plastic multiplier $d\lambda$ is obtained,

$$d\lambda = \left[\frac{\{a\}^T [D]}{H' + \{a\}^T [D]\{a\}} \right] d\{\varepsilon\} \qquad \ldots(3.52)$$

By substituting Eq. (3.52), into Eq. (3.48), and pre-multiplying both sides by [D], the complete elastic incremental stress-strain relationship can be expressed as:

$$d\{\sigma\} = \left[[D] - \frac{[D]\{a\}\{a\}^T [D]}{H' + \{a\}^T [D]\{a\}} \right] d\{\varepsilon\} \qquad \ldots(3.53)$$

where the second term in the brackets represents the stiffness degradation due to the plastic deformation.

3.8.1.5 Crushing condition

Crushing indicates the complete rupture and disintegration of the material under compressive stress state. After crushing, the current stresses drop rapidly to zero and the concrete is assumed to lose its resistance completely against further deformation. In the adopted model, concrete is considered to crush when the strain reaches a specified ultimate value. Hence, rewriting the yield condition from Eq. (3.30) in terms of the peak strain, the following crushing criterion is obtained:

$$C\ \bar{I}_1 + \sqrt{\left(C\bar{I}_1\right)^2 + \beta\bar{J}_2} = \varepsilon_{cu} \qquad \ldots(3.54)$$

where $\bar{I}_1$: is the first strain invariant

$\bar{J}_2$: is the second deviatoric strain

ε_{cu}:is the ultimate concrete strain that can be extrapolated from the compression test.

3.8.2 Modeling of Concrete in Tension

3.8.2.1 Cracking criterion

The maximum tensile stress criterion is used in this research to monitor cracking. For a previously uncracked sampling point, if the principal stress exceeds the limiting value of tensile stress f_t, a crack is assumed to form. The limiting tensile stress required to define the onset of cracking can be calculated for states of triaxial tensile stress and for combination of tension and compression principal stresses as follows (Bathe and Ramaswamy,(1979)):

a) For triaxial tension zone ($\sigma_1 \geq \sigma_2 \geq \sigma_3 \geq 0$)

$\sigma_i = \sigma_{cr} = f_t$ i = 1,2,3

b) For the tension-tension-compression zone ($\sigma_1>0$, $\sigma_3 \le \sigma_2 \le 0$)

$$\sigma_i = \sigma_{cr} = f_t\left[1+\frac{0.75\,\sigma_3}{f'_c}\right] \qquad i=1,2 \qquad \ldots(3.56)$$

c) For the tension-compression-compression zone $(\sigma_1 \rangle 0, \sigma_3 \le \sigma_2 \le 0)$

$$\sigma_1 = \sigma_{cr} = f_t\left[1+\frac{0.75\,\sigma_2}{f'_c}\right]\left[1+\frac{0.75\,\sigma_3}{f'_c}\right] \qquad \ldots(3.57)$$

where $\boldsymbol{\sigma_{cr}}$ is the cracking stress and both $\boldsymbol{ft}$ and $\boldsymbol{f'_c}$ are given positive values, Eq. (3.56) incorporates the fact that compression in one direction favors the cracking in the others and thus reduces the tensile capacity of the material.

When the major principal stress $\boldsymbol{\sigma_1}$ violates the cracking criterion, planes of failure develop perpendicular to its direction. Concrete behavior is no longer isotropic; it becomes orthotropic with the direction of orthotropy coinciding with the direction of $\boldsymbol{\sigma_1}$. Therefore, the normal and shear stresses across the plane of failure and the corresponding normal and shear stiffness are reduced, and the concrete is assumed to be transversely isotropic with axes of isotropy being perpendicular to the direction of $\boldsymbol{\sigma_1}$. Thus, the incremental stress-strain relationship in the local axes can be expressed as:

$$\begin{Bmatrix} \Delta\sigma_1 \\ \Delta\sigma_2 \\ \Delta\sigma_3 \\ \Delta\tau_{12} \\ \Delta\tau_{23} \\ \Delta\tau_{31} \end{Bmatrix} = \begin{bmatrix} E_1 & 0 & 0 & 0 & 0 & 0 \\ 0 & E/\left(1-\nu^2\right) & \nu E/\left(1-\nu^2\right) & 0 & 0 & 0 \\ 0 & \nu E/\left(1-\nu^2\right) & E/\left(1-\nu^2\right) & 0 & 0 & 0 \\ 0 & 0 & 0 & \beta_1 G & 0 & 0 \\ 0 & 0 & 0 & 0 & G & 0 \\ 0 & 0 & 0 & 0 & 0 & \beta_1 G \end{bmatrix} \begin{Bmatrix} \Delta\varepsilon_1 \\ \Delta\varepsilon_2 \\ \Delta\varepsilon_3 \\ \Delta\gamma_{12} \\ \Delta\gamma_{23} \\ \Delta\gamma_{31} \end{Bmatrix} \quad \ldots(3.58)$$

or in a condensed form:

$$\{\Delta\sigma\} = [D_{cr}]\{\Delta\varepsilon\} \quad \ldots(3.59)$$

where $\boldsymbol{E_1}$ is the reduced modulus of elasticity in the direction of $\boldsymbol{\sigma_1}$, $\boldsymbol{\beta_1 G}$ is the reduced shear modulus across the failure plane.

$[\boldsymbol{D_{cr}}]$ is the material stiffness in the local axes. The stress increments in the global axes ($\boldsymbol{x}$, $\boldsymbol{y}$, $\boldsymbol{z}$) may be obtained by using the coordinate transformation matrix such that:

$$\{\Delta\sigma\} = [T]^T [D_{cr}][T]\{\Delta\varepsilon\} \quad \ldots(3.60)$$

where ***[T]*** is the transformation matrix expressed in terms of the direction cosines as:

$$[T] = \begin{bmatrix} l_1^2 & m_1^2 & n_1^2 & l_1 m_1 & m_1 n_1 & n_1 l_1 \\ l_2^2 & m_2^2 & n_2^2 & l_2 m_2 & m_1 n_1 & n_1 l_1 \\ l_3^2 & m_3^2 & n_3^2 & l_3 m_3 & m_1 n_1 & n_1 l_1 \\ 2l_1 l_2 & 2m_1 m_2 & 2n_1 n_2 & l_1 m_2 + l_2 m_1 & n_2 m_1 + n_1 m_2 & l_2 n_1 + l_1 n_2 \\ 2l_2 l_3 & 2m_2 m_3 & 2n_2 n_3 & l_2 m_3 + l_3 m_2 & n_3 m_2 + n_2 m_3 & l_3 n_2 + l_2 n_3 \\ 2l_3 l_1 & 2m_3 m_1 & 2n_3 n_1 & l_3 m_1 + l_1 m_3 & n_1 m_3 + n_3 m_1 & l_1 n_3 + l_3 n_1 \end{bmatrix} \quad \ldots(3.61)$$

where l_i, m_i and n_i represent the direction cosines of the local coordinate axes (x, y, z) direction respectively.

For the tension–tension–compression and the triaxial tension states of stress, the cracking criterion may be violated by the major principal stress σ_1, and the second principal stress σ_2, simultaneously. Thus, two sets of orthogonal cracked planes may be developed and the constitutive matrix in the local material axes become diagonal:

$$[D]_{cr} = \begin{bmatrix} E_1 & 0 & 0 & 0 & 0 & 0 \\ 0 & E_2 & 0 & 0 & 0 & 0 \\ 0 & 0 & E_3 & 0 & 0 & 0 \\ 0 & 0 & 0 & \beta_1 G & 0 & 0 \\ 0 & 0 & 0 & 0 & \beta_2 G & 0 \\ 0 & 0 & 0 & 0 & 0 & \beta_1 G \end{bmatrix} \quad \ldots(3.62)$$

In the current model, a maximum of three sets of cracking is allowed to form at each sampling point.

3.8.2.2 Post-cracking models

3.8.2.2.1 Tension- Stiffening Model

The tensile stresses normal to the cracked planes are gradually released, and represented by an average stress-strain curve. In the present study, such a relationship may be obtained by using the tension-stiffening model. This is specified by a linear descending stress-strain curve similar to that shown in Fig. (3.12) and this is given by (Bathe and Ramaswamy,(1979)) :

a) for $\varepsilon_{cr} \leq \varepsilon_n \leq \alpha_1 \varepsilon_{cr}$

$$\sigma_n = \alpha_2 \sigma_{cr} \left[\frac{\alpha_1 - \frac{\varepsilon_n}{\varepsilon_{cr}}}{\alpha_1 - 1.0} \right] \quad \ldots(3.63)$$

b) for

$$\varepsilon_n \rangle \alpha_1 \varepsilon_{cr} \qquad \ldots(3.64)$$

$$\sigma_n = 0.0$$

where σ_n and ε_n are the stress and strain normal to the cracked plane, ε_{cr} is the cracking strain associated with the cracking stress σ_{cr}, α_1, and α_2 are the tension-stiffening parameters. α_1 represents the rate of stress release as the crack widens, while α_2 represents the sudden loss of stress at instant of cracking.

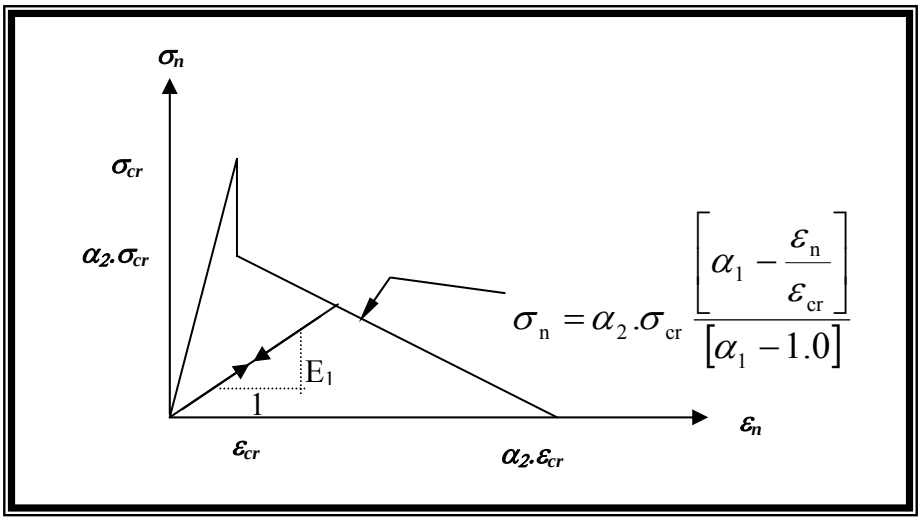

Figure (3.12): Post-Cracking Model for Concrete

3.8.2.2.2 Shear Retention Model

At a cracked sampling point, the shear stiffness across the cracked plane becomes progressively smaller as the crack widens. A reduced shear

modulus βG, has been used across the cracked plane. The value of β depends on the stage of loading and it is given by:

a) For $\varepsilon_n \leq \varepsilon_{cr}$

$$\beta = 1 \qquad \ldots(3.65)$$

b) For $\varepsilon_{cr} \leq \varepsilon_n \leq \gamma_1 \varepsilon_{cr}$

$$\beta = \frac{\gamma_2 - \gamma_3}{\gamma_1 - 1}\left[\gamma_1 - \frac{\varepsilon_n}{\varepsilon_{cr}}\right] + \gamma_3 \qquad \ldots(3.66)$$

c) For $\varepsilon_n \rangle \gamma_1 \varepsilon_{cr}$

$$\beta = \gamma_3 \qquad \ldots(3.67)$$

Figure (3.13) shows schematically the value of (β) for different stages. γ_1, γ_2, *and* γ_3 are shear retention parameters. γ_1 represents the rate of decay of shear stiffness as the crack widens, γ_2 is the sudden loss in shear stiffness at the instant of cracking, while γ_3 is the residual shear stiffness due to the dowel action.

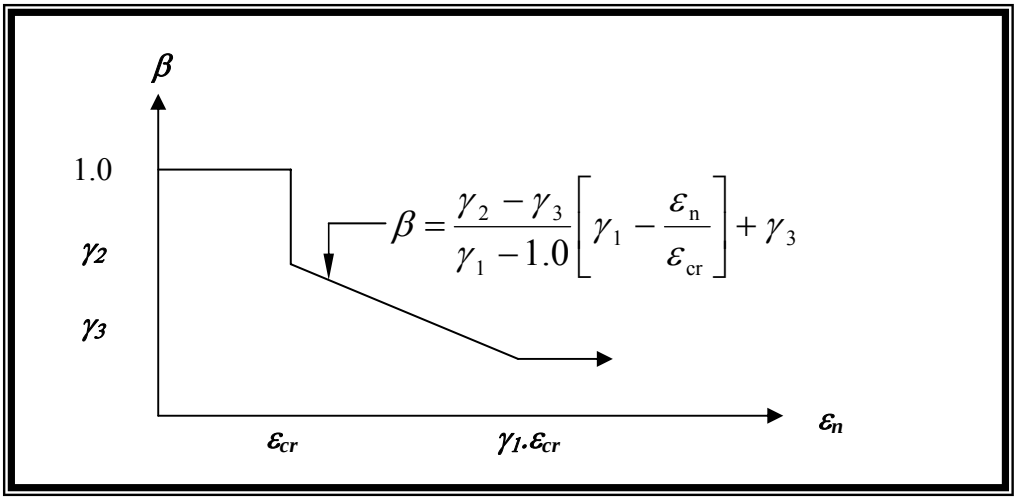

Figure (3.13): Shear Retention for Concrete

3.8.2.3 Modeling of the Compressive Strength Reduction due to Orthogonal Cracks:

In a reinforced concrete member, a significant degradation in the compressive strength can result due to presence of transverse tensile strain after cracking In plasticity based model, the effect of these tensile strains on the yield criterion and the evolution of the subsequent loading surface can be simulated by scaling the equivalent uniaxial stress-strain relationships given by Eqs. (3.34) and (3.36) according to the current value of the compressive strength reduction factor (Cervenka,(1985).

The model used here is due to Cervenka and this depends on the reduction factor $(\lambda)$to reduce both the peak stress and the corresponding strain, Fig. (3.14). From Eqs. (3.34 and 3.36), the modified stress-strain relationship may be written as (Cervenka,(1985):

a) for $\bar{\sigma} \leq Cp \,.\, f_c'$

$$\bar{\sigma} = \lambda E\, \varepsilon_c \qquad \ldots(3.68)$$

b) for $\lambda \;\; Cp \;\; f_c' \leq \bar{\sigma} \leq \lambda \; f_c'$

$$\bar{\sigma} = \lambda\, Cp\, f_c' + E\left[\varepsilon_c - \frac{\lambda\, Cp\; f_c'}{E}\right] - \frac{E}{2\,\varepsilon_0}\left[\varepsilon_c - \frac{\lambda\;\; Cp\; f_c'}{E}\right] \qquad \ldots(3.69)$$

c) for $\varepsilon_c \geq (2 - Cp)\lambda\, f_c' / E$

$$\bar{\sigma} \leq \lambda\; f_c' \qquad \ldots(3.70)$$

where

$$\varepsilon'_o = 2(1-Cp)\lambda . f_c' / E \qquad \ldots(3.71)$$

The effective stress-plastic strain relation can be modified as:

$$\bar{\sigma} = \lambda\, c_p\, f_c' E.\varepsilon_p + \left(2E^2\, \lambda.\varepsilon'_o \quad \varepsilon_p\right)^{1/2} \qquad \ldots(3.72)$$

and the hardening parameter can be expressed as:

$$\bar{H} = \frac{d\bar{\sigma}}{d\varepsilon_p} = E\left\{\left[\frac{\lambda\,\varepsilon_o}{2\,\varepsilon_p}\right]^{1/2} - 1.0\right\} \qquad \ldots(3.73)$$

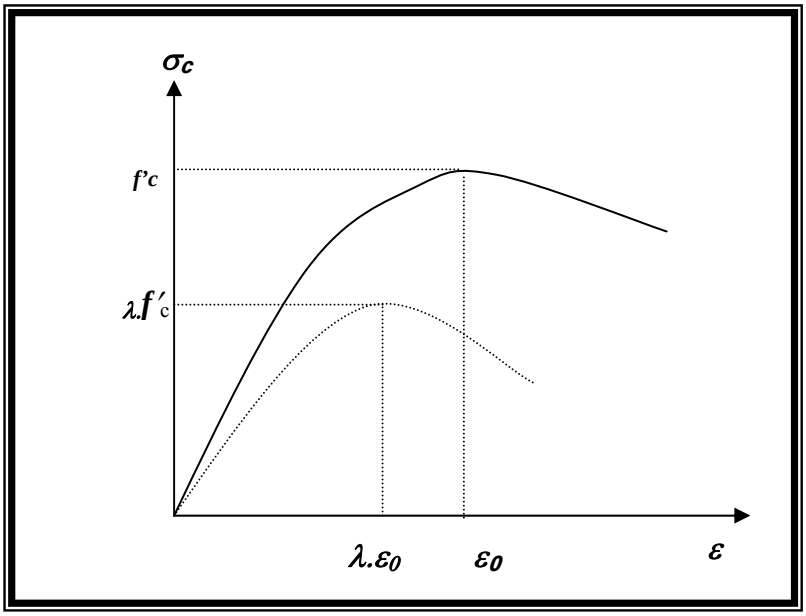

Figure (3.14):Uniaxial Compressive Stress-Strain Relationship for Cracked Concrete

For a singly cracked sampling point, the compression reduction factor is given by:

$$\lambda = 1.0 - K_1 \frac{\varepsilon_1}{0.005} \leq 1.0 - K_1 \qquad \ldots(3.74)$$

where ε_1 is the transverse tensile strain in principal direction (1), the strain is normal to the cracked plane. Also for doubly cracked sampling point, the reduction factor may be taken as:

$$\lambda = 1.0 - K_1 \frac{\left(\varepsilon_1^2 + \varepsilon_2^2\right)}{0.005} \leq 1.0 - K_1 \qquad \ldots(3.75)$$

where ε_2 is the tensile strain normal to the second crack.

3.9 Modeling of Reinforcement

Compared to concrete, steel is a much simpler material to represent. Its stress-strain behavior can be assumed to be identical in tension and compression. In reinforced concrete members, reinforcing bars are normally long and relatively slender and therefore they can be assumed to be capable of transmitting axial forces only. In the current study, the uniaxial stress-strain behavior of reinforcement is simulated by an elastic-linear work hardening model, as shown in Fig. (3.15).

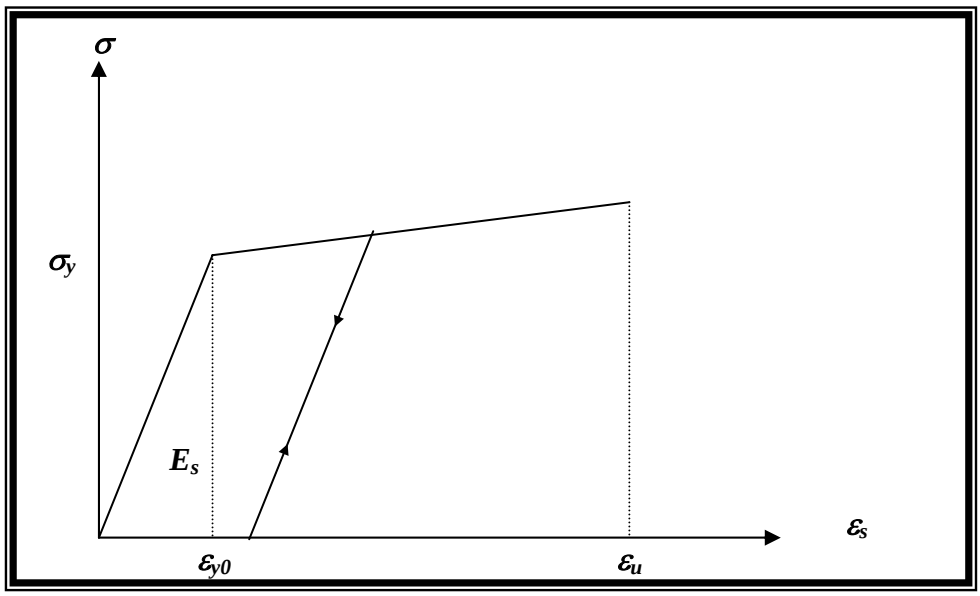

Figure (3.15): Stress-Strain Relationship of Steel Bars Used in the Analysis

Chapter Four

SOLUTION ALGORITHM FOR THE NONLINEAR PROBLEM AND COMPUTER PROGRAM

4.1 Introduction

This chapter presents a description of the different numerical techniques used in solving nonlinear simultaneous equations. The nonlinear behavior of any reinforced concrete structure may be generally attributed to either material or geometric nonlinearity or a combination of both types. In reinforced concrete members, the geometric nonlinearity is usually neglected as a result of early onset of the material nonlinearity, with large deflections occurring only close to structural collapse. So, only material nonlinearity is considered in the present study.

4.2 Solution Techniques for Nonlinear Problems

The techniques used in solving nonlinear problems are:

1. Linear incremental technique.
2. Iterative technique.
3. Incremental – iterative technique.

4.2.1 Linear – Incremental Technique

In this method, Fig. (4.1), the nonlinear behavior is determined by solving a sequence of linear problems. The load is applied as a sequence of sufficiently small increments, so that during each load increment, the

structure is assumed to respond linearly. The basic disadvantage of this method is that a real estimate of the solution accuracy is not possible, since equilibrium is not satisfied at any given load level. So, for stability requirements, it is necessary to use small load increments, which in turns will increase the computation cost if compared with the other techniques.

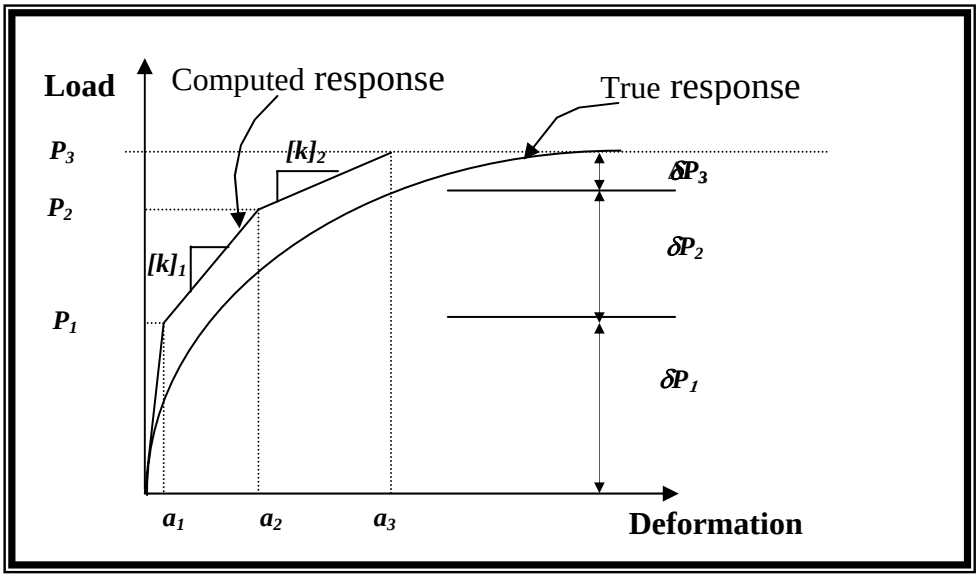

Figure (4.1): Linear Incremental Method

4.2.2 Iterative Technique

The iterative procedure is a sequence of calculations in which the structure is fully loaded in one step to get an initial approximate solution. Then, this solution is improved step by step by using an iteration process until equilibrium is satisfied within a prescribed tolerance.

After each iteration, the portion of the total loading that is not balanced is calculated and used in the iterative process as an additional load to compute an approximate additional increment of the total displacements. This process is repeated until equilibrium is approximated to some acceptable degree. These techniques fail to reach the required convergence for structures with high nonlinearity. There are several types of iteration procedures, some of them are:

1.Conventional Newton – Raphson method.

2.Modified Newton – Raphson method.

3.Combined (conventional and modified) Newton – Raphson method.

4.2.2.1 Conventional Newton – Raphson Method

The conventional Newton – Raphson method, Fig. (4.2), is one of the earliest known methods used in solving nonlinear problems. For simplicity, a single degree of freedom system is considered with a load level $\{P\}_0$, with the assumption that the corresponding deformed configuration of the system which may be denoted symbolically by $\{a\}_0$ is known. Then, to determine a new configuration, $\{a\}_1$, corresponding to a load level $\{p\}_1$ where:

$$\{P\}_1 = \{P\}_0 + \{\delta P\}_1 \qquad \ldots(4.1)$$

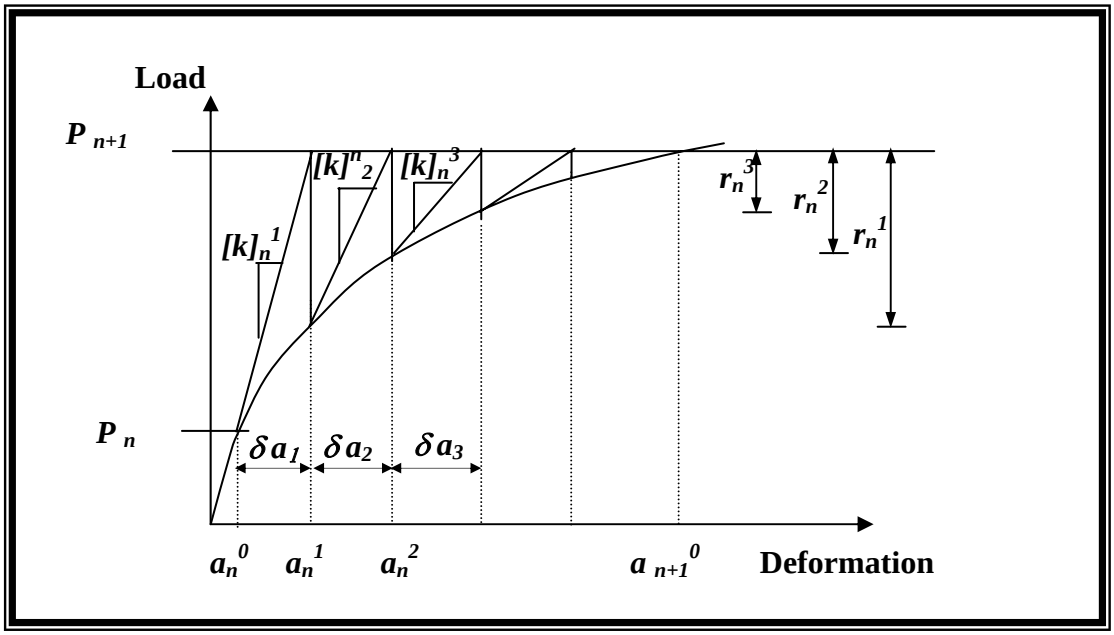

Figure (4.2): Conventional Newton – Raphson Method [35]

and where $\{\delta P\}_1$ is the additional applied load is obtained by using a linearized analysis, where the change in configuration $\{\delta a\}_1$ is first computed from:

$$\{\delta P\}_1 = [k]_0 \{\delta a\}_1 \qquad \ldots(4.2)$$

in which the tangent stiffness matrix $[\boldsymbol{k}]_0$ is evaluated at the beginning of the load interval, i.e. the load level $\{\boldsymbol{P}\}_0$. The term $\{\boldsymbol{a}\}_1 = \{\boldsymbol{a}\}_0 + \{\delta \boldsymbol{a}\}_1$ represents an approximate configuration which is then corrected by updating a new tangent stiffness matrix from the approximate configuration $\{\boldsymbol{a}\}_1$. The internal forces $\{f\}_1$ corresponding to this configuration can be determined as:

$$\{f\}_1 = [k]_1 \{a\}_1 \qquad \ldots(4.3)$$

Generally for any level of iteration (j):

$$\{a\}_j = \{a\}_{j-1} + \sum_{m=1}^{n} \{\delta a\}_m \qquad \ldots(4.4)$$

where:

$\{\boldsymbol{a}\}_j$ is the vector of displacement after the iteration. Then, the out of balance force vector $\{\boldsymbol{r}\}_j$ can be obtained from:

$$\{r\}_j = \{P\}_f - \{f\}_j \qquad \ldots(4.5)$$

The unbalanced joint forces are then treated as load increments and the correction vector $\{\delta \boldsymbol{a}\}_{j+1}$ is then obtained from the incremental relationship:

$$[k]_j \{\delta a\}_{j+1} = \{r\}_j \qquad \boldsymbol{\ldots(4.6)}$$

The conventional Newton – Raphson method requires that the tangent stiffness matrix is to be updated and a new system of equations is solved for each iteration. This is expensive if the problem to be solved is too large. Accordingly various modifications have been proposed (Oran and Kassimali,(1976)).

4.2.2.2 Modified Newton – Raphson Method

In this method, Fig. (4.3), the stiffness matrix is updated only once for each increment of loading. As compared with the conventional Newton – Raphson method, the modified Newton – Raphson method is more economical. However, this method requires more steps for convergence, but each step is done quickly by avoiding time consuming repetitions of forming the tangent stiffness matrix.

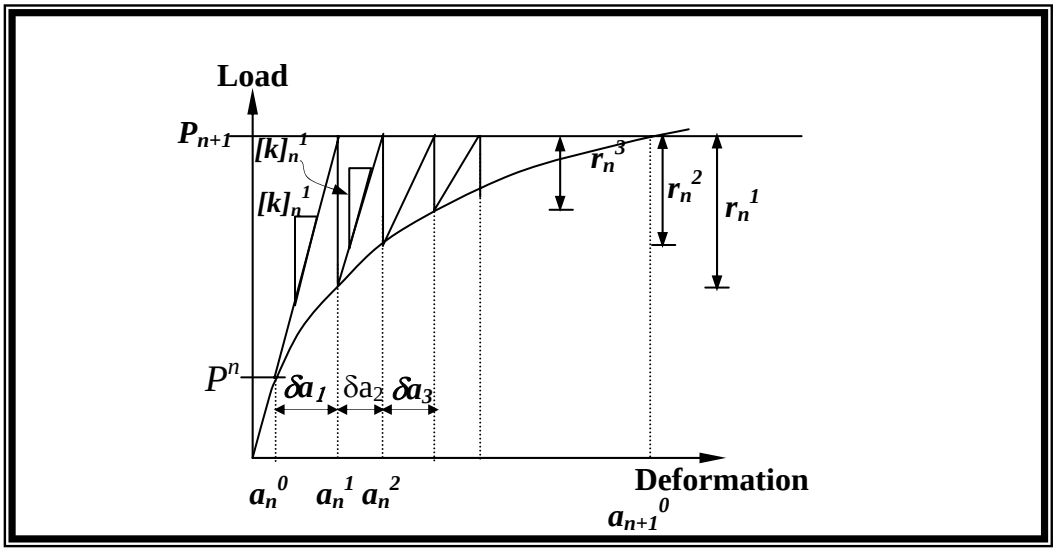

Figure (4.3): Modified Newton – Raphson Method

4.2.2.3 Combined Newton - Raphson Method

This method, Fig. (4.4), is a modification of the conventional Newton – Raphson method. It involves updating the stiffness matrix after remaining constant for a certain number of iterations. The stiffness matrix can be recalculated at:

The beginning of first iteration of each increment.

Beginning of second iteration.

First, eleventh, twenty first, … stiffness matrices over each load increment.

Second, twelfth, twenty second, … stiffness matrices over each load increment.

The disadvantage of this method is represented in the fact that the convergence is slower than the conventional Newton – Raphson method and requires a great number of iterations to achieve the solution within each load increment.

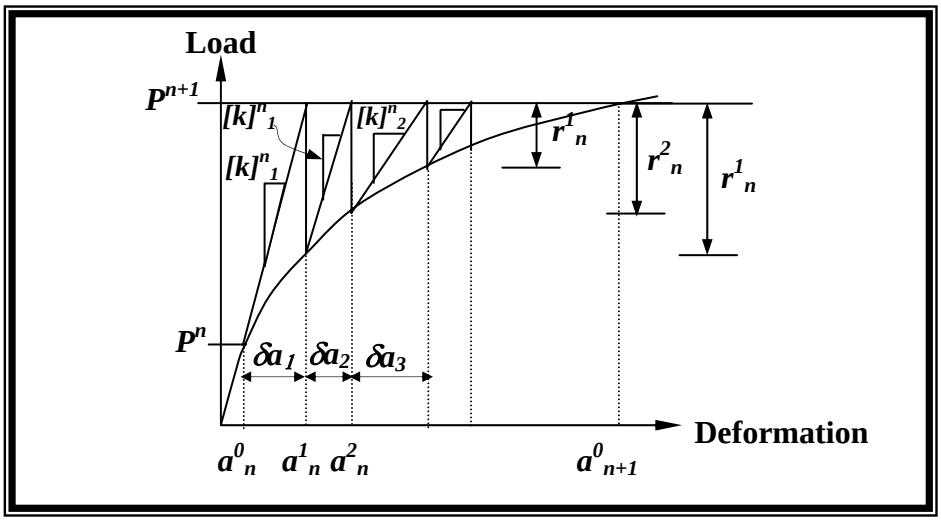

Figure (4.4) :Combined Newton – Raphson Method

4.2.3 Incremental – Iterative Techniques

In this type of technique, the load is applied as a series of increments, and at each increment, iterative solution is carried out to find the truest response of the structure. The conventional, modified and combined Newton – Raphson methods may also be used in the iteration process, Fig.(4.5).

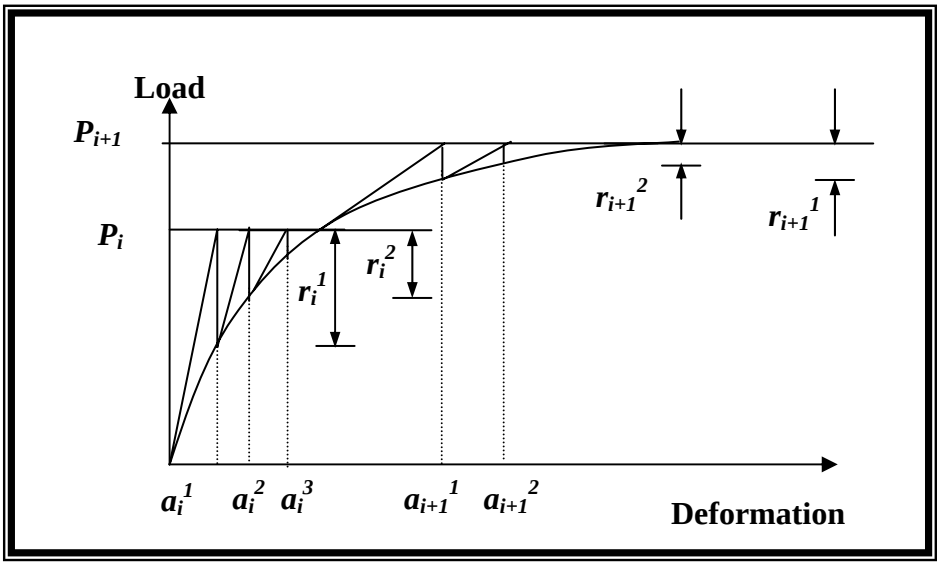

Figure (4.5): Incremental - Iterative Technique

4.3 Convergence Criterion

A termination criterion for the iterative process should be used to stop the iteration when a sufficient accuracy is achieved, i.e, when no further iterations are necessary. The different useful criteria are the displacement, the force and the work done criteria. Only the force criterion is adopted in the present study. This criterion depends on comparing the internal force vector $\{f\}$ and the applied load vector $\{P\}$. In other words, a vector called "unbalanced force vector" is used to be small within a prescribed tolerance. The convergence is assumed to occur when the inequality:

$$\left[\frac{\sum_{i=1}^{n}(\{P\}_i - \{f\}_i)^2}{\sum(\{P\}i)^2}\right]^{0.5} \leq tol. \qquad \ldots(4.7)$$

is satisfied.

4.4 Analysis Termination Criterion

The nonlinear finite element analysis must be provided with a criterion to detect failure of the solution. In the physical test under load control, the collapse of a structure takes place when no further loading can be sustained. This is usually indicated in the numerical tests by successively increasing iterative displacements and continuous growth in the dissipated energy. Hence, convergence of the iterative procedure can not be achieved and therefore, it is necessary to specify a suitable criterion to terminate the analysis and save computation efforts.

In the present study, the nonlinear analysis is terminated when the stiffness matrix is no longer positive definite, a steel bar has fractured, or excessive concrete crushing at sampling points has taken place.

4.5 Outline of Computer Program

The computer program ***P3DNFEA*** (three – dimensional nonlinear finite element analysis) has been used in the present study. This program was developed by Al – Shaarbaf (Al – Shaarbaf 1990). The program is coded in ***FORTRAN 77*** language. This program is used to analysis reinforced concrete deep beams with openings and subjected to static load up to failure.

In the present study, the ***Fortran PowerStation 4.0*** compiler produced by Microsoft incorporation was used to operate the program under Pentium III with Intel MMX 633 MHz processor and 128 MB RAM.

Chapter Five

APPLICATION AND DISCUSSION

5.1 General

In this chapter, some numerical examples are worked out and the result obtained by the finite element analysis are compared with those obtained from experimental and other numerical solutions. The numerical examples have been analyzed with the computer program (**P3DNFEA**).

The examples are used first to check the validity of the material models used. And to demonstrate the applicability and capability of the analysis method adopted in this study to a variety of three-dimensional reinforced concrete structures.

It is important to mention that the theoretical study is approximate in nature due to different factors mainly:

1- Approximations in the material modeling of concrete and steel.
2- Approximation inherent in the finite element modeling technique.
3- Approximation in the integration functions used in the numerical analysis.
4- Approximation introduced due to the type of procedure used in solving the nonlinear system of equations.

5.2 Simply Support Reinforced Concrete Deep Beams

Simply support reinforced concrete deep beams are analyzed using the computer program (**P3DNFEA**). Details of three deep beams tested experimentally by Ramakrishan and Anathanarayana (1968) are shown in Fig. (5.1). The first beam (A_4) was subjected to two point loads located at the third portion of the beam, while the second (K_2) was loaded with a uniform load and the thrid beam (K'_1) was analyzed under one concentrated load applied at mid-span. Input and output data of beam A_4 are listed in Appendix C.

Due to symmetry of loading and geometry, only one half of the beam is analyzed using sixteen 20-node brick elements for the first beam and twelve 20-node brick elements for the second and third as shown in Fig. (5.2). The steel reinforcement is represented by embedded bar along span length. Material properties of concrete and steel are given inTable (5.1).

Fig. (5.3) to Fig. (5.5) show the load-deflection response at mid-span of the beams. The computed response of load-deflection refers to good agreement with experimental result for most loading levels with difference in ultimate load about (3%), (2%) and (5%) for beams (A_4), (K_2), and (K'_1), respectively.

The beams (A_4 and K_2) were analyzed by Cervera et al. (1987) using the three-dimentional finite element method. Fig. (5.6) and Fig. (5.7) show a comparison of the calculated load-deflection with this study. Table (5.2) shows the comparison of shear strengths of deep beams obtained by previous study Cervera et al.(1987) and ACI-code .

The formula given in section 11.8 of the ACI code for the nominal shear strength of reinforced concrete deep beams with web reinforcement is:

$V_u = \emptyset (V_c + V_s)$ ....(5.1)

in which the shear strength V_c is computed by:

$$V_c = \left\{3.5 - 2.5\left(\frac{Mu}{V_u.d}\right)\right\}\left\{0.16\sqrt{f'} + 17\rho_w\left(\frac{V_u.d}{M_u}\right)\right\}b_w.d \quad ....(5.2)$$

and this should not be greater than the upper bound $0.49\ \sqrt{f'}\ b_w\ d$. Furthermore the shear strength V_u for the deep beam should not be greater than $0.66\ \sqrt{f'}\ b_w\ d$ when Ln/d < 2. When Ln/d is between 2 and 5, then $0.055\ (10 + Ln/d)\ \sqrt{f'}\ b_w\ d$ is to be used. The shear strength V_s is computed by:

$$V_s = \left[\frac{A_v}{s}\left(\frac{(1+\frac{L_n}{d})}{12}\right) + \frac{A_{vh}}{s_2}\left(\frac{(11-\frac{L_n}{d})}{12}\right)\right] f_y d \quad ....(5.3)$$

where

V_u = shear strength of the deep beam (N)

V_c and V_s = shear strengths provided by concrete and shear reinforcements (N)

$\emptyset$ = reduction factor (equal to 0.85)

V_u and M_u = factored shear force and moment at the critical section

d = effective depth of the section (mm)

b_w = width of the section (mm)

Ln = clear span of concrete (mm)

f'_c = compressive strength of concrete (N/mm^2)

ρ_w = ratio of flexural tensile reinforcement

A_v, A_{vh} = area of shear reinforcement perpendicular and parallel to flexural tension reinforcement within a distance s_1 and s_2, respectively

f_y = yield strength of shear reinforcement (N/mm^2)

The cracking pattren of the beam for different load levels are shown in Fig.(5.7). The first crack initiates at bottom surface of the middle zone of the beam at load (21.4%), (22.9%), and (22.1%) of ultimate load for the beam A_4, K_2, and K'_1, respectively. The cracks develop in all three directions of the beam, throughout the increase in the loading levels.

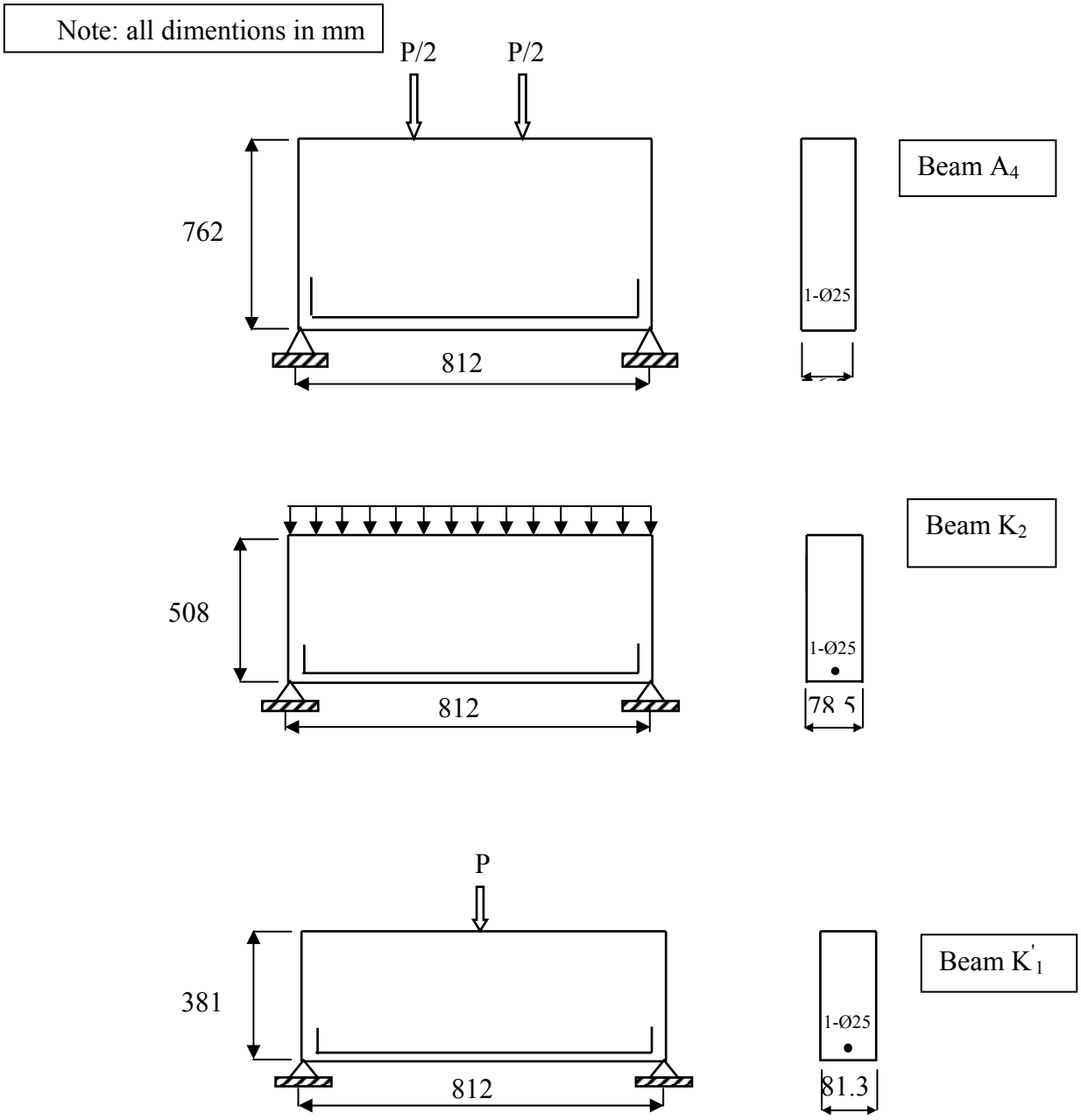

Figure(5.1): Simply Supported Reinforced Concrete Deep Beams /Geometry, Loading arrangement, and Reinforcement Details

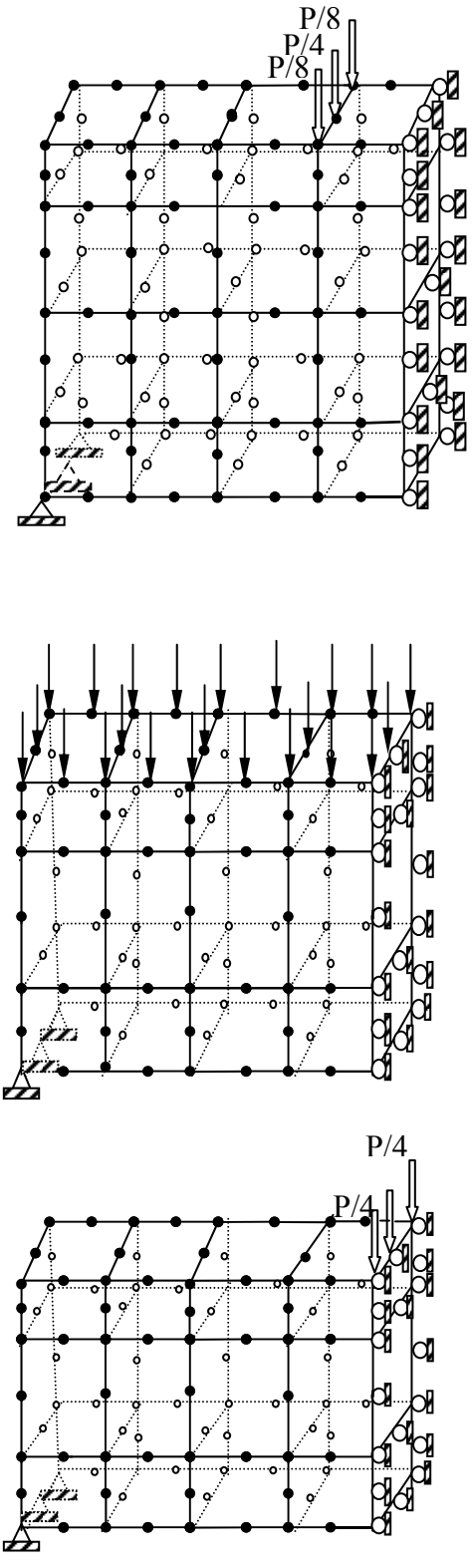

Figure (5.2): Finite Element idealization of Half of the Simply Supported Deep Beams

Table (5.1): Material Properties and Additional Parameters of Deep Beams

	Material properties and material parameters	Symbol	A_4	K_2	K'_1
Concrete	Young's modulus	$E_c(N/mm^2)$	23460	17836	18503
	Compressive strength	$f'_c(N/mm^2)$	27.12	14.2	15.5
	Tensile strength	$f_t(N/mm^2)$	2.5	1.6	1.6
	Poisson's ratio	ν	0.2	0.2	0.2
Reinforcement	Young's modulus	$E_s(N/mm^2)$	200000	200000	200000
	Yield stress	$f_y(N/mm^2)$	317	317	317
	Hardening parameter	H	0.0	0.0	0.0
Tension stiffening parameterS	Rate of stress release	α_1	20.0	20.0	20.0
	Sudden loss of tension stiffness at the instant of cracking	α_2	0.5	0.5	0.5
Shear retention parameters	Rate of decay of shear stiffness	γ_1	10.0	10.0	10.0
	Sudden loss of shear stiffness at the instant of cracking	γ_2	0.5	0.5	0.5
	Residual shear stiffness due to the dowel action	γ_3	0.1	0.1	0.1

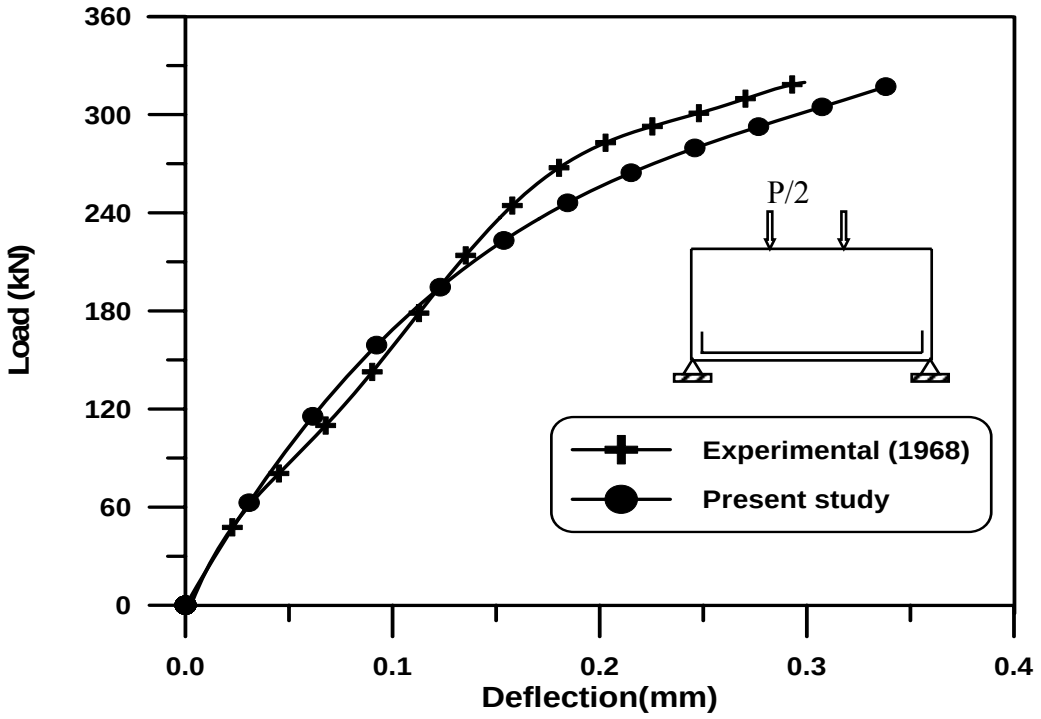

Figure(5.3): Load-Deflection Curve at Mid-span for (A_4) Deep Beam

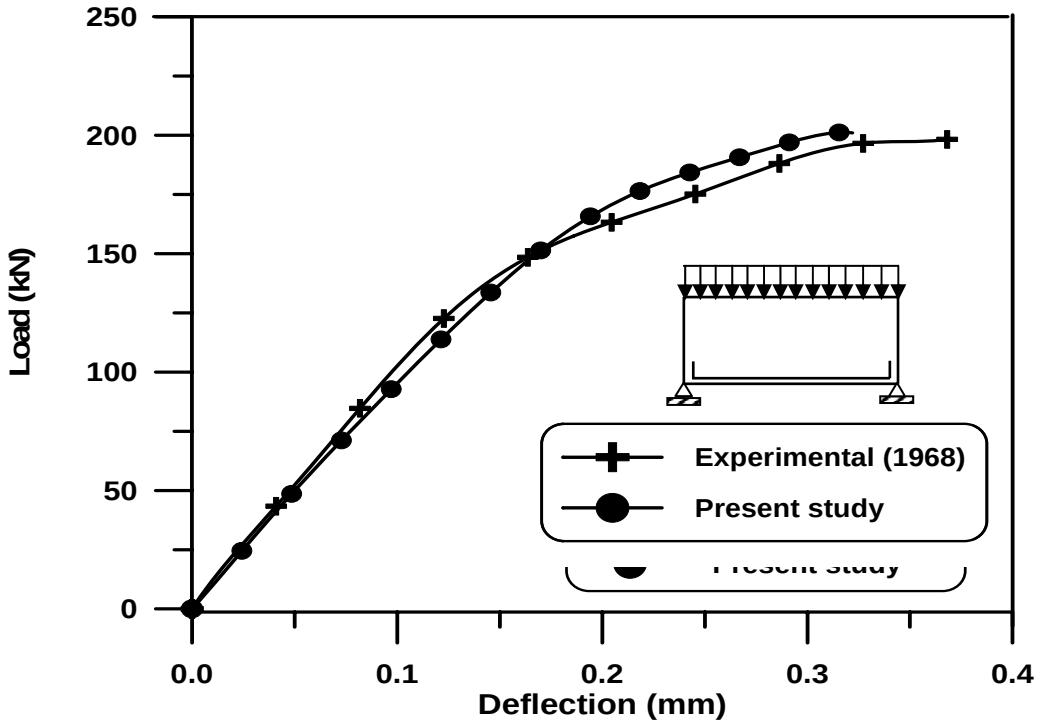

Figure(5.4): Load-Deflection Curve at Mid-Span for (K_2) Deep Beam

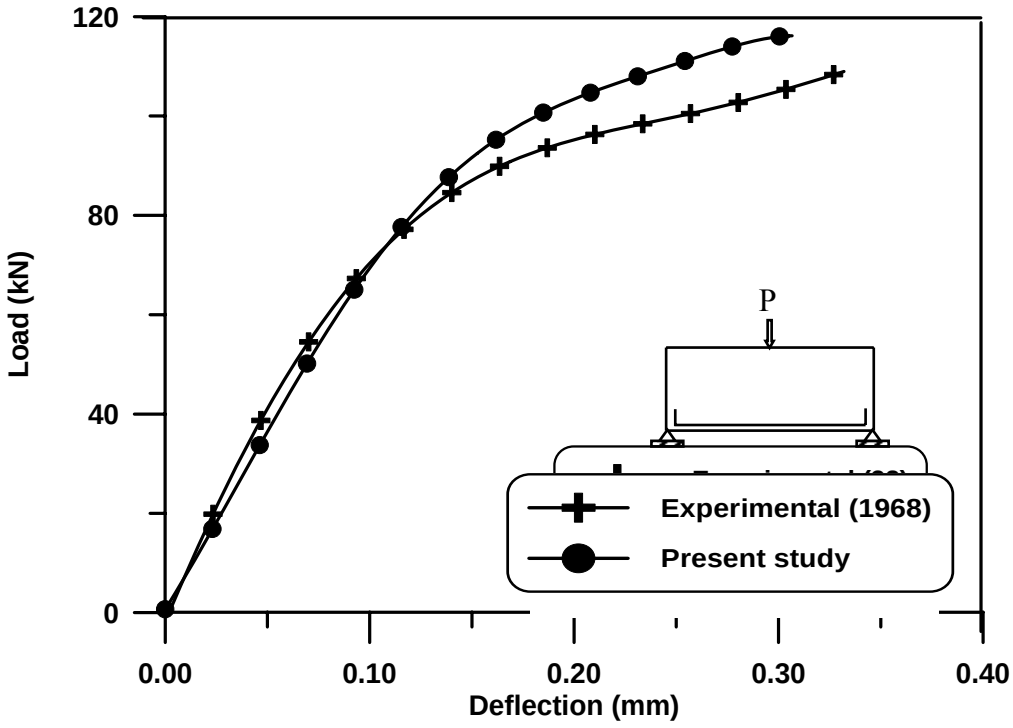

Figure(5.5): Load-Deflection Curve at Mid-Span for (K'_1) Deep Beam

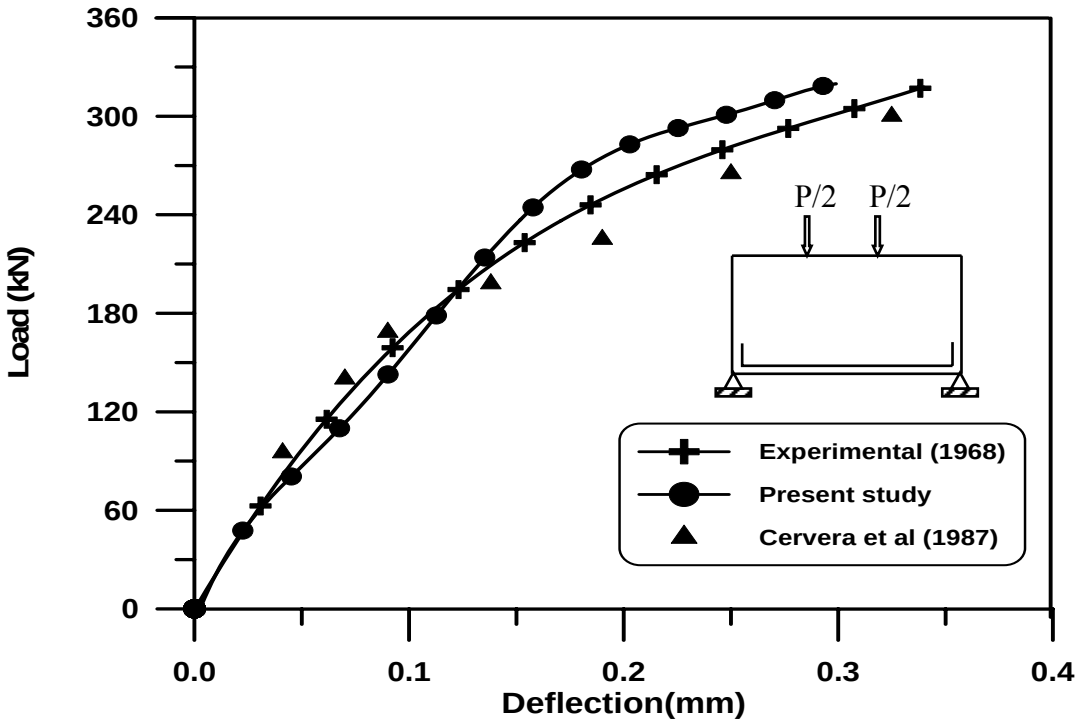

Figure(5.6): Load-Deflection Curve at Mid-Span for (A_4) Deep Beam (Comparison with previous studies)

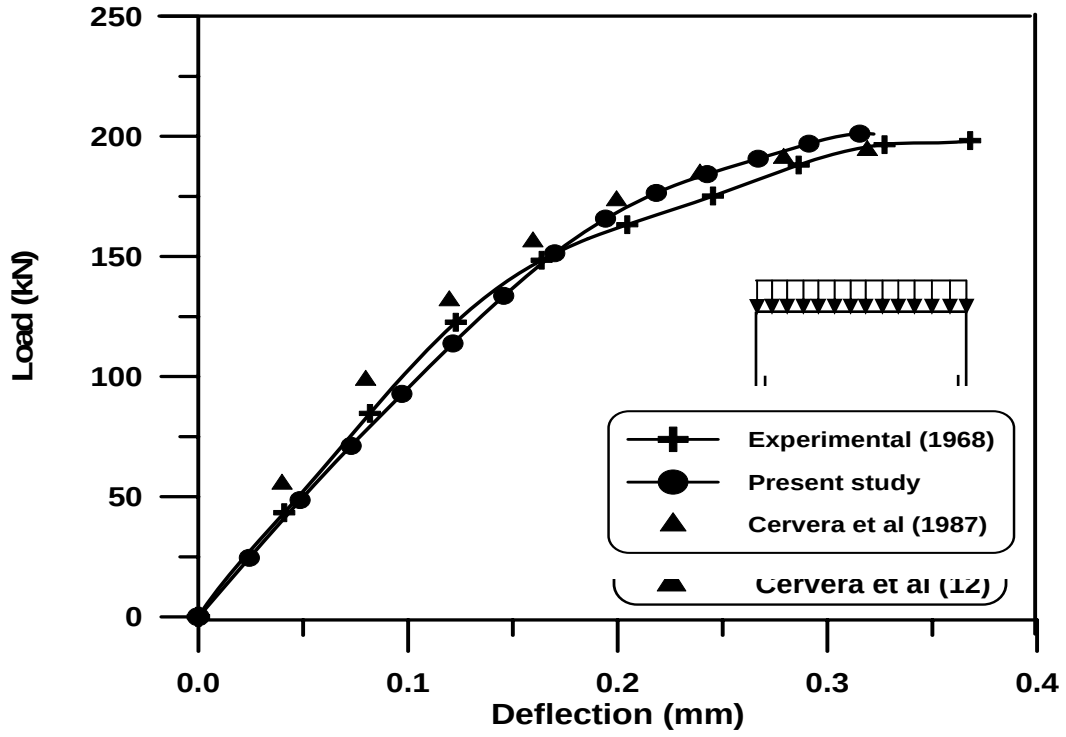

Figure(5.7): Load-Deflection Curve at Mid-Span for (K_2) Deep Beam (Comparison with previous studies)

Table (5.2): Comparison of Shear Strengths for Deep Beams

Shear Strength	**A4**	**K_2**	**K'_1**	**$V_{Exp.}/V_{Predicted}$ average**
$V_{Exp.}$	160	99	55	-
$V_{F.E.}$	164	101	58	0.97
$P_{previous\ study}$	159	98	-	1.01
$V_{ACI\text{-}code}$	147	72	50	1.2

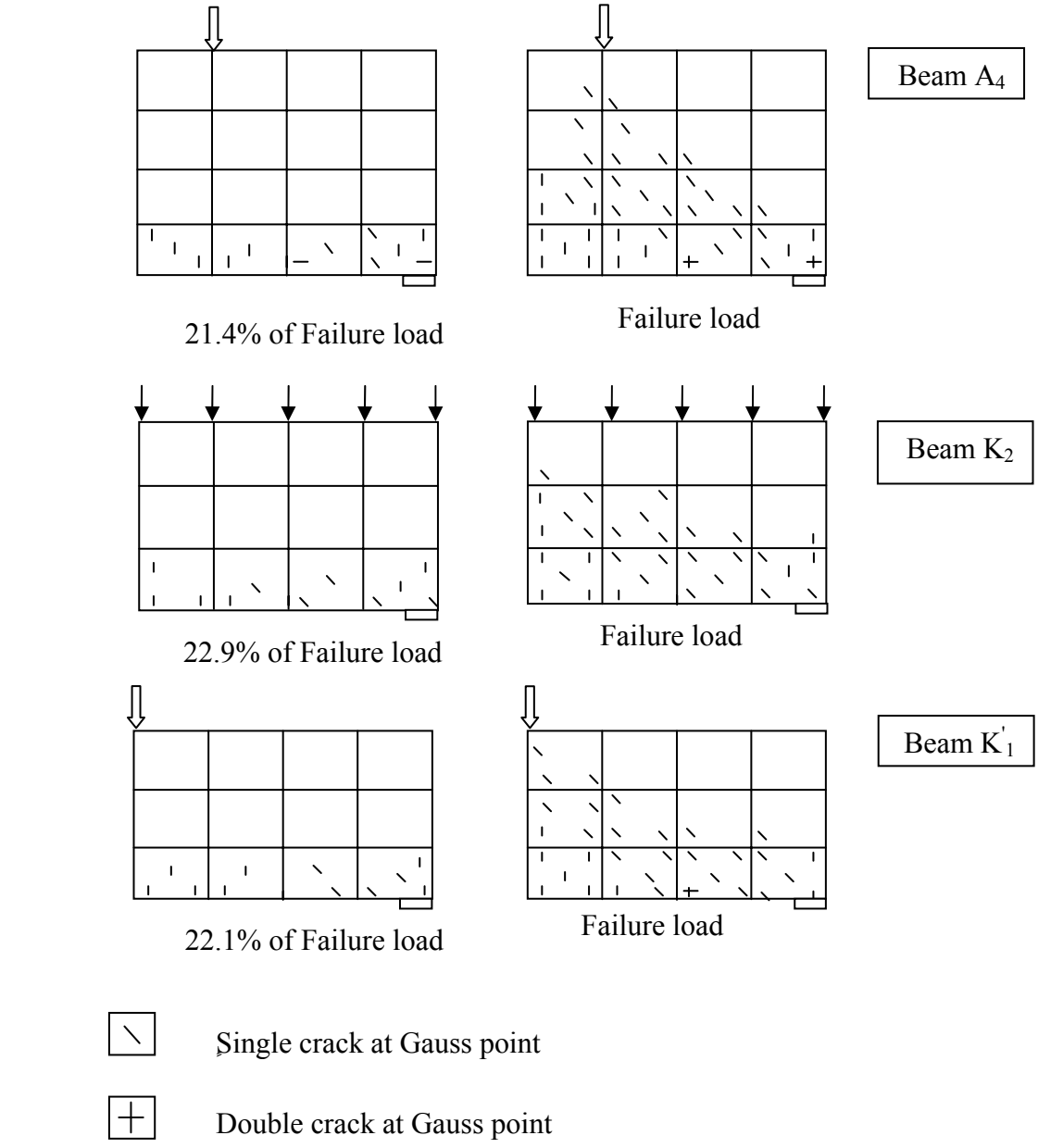

Figure(5.8): Cracking Patterns of Simply Supported Deep Beams

5.3 Continuous Reinforced Concrete Deep Beam

A deep beam with three supports has been chosen for the numerical analysis in the present example. This beam was tested experimentally by Leonhardt and Walther (1987) and was analyzed later by Mahmoud (1992), utilizing the two-dimentional finite element method. The dimensions of the beam as well as details of the reinforcement are given in Fig. (5.9). Due to symmetry of loading and geometry, only one span of the beam is analyzed using thirty 20-node brick elements, as shown in Fig. (5.10).

Material properties of concrete and steel are given in Table (5.3). The deflection was measured in the middle of each span. The computed response shows reasonable agreement with experimental result, as shown in Fig. (5.11), with difference about (3%) in ultimate load and (11%) in deflection. Fig. (5.12) shows a comparison of the load-deflection response with that of Mahmoud (1992).

The crack patterns of the beams at failure load are shown in Fig. (5.11). The first cracking initiates at load about (20%) of the ultimate load, in a region of mid-span at bottom surface. The cracks developed in all direction of the beam, through increasing the load. Crushing at Gauss point was initiated at load (96%) of ultimate load. This crushed point began at the top surface, when the Gauss point was considered to be crushed. Zero stress and stiffness were assigned to them.

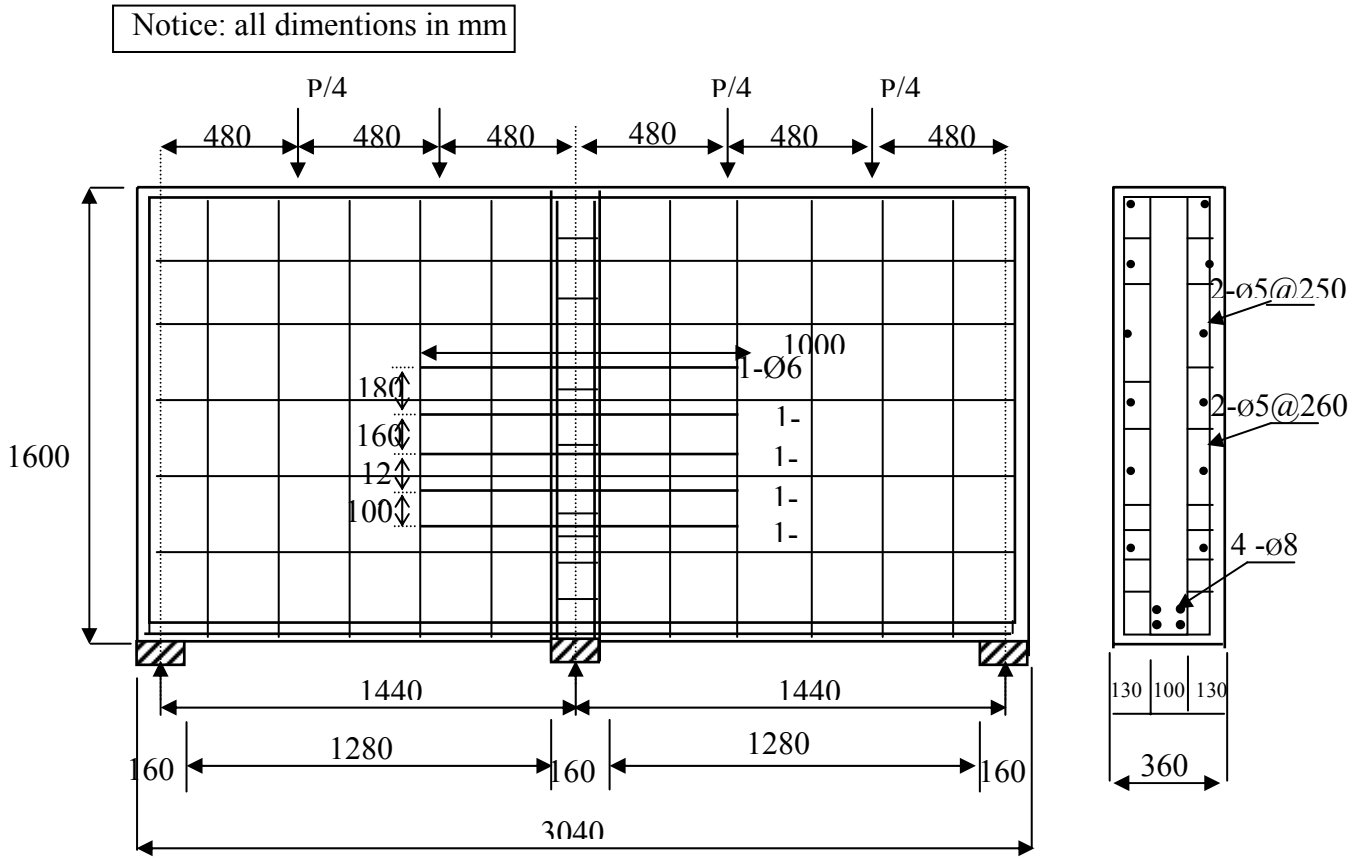

Figure(5.9): Continuous Deep Beam /Geometry and Reinforcement Detailes

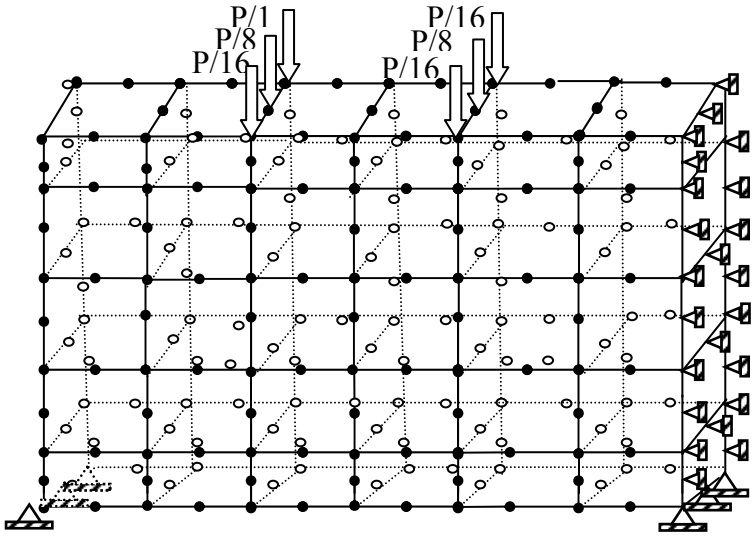

Figure(5.10): Finite Element Idelization of One Span of Continuous Deep Beam

Table (5.3): Material Properties and Additional Parameters of Continuous Deep Beam

	Material properties and material parameters	Symbol	value
Concrete	Young's modulus	Ec(N/mm^2)	32000
	Compressive strength	$f'c$(N/mm^2)	30.2
	Tensile strength	ft(N/mm^2)	3.0
	Poisson's ratio	ν	0.2
Steel	Young's modulus	Es(N/mm^2)	210000
	Yield stress	f_y(N/mm^2)	430
	Hardening parameter	H	0.0
Tension stiffening parameters	Rate of stress release	α_1	20.0
	Sudden loss of tension stiffness at the instant of cracking	α_2	0.5
Shear retention parameters	Rate of decay of shear stiffness	γ_1	10.0
	Sudden loss of shear stiffness at the instant of cracking	γ_2	0.5
	Residual shear stiffness due to the dowel action	γ_3	0.1

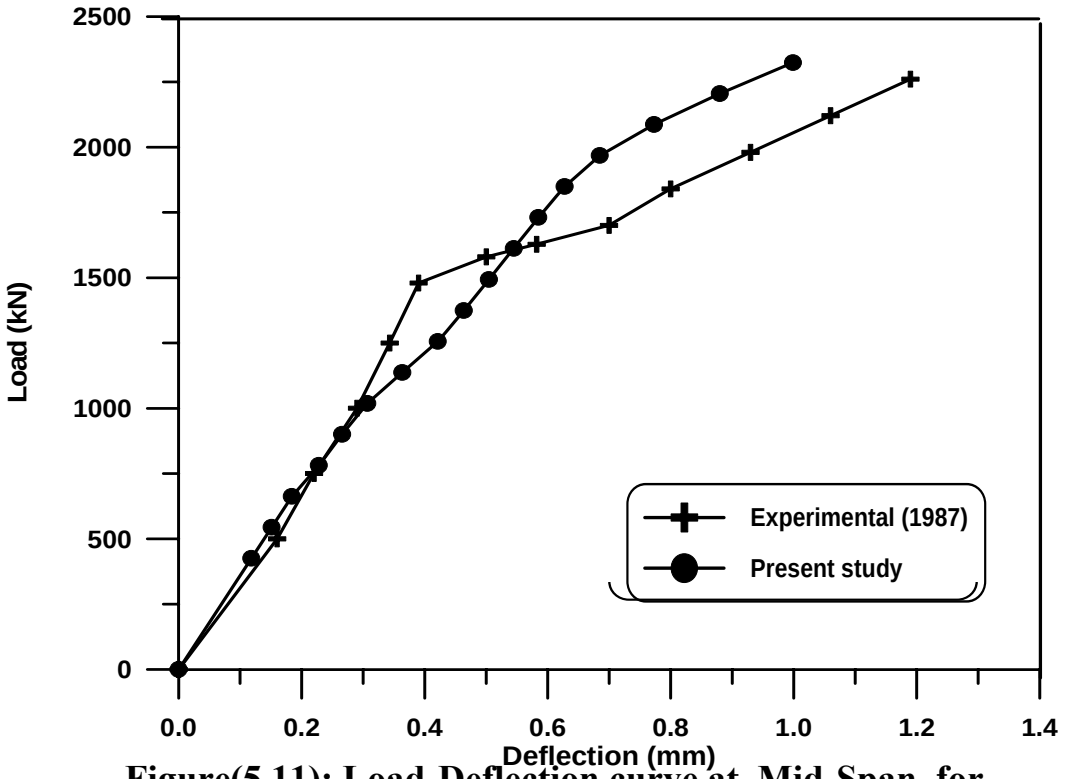

Figure(5.11): Load-Deflection curve at Mid-Span for Continuous Deep Beam

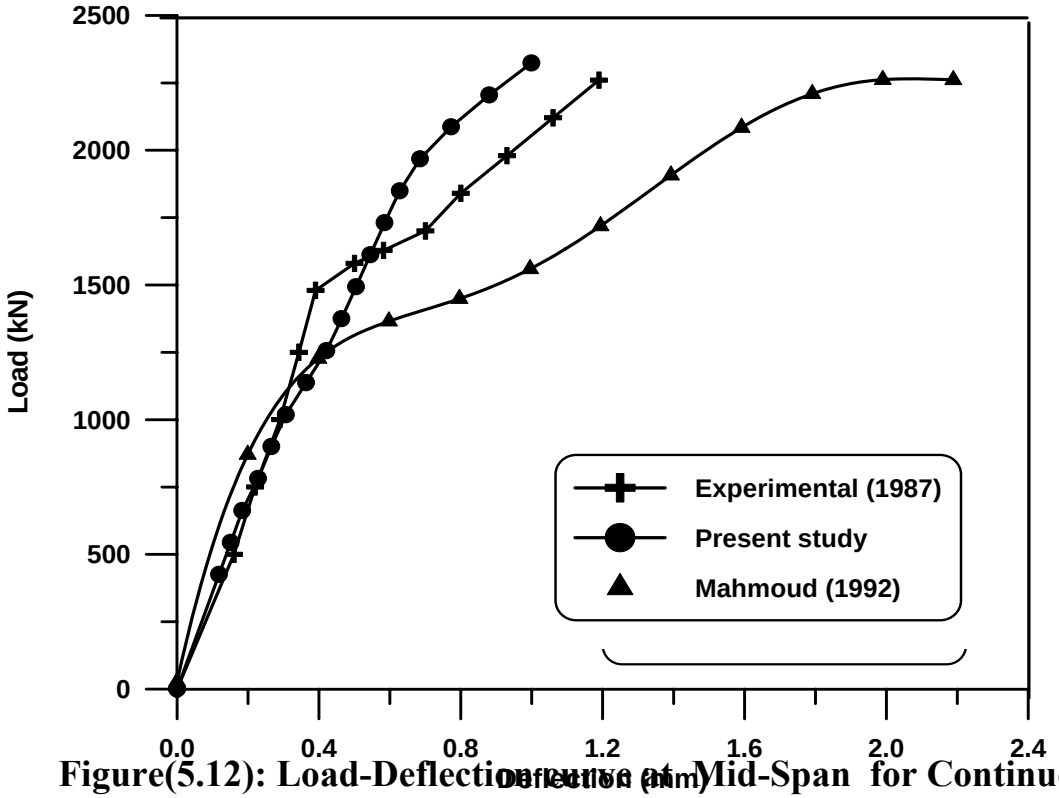

Figure(5.12): Load-Deflection curve at Mid-Span for Continuous Deep Beam (Comparison with previous studies)

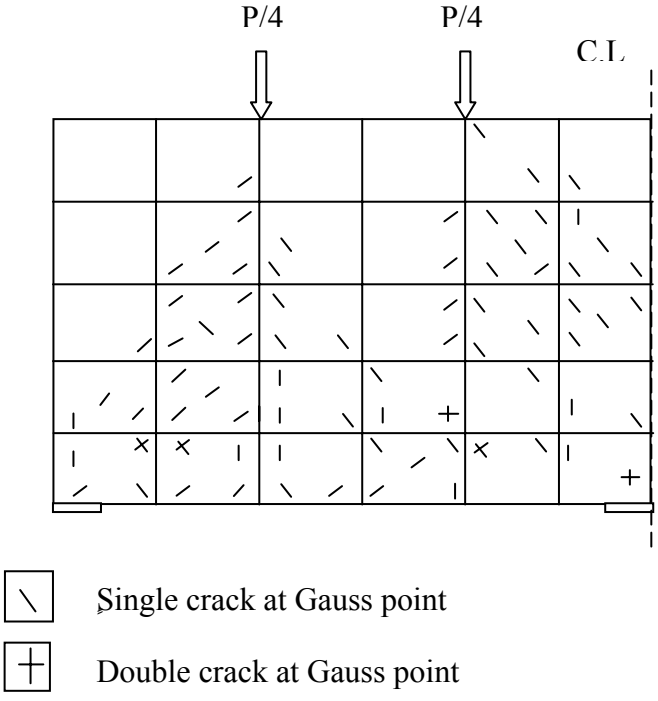

Figure(5.13): Cracking Patterns of Continuous Deep Beam at Failure for one Span

5.4 Simply Supported Reinforced Concrete Deep Beams With Openings

Simply supported reinforced concrete deep beams with openings are analyzed by using the computer program (**P3DNFEA**). Details of three beams tested by Kong and Sharp (1973) are shown in Fig. (5.14). Area of each opening is equal to 2% of side view area of the beam. Due to symmetry of loading and geometry, only one-half of the beams are analyzed by using twenty nine 20-node brick elements for beams as shown in Fig. (5.15).

The main reinforcement consists of one bar of diameter 20mm. The web reinforcement had a rectangular mesh of 6mm diameter bar with 100mm vertical spacing and 140mm horizontal spacing and a 6mm diameter bar of rectangular loop to trim each opening. The reinforcement is represented by embedded bar. Material properties of the concrete and steel are given in Table (5.4). The computed ultimate load gives a good agreement with the experimental result with a difference about (5%) as average in ultimate load as shown in Fig. (5.16) and Table (5.5).

The crack patterns of the beam (M-0.4/5) for different loading levels are shown in Figure (5.17). The first cracking initiates at load (21%) of the ultimate load at corners of the openings. The crack develops in all directions of the beam through the increase of the loading.

.

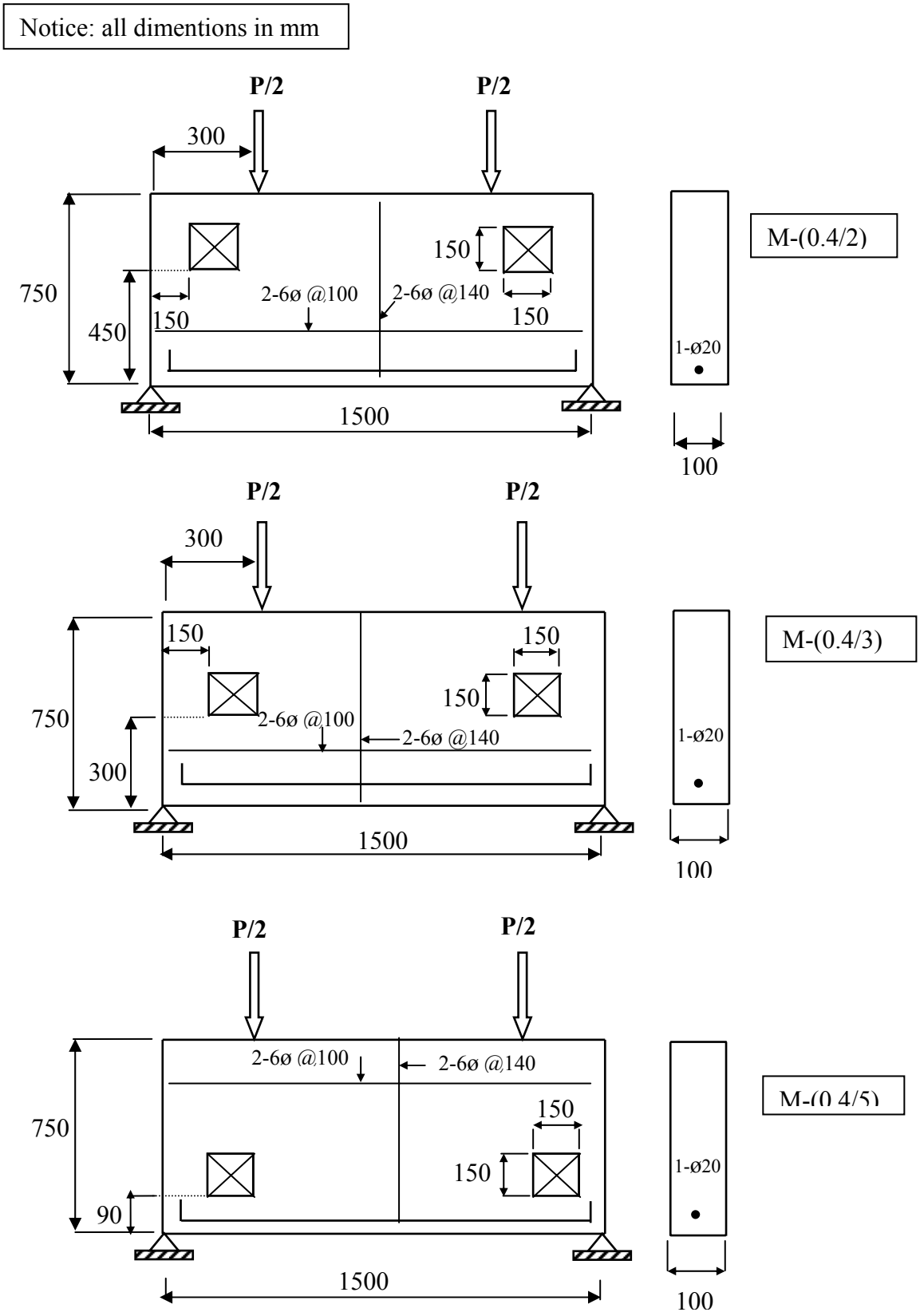

Figure(5.14): Simply Supported Deep Beams with Opening

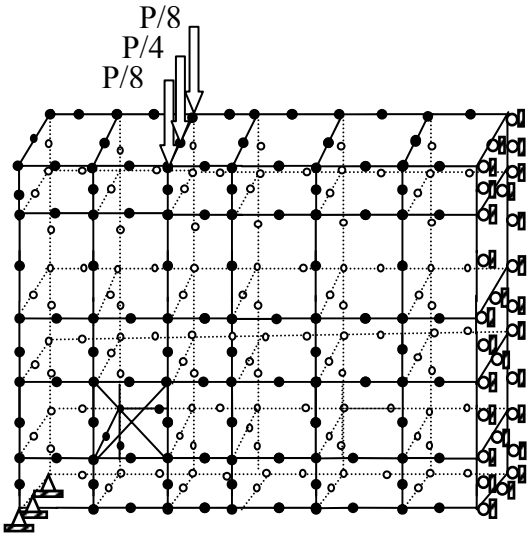

Figure (5.15): Finite Element Idealization of Beam (M-0.4/5)

Table (5.4): Material Properties and Additional Parameters of Simply Supported Deep Beams with Openings.

	Material properties and material parameter	Symbol	M-0.4/2	M-0.4/3	M-0.4/5
Concrete	Young's modulus	Ec(N/mm^2)	25786	26795	26379
	Compressive strength	f'_c (N/mm^2)	30.1	32.5	31.3
	Tensile strength	f_t (N/mm^2)	2.5	2.18	2.3
	Poisson's ratio	ν	0.2	0.2	0.2
Main Reinforcement	Young's modulus	Es(N/mm^2)	200100	200100	200100
	Yield stress	f_y(N/mm^2)	430	430	430
	Hardening parameter	H	0.0	0.0	0.0
Web Reinforcement	Young's modulus Yield stress Hardening parameter	Es(N/mm^2) f_y(N/mm^2) H	200000 425 0.0	200000 425 0.0	200000 425 0.0
Tension stiffening parameter	Rate of stress release	α_1	20.0	20.0	20.0
	Sudden loss of tension stiffness at the instant of cracking	α_2	0.5	0.5	0.5
Shear retention parameters	Rate of decay of shear stiffness	γ_1	10.0	10.0	10.0
	Sudden loss of shear stiffness at the instant of cracking	γ_2	0.5	0.5	0.5
	Residual shear stiffness due to the dowel action	γ_3	0.1	0.1	0.1

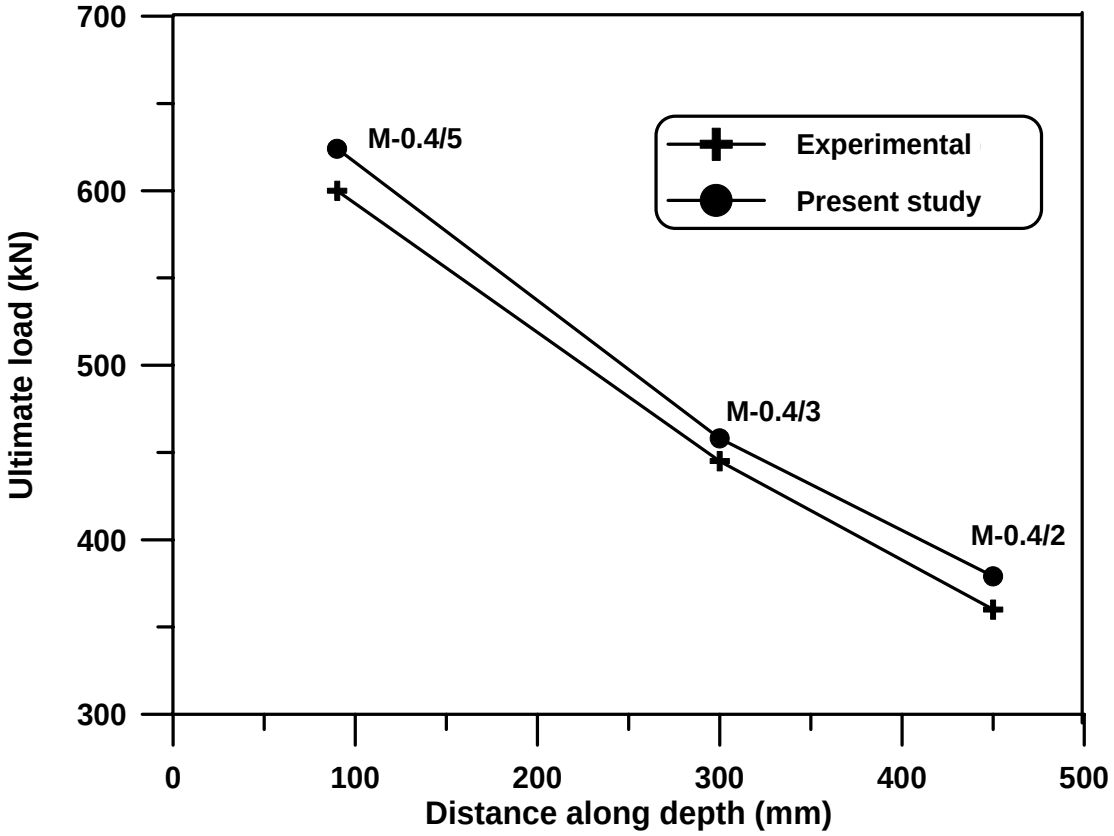

Figure(5.16): Influence of Opening Location through Depth of the Beam

Table (5.5): Measured and Computed Ultimate Loads

Beams Ref. No.	Ultimate Load		$P_{Exp.}/P_p$
	Experimantal ($P_{Exp.}$)	Predicted (P_p)	
M 0.4/2	360	384	0.94
M 0.4/3	445	458	0.97
M 0.4/5	600	624	0.96

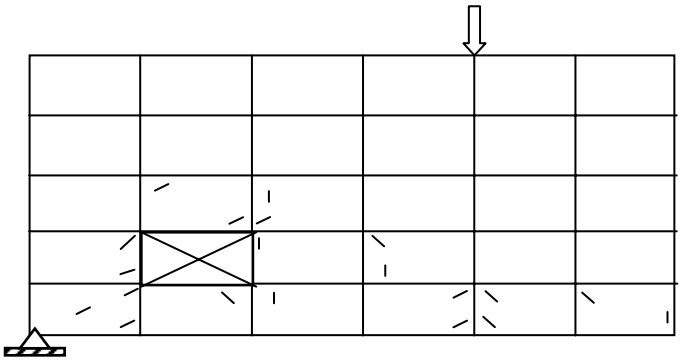

20% of Failure load

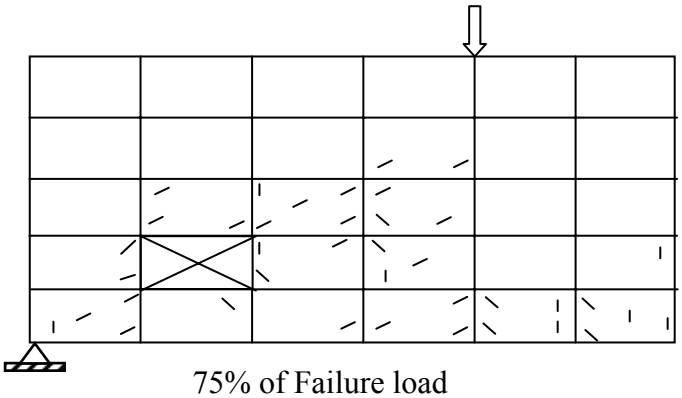

75% of Failure load

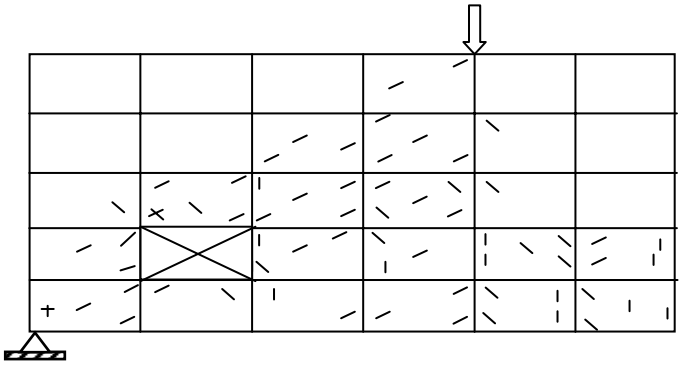

at Failure load

Single crack at Gauss point

Double crack at Gauss point

Figure (5.17): Cracking Patterns of Simply Supported Deep Beam (M-0.4/5)

5.5 Parametric study of Simply Supported Reinforced Concrete Deep Beams with openings

Simply supported reinforced concrete deep beams with openings are considered. All the openings with position and size are indicated by symbols, which are ranging from B0 to B10 as explained in Fig. (5.18) and Table (5.6). Two openings are provided in each beam symmetrically about the mid-span except (B6, B7, B8, B9, B10) that has only one opening at mid-span, and B0 that is solid without opening. Area of each opening is equal to (4%) of the side view area of the beam.

Due to symmetry of loading and geometry, only one half of the beams is analyzed as shown in Fig.(5.19). Sixteen 20- node brick elements were used for B0, twenty two 20- node brick elements for B5 and B10, and twenty three 20- node brick elements for the other. The steel reinforcement is represented by embedded bar in x-direction. Material properties of the concrete and steel are given in Table (5.7)

A Parametric study is presented including the influence of both beam and opening proportions in many items:

1. Effect of opening location along the beam span and through the depth.
2. Effect of web reinforcement.
3. Effect of span to depth ratio.
4. Effect of compressive strength.
5. Effect of boundary conditions.

Notice: all dimentions in mm

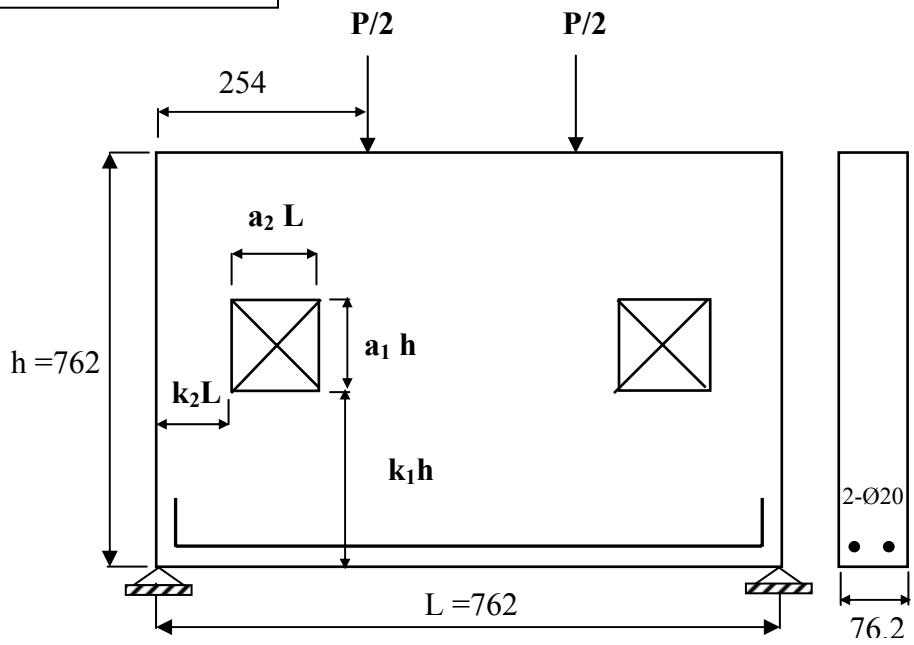

Figure (5.18): Simply Supported Deep Beams with Openings / Geometry, Loading arrangement, and Reinforcement Details

Table (5.6): Open Notations

Beam No.	Open No.	Size		Position	
		a_1	a_2	k_1	k_2
B0	-	-	-	-	-
B1	1	0.2	0.2	0.2	0.1
B2	2	0.2	0.2	0.4	0.1
B3	3	0.2	0.2	0.6	0.1
B4	4	0.1	0.4	0.45	0.05
B5	5	0.4	0.1	0.3	0.15
B6	6	0.2	0.2	0.4	0.4
B7	7	0.1	0.4	0.45	0.3
B8	8	0.075	0.53	0.481	0.235
B9	9	0.4	0.1	0.3	0.45
B10	10	0.53	0.075	0.235	0.481

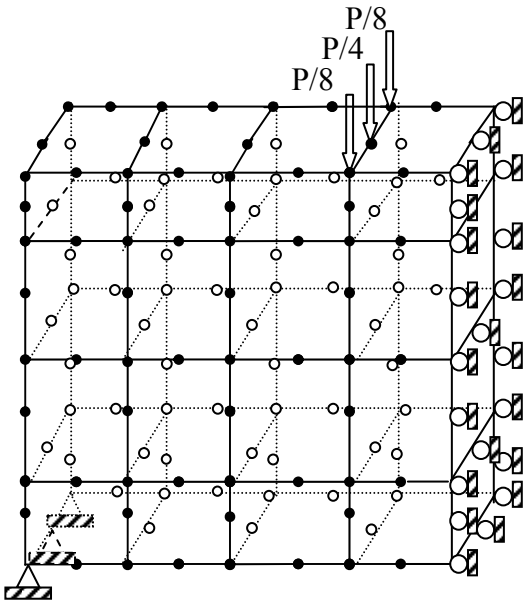

(a): Finite Element idealization of B0

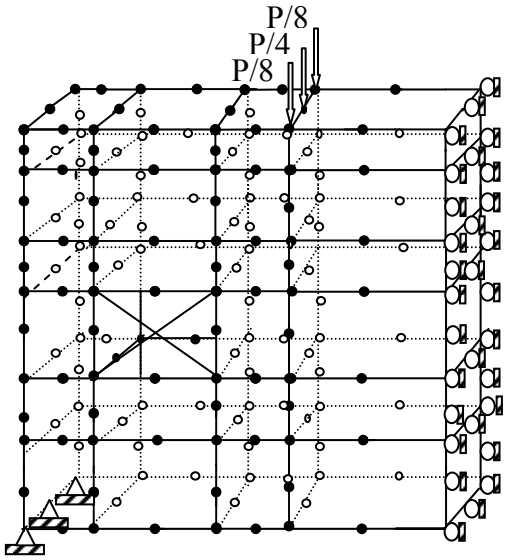

(b): Finite Element idealization of B2

Figure (5.19): Finite Element idealization of B0 and B2

5.5.1 Effect of Opening Location along the Beam Span and through the Depth

To explain the effect of openings on the behavior of deep beams, the openings are provided at different positions along beam span and throught depth as shown in Fig (5.18). Fig (5.20) to Fig (5.23) show the influence of opening position on the ultimate load. These figures illustrate that the effect of an opening on the ultimate load depends on the extent to which it interrupts the load path joining the bearing block at the load and reaction points.

Presence of openings in the shear zone of a deep beam leads to reduce considerably the ultimate load as shown in Fig.(5.20). The ultimate load in beams B1, B2, and B3 is about (31%, 49%, and 38%) less than that of the case of no opening of similar solid beam B0, respectively.

In beams B4 and B5, the reduction in ultimate load is about (40% and 56%) of the solid beam B0, respectively, where the openings completely interrupted the load path, therefore; serious strength reduction occurred as shown in Fig.(5.21).

Ultimate load in beams B6 and B7, at which there is one opening made in the beam center and far away from the load path , is about (8% and 19%) less than that of B0, respectively. On the other hand, for B8 the opening piercing the critical shear zone, ultimate load is about (39%) less than that of B0 as shown in Fig. (5.22).

In beams B9, and B10, the openings are provided in mid-span and are reasponsably clear from the load path, Fig.(5.23) shows that their ultimate loads were comparable to that of solid beam B0 with a difference about (13%). ACI-Code formulas are used to determine the shear strength of these beams. From Table (5.8) it can be noticed that ACI-Code formulas could not sensitize to opening location, inverse to the finite element method.

Table (5.7): Material Properties and Additional Parameters of Simply Supported Deep Beams with Openings

	Material properties and material parameter	Symbol	value
Concrete	Young's modulus	Ec(N/mm^2)	244210
	Compressive strength	f′$_c$(N/mm^2)	27.8
	Tensile strength	f$_t$(N/mm^2)	2.6
	Poisson's ratio	ν	0.17
Steel	Young's modulus	Es(N/mm^2)	200000
	Yield stress	f$_y$(N/mm^2)	350
	Hardening parameter	H	0.0
Tension stiffening parameter	Rate of stress release	α_1	20.0
	Sudden loss of shear stiffness at the instant of cracking	α_2	0.5
Shear retention parameters	Rate of decay of shear stiffness	γ_1	10.0
	Sudden shear stiffness at the instant of cracking	γ_2	0.5
	Residual shear stiffness due to the dowel action	γ_3	0.1

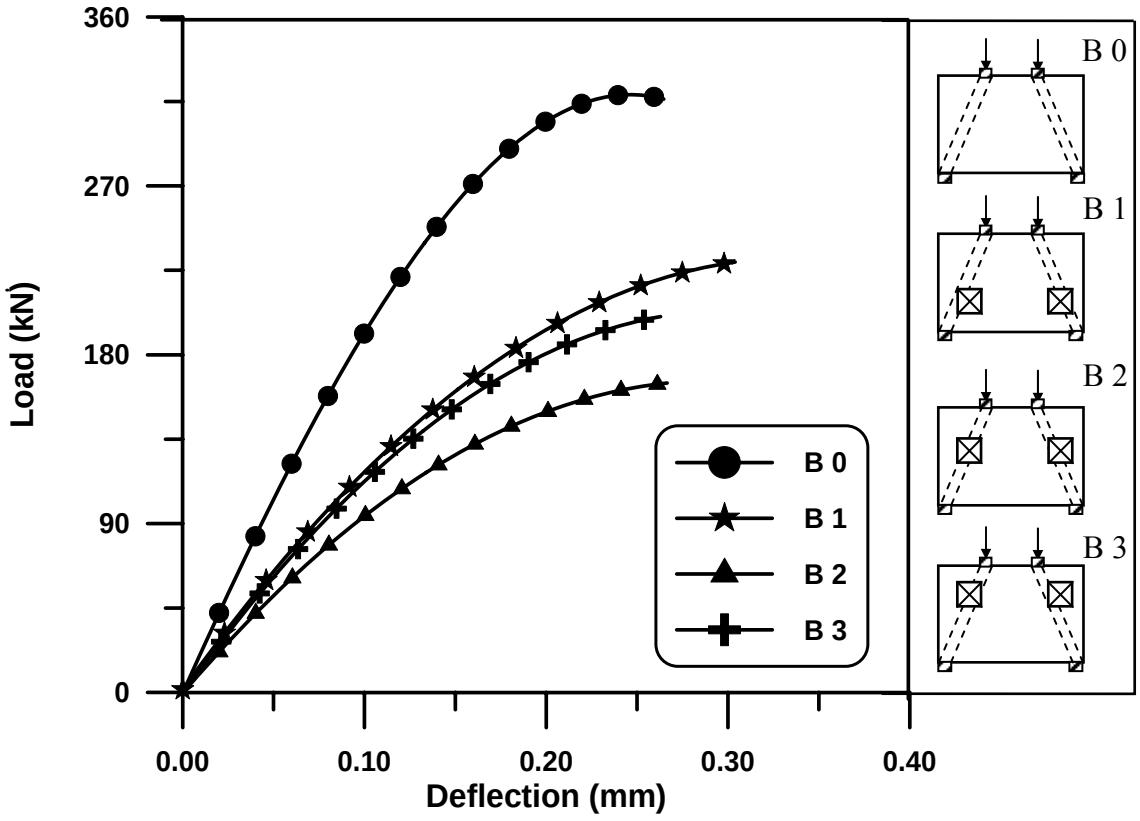

Figure(5.20): Load-Deflection Curve at Mid-Span for Deep Beams (B0, B1, B2, and B3)

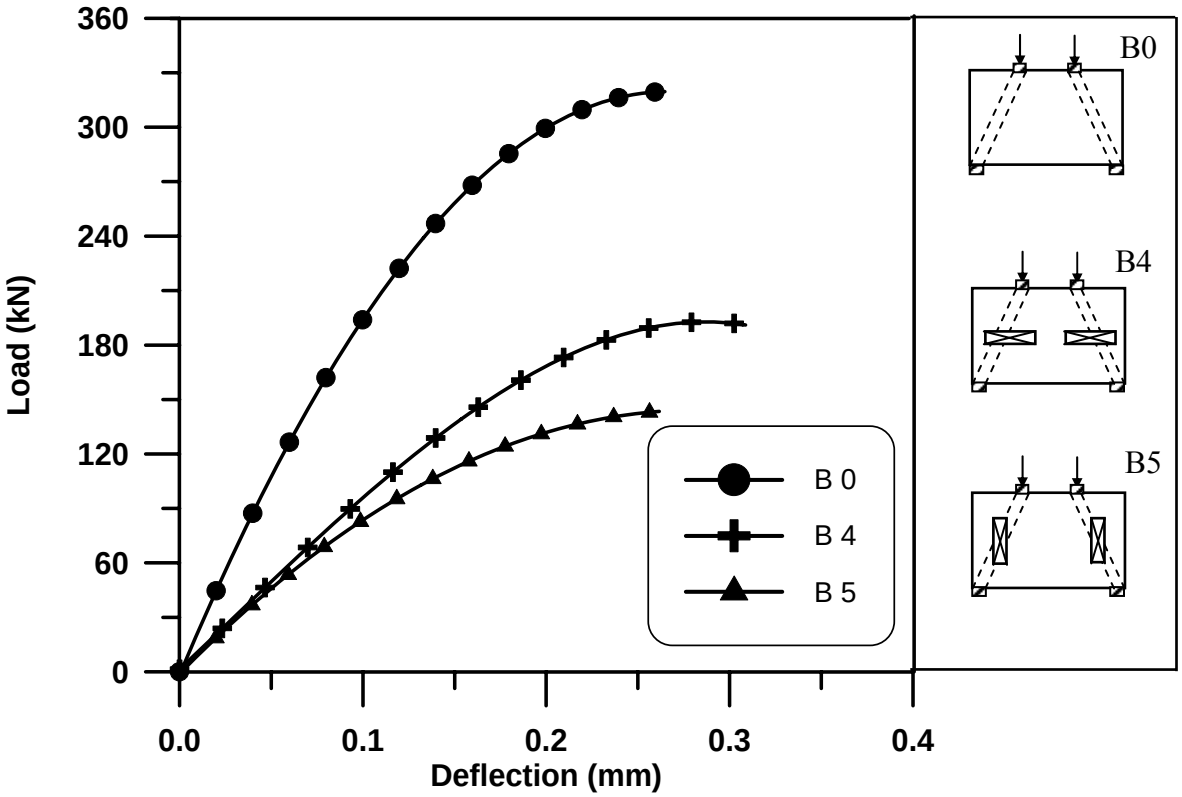

Figure (5.21): Load-Deflection Curve at Mid-Span for Deep Beams (B0, B4, and B5)

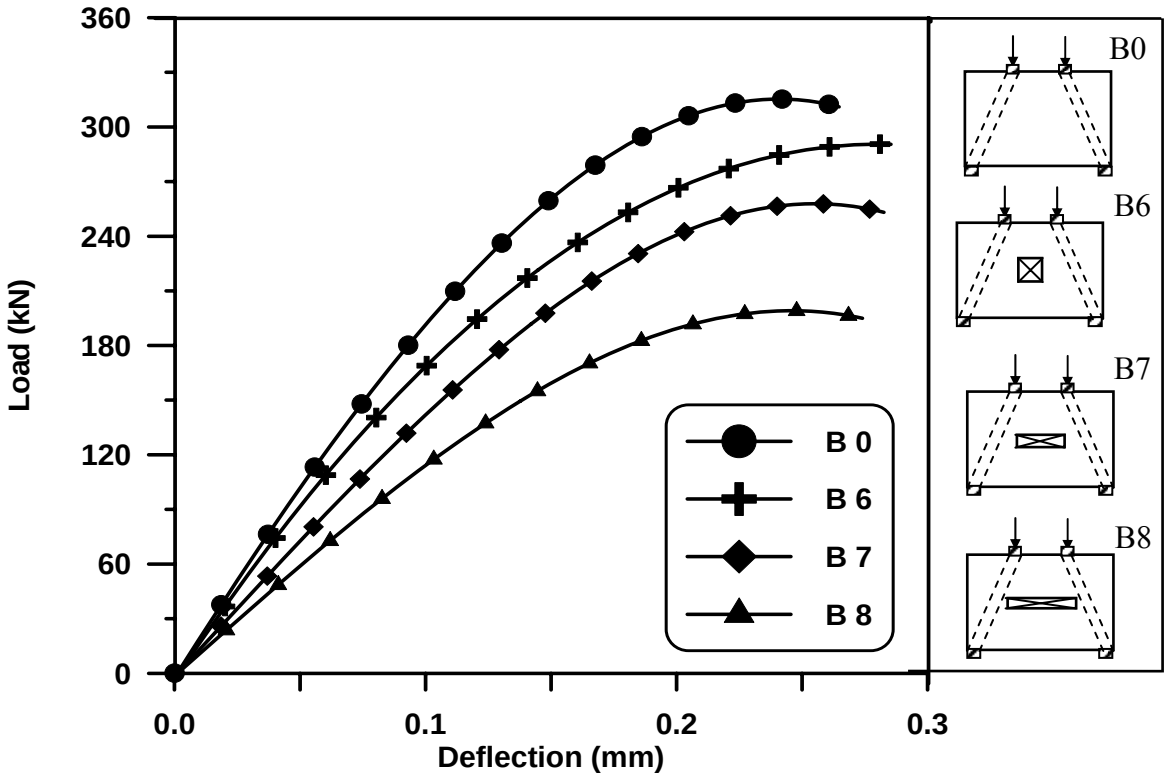

Figure (5.22): Load-Deflection Curve at Mid-Span for Deep Beams (B0, B6, B7, and B8)

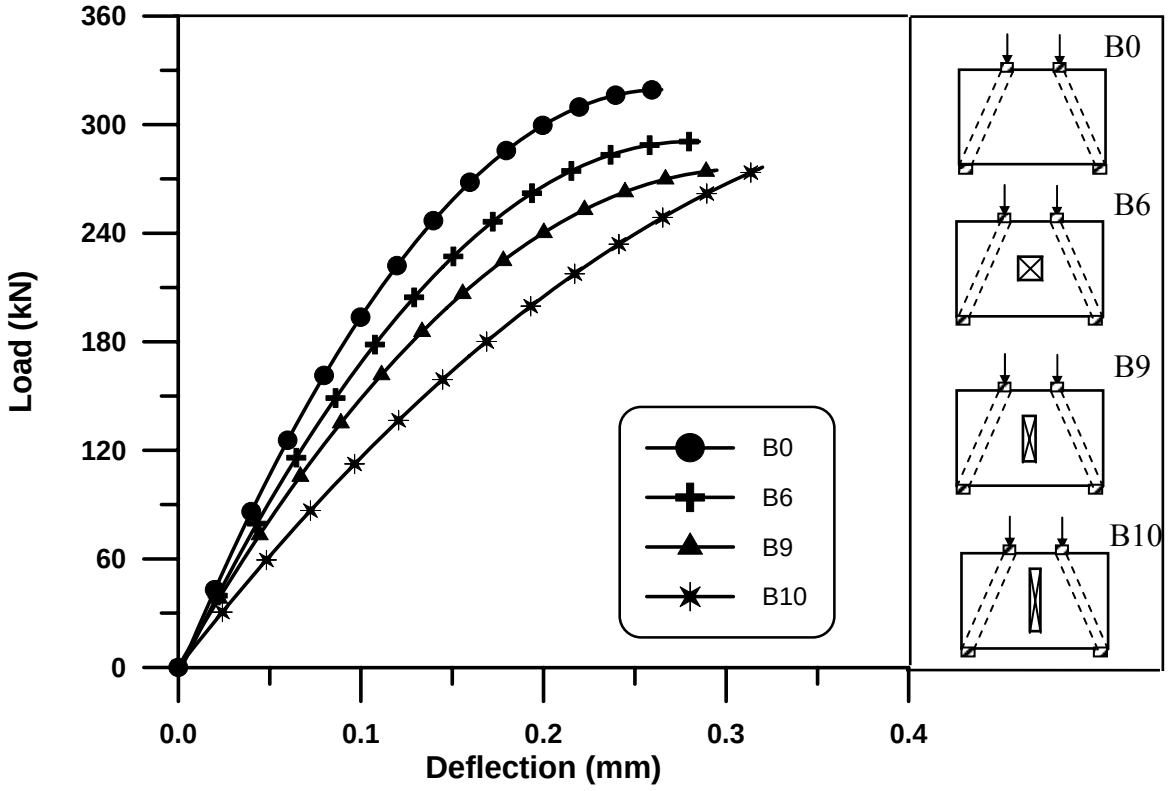

Figure (5.23): Load-Deflection Curve for at Mid-Span for Deep Beams (B0, B6, B9, and B10)

Table (5.8): Shear Strength of Simply Supported Deep Beams with Openings

Beam No.	$V_{F.E}$ kN	V_{ACI} kN
B0	160	141
B1	80	116
B2	101	116
B3	117	116
B4	100	127
B5	55	83
B6	145	141
B7	133	141
B8	100	141
B9	143	141
B10	139	141

5.5.2 Effect of Web Reinforcement

To investigate the effect of web reinforcement, deep beams B0 and B2 are considered. All information are shown in Fig.(5.18) and Table(5.6). Reinforcement details of beams include in addition:

1. A rectangular mesh of 10mm diameter bar at 150 mm vertical spacing and bar of diameter 10mm horizontal at spacing 210 mm.
2. Bar of diameter 10mm rectangular loop are provided to trim each opening.

From Fig.(5.24) and Fig.(5.25), it can be noticed that the ultimate load increases with web reinforcement by about (6% and 12%) for B0 and B2, respectively.

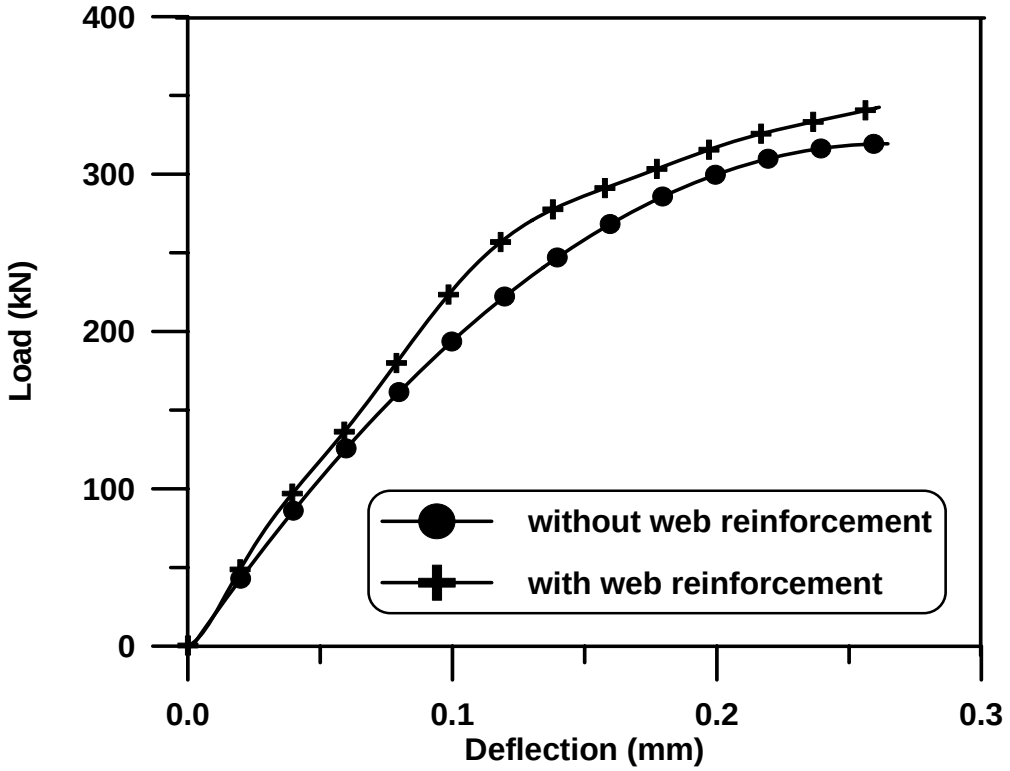

Figure (5.24): Load-Deflection Curve at Mid-Span for Beam B0 with Effect of Web Reinforcement

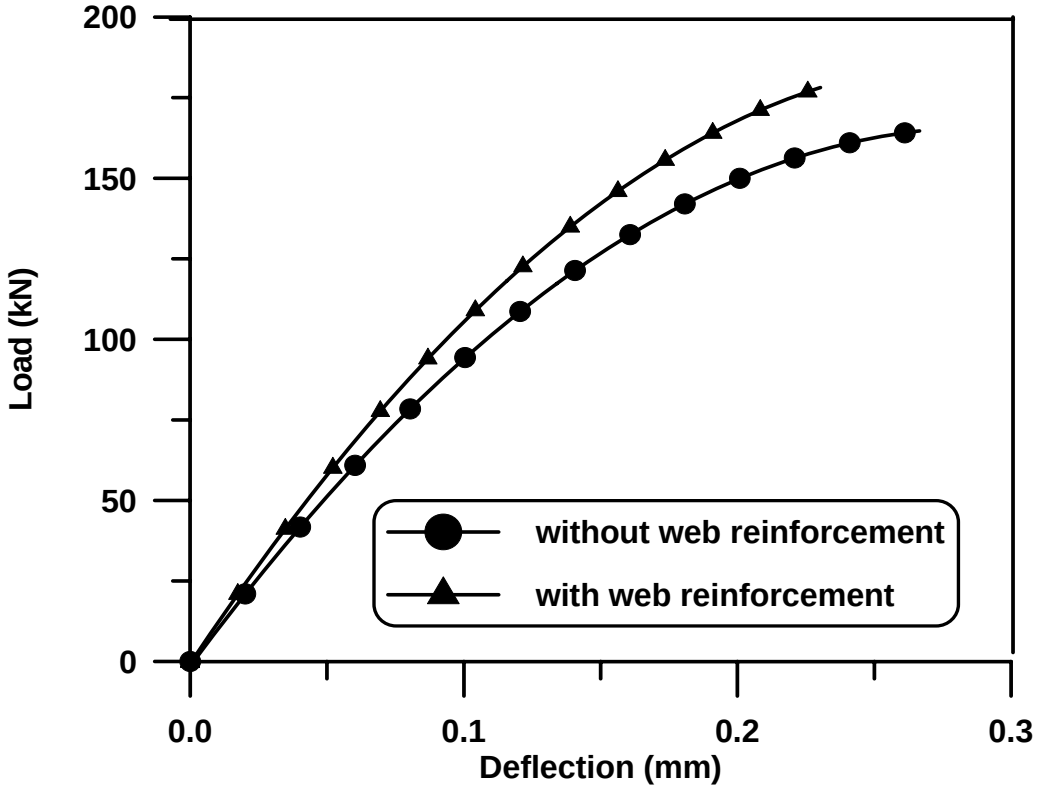

Figure(5.25): Load-Deflection Curve at Mid-Span for Beam B2 with Effect of Web Reinforcement

5.5.3 Effect of Span-Depth ratio

Reinforced concrete deep beam B2 is considered. All information is shown in Fig. (5.18) and Table (5.6). Fig. (5.26) illustrates the influence of beam span to depth ratio on the ultimate load. The curve indicates that increasing the span to depth ratio from 1 to 3 leads to a decrease in the ultimate load by about (53%).

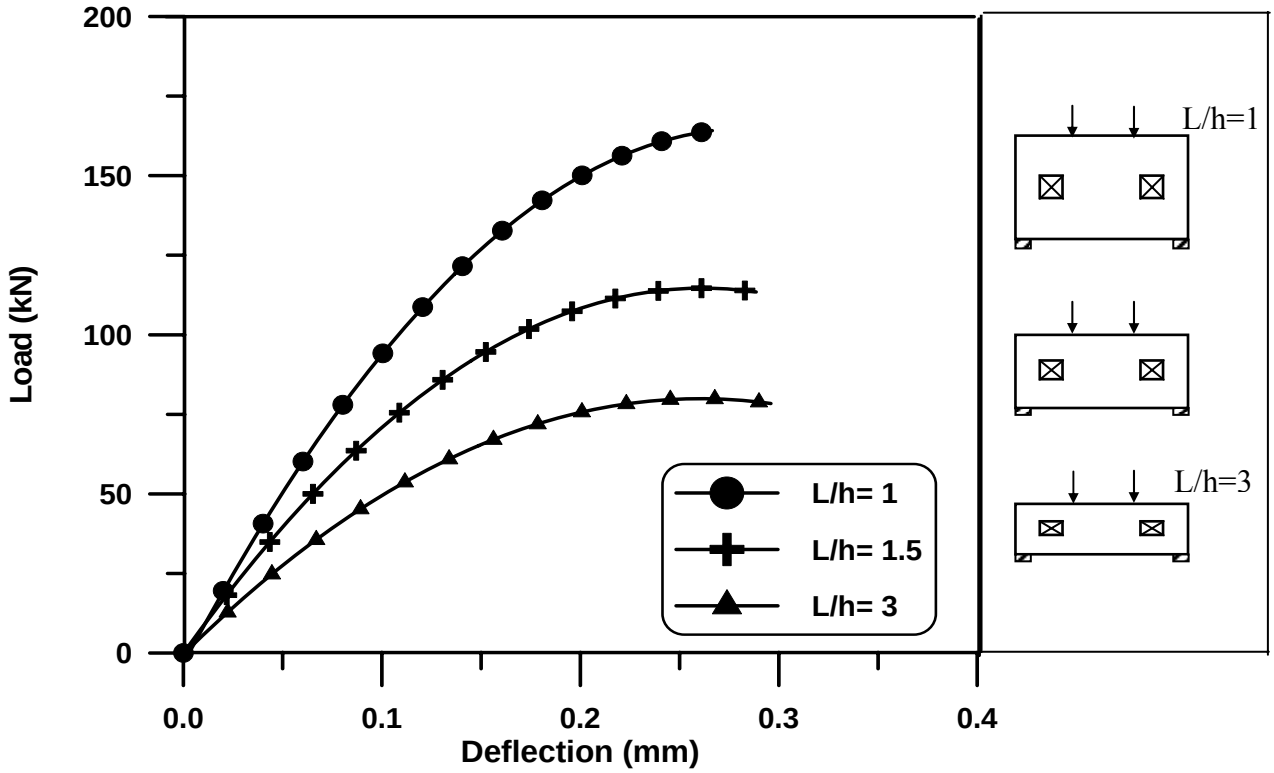

Figure (5.26): Load-Deflection Curve at Mid-Span for Beam B2 with Different Span–Depth Ratio

5.5.4 Effect of Compressive Strength

To show the effect of compressive strength, reinforced concrete deep beam B2 is considered. Fig. (5.27) shows the effect of concrete grade on the ultimate load of deep beam. As may be seen from the figure, the ultimate loads for grades 27.8 and 30 are about (78%) and (88%), respectively; of that for grade 35.

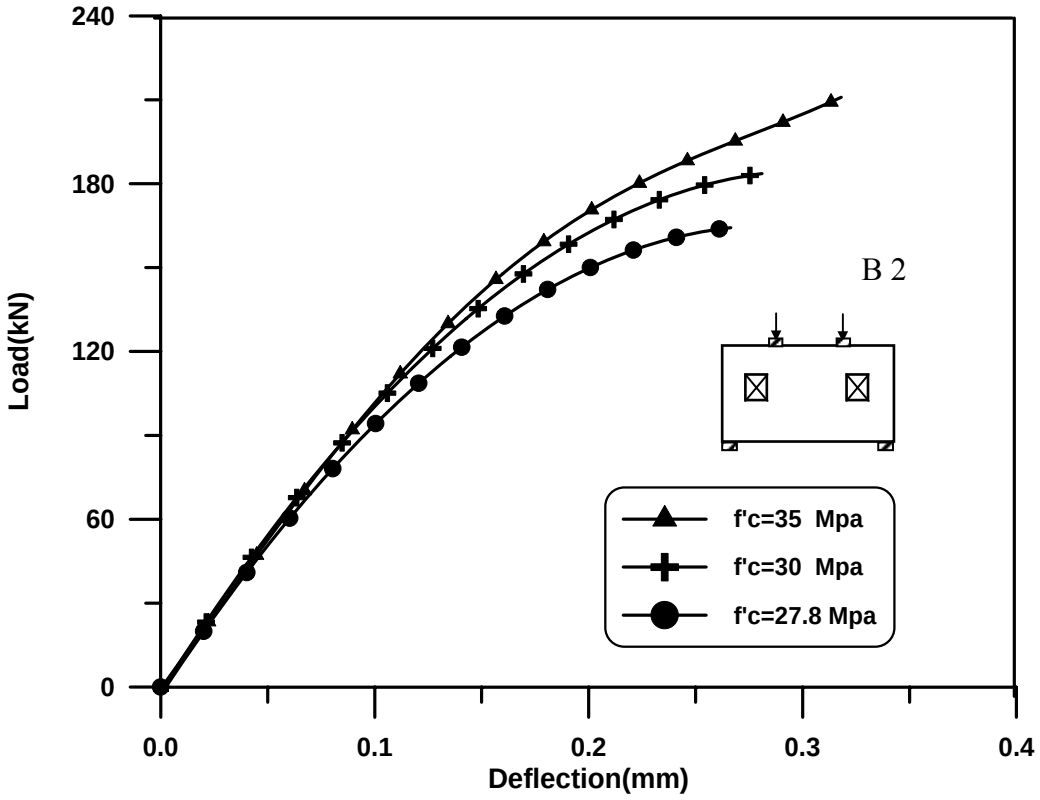

Figure (5.27): Load-Deflection Curve at Mid-Span for Beam B2 with Different Compressive Strength

5.5.5 Effect of Boundary Condition

To show the effect of boundary condition, the load-deflection curve for simply supported, fixed- fixed supported and fixed-simply supported ends are plotted. Fig.(5.28) shows the load-deflection curve for simply supported, fixed ends, and fixed-simply supported ends for beam B0. From this figure it can be noticed that:

1. The load-deflection curves show that the ultimate load for the fixed-fixed supported deep beam is greater than that of the simply supported beam by about (6%) and the ultimate load for the fixed-simply supported ends is greater than that of the simply supported ends by about (5%).
2. The deflection for the simply supported deep beam is greater than that for the fixed- fixed supported deep beam by about (50%) and (19%) for the fixed-simply supported ends.

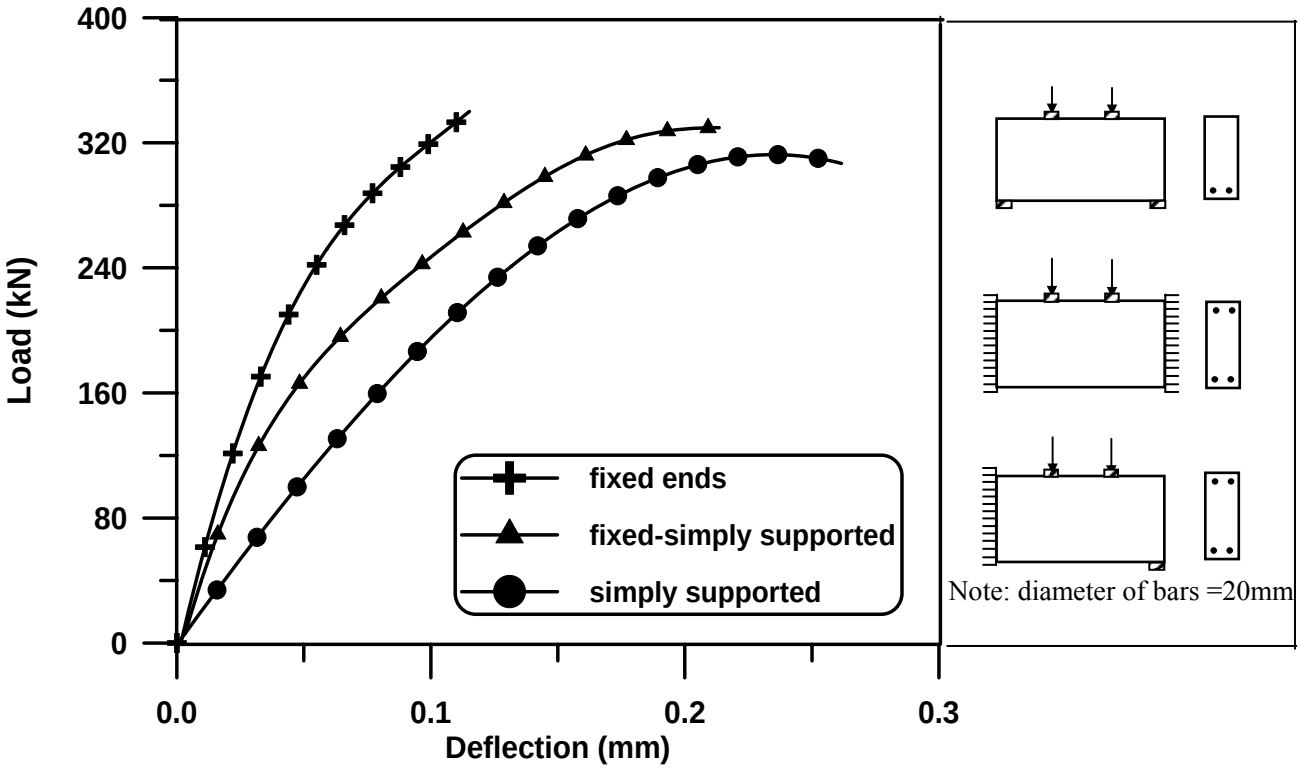

Figure (5.28): Load-Deflection Curve at Mid-Span for Beam B0 with Different Boundary Conditions

5.6 Continuous Reinforced Concrete Deep Beams with Openings

Three continuous reinforced concrete deep beams are considered. Fig(5.29) and Table (5.9) shows the geometry and details of these beams. Two openings are provided in each span symmetrically about mid-span. Bc0 is a solid beam without any opening. All the openings have area equal to (4%) of side view area of the beam.

Due to symmetry of loading and geometry, only one half of the beams is analyzed by using twenty four 20- node brick elements for Bc0, and twenty eight 20-node element for other beams as shown in Fig.(5.30). The steel reinforcement is represented by embedded bars in x-direction. Material properties of the concrete and the steel are given in Table (5.10). Fig. (5.31) to Fig. (5.33) show the load- deflection response at mid-span of the beams. From these figures, it can be noticed that:

1. In Bc1, where the openings are provided at location cutting small area from the compressive-strut arch, the reduction in the ultimate strength is about (8%) of the solid deep beam.

2. In Bc2 and Bc3, where the openings are provided along the depth towards the supports, the reduction in ultimate load is about (30% and 24%)of the solid deep beam, respectively.

Note: all dimensions in mm

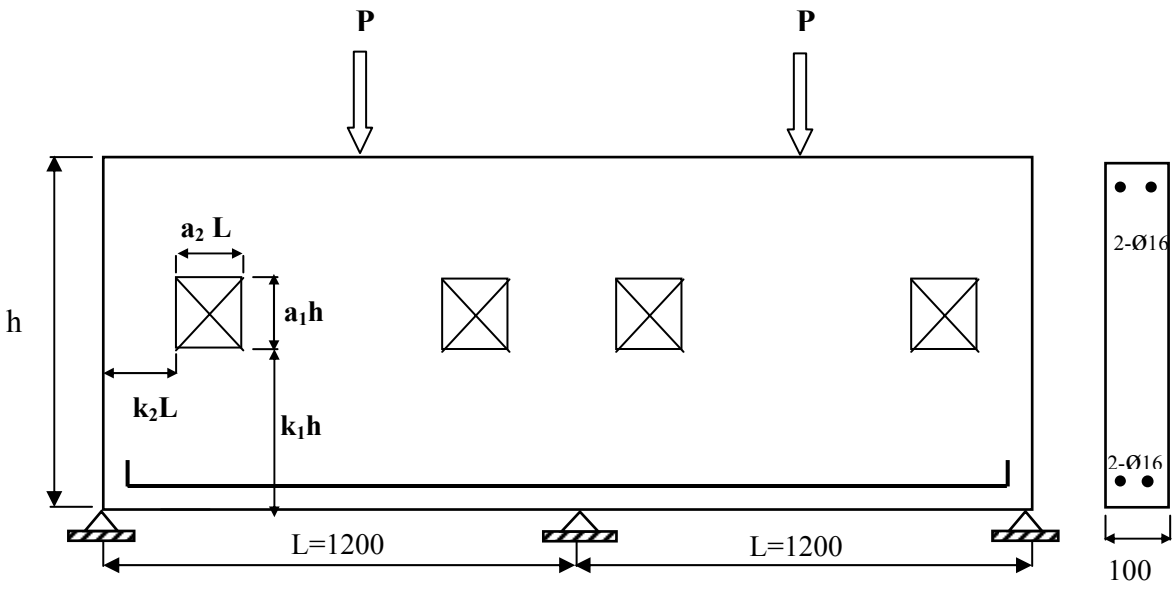

Figure(5. 29): Continuous Deep Beams with Openings/ Geometry, Loading arrangement, and Reinforcement Details

Table (5.9): Opening Notations

Beam No.	Open No.	Size		Position	
		a_1	a_2	k_1	k_2
Bc0	-	-	-	-	-
Bc1	1	0.2	0.2	0.2	0.1
Bc2	2	0.2	0.2	0.4	0.1
Bc3	3	0.2	0.2	0.6	0.1

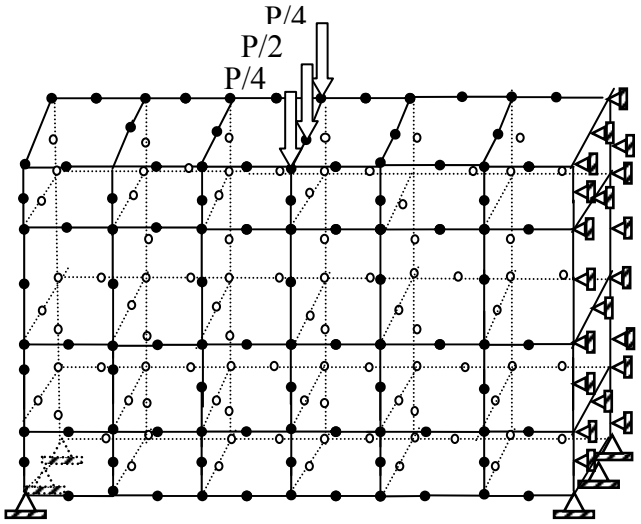

(a): Finite Element Mesh of Half of Bc0

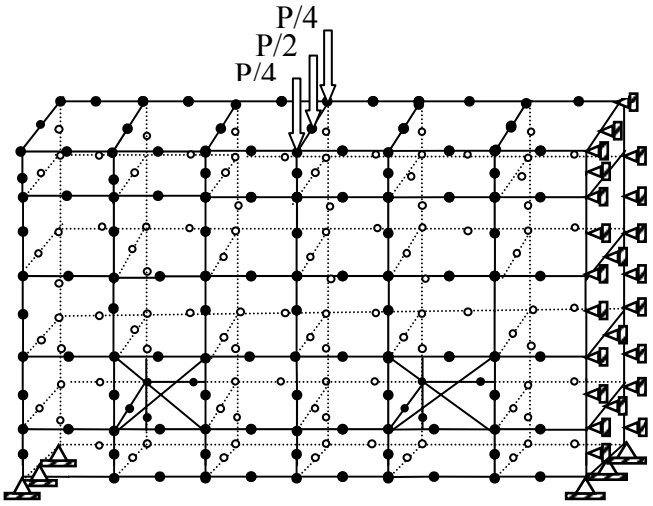

(b): Finite Element Mash of Half of Bc1

Figure(5. 30): Finite Element Mash of Half Bc0 and Bc1

Table (5.10): Material Properties and Additional Parameters of Continuous Deep Beams with openings

	Material properties and material parameters	Symbol	value
Concrete	Young's modulus	Ec(N/mm^2)	25743
	Compressive strength	f´$_c$(N/mm^2)	30
	Tensile strength	f_t(N/mm^2)	2.73
	Poisson's ratio	ν	0.2
Steel	Young's modulus	Es(N/mm^2)	230000
	Yield stress	f_y(N/mm^2)	430
	Hardening parameter	H	0.0
Tension stiffening parameter	Rate of stress release	α_1	20.0
	Sudden loss of tension stiffness at the instant of cracking	α_2	0.5
Shear retention parameters	Rate of decay of shear stiffness	γ_1	10.0
	Sudden loss of shear stiffness at the instant of cracking	γ_2	0.5
	Residual shear stiffness due to the dowel action	γ_3	0.1

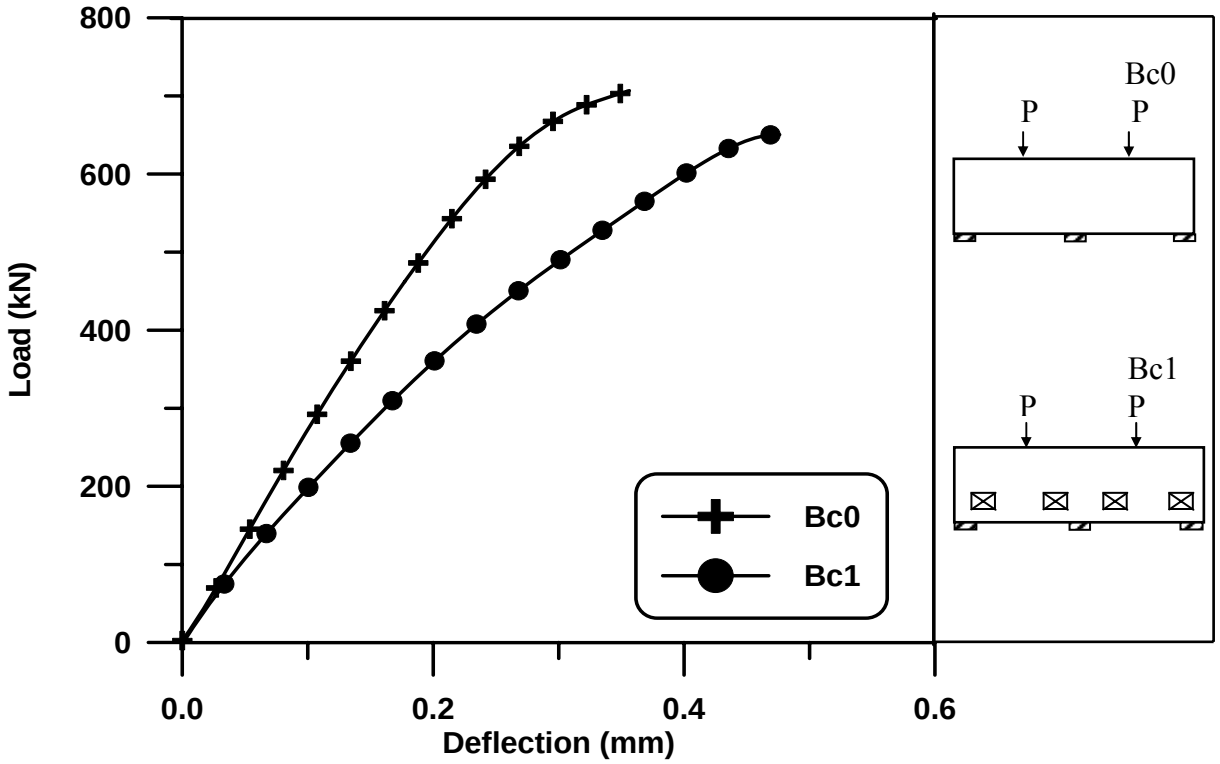

Figure (5. 31): Load -Deflection Curve at Mid-Span for Bc0 and Bc1

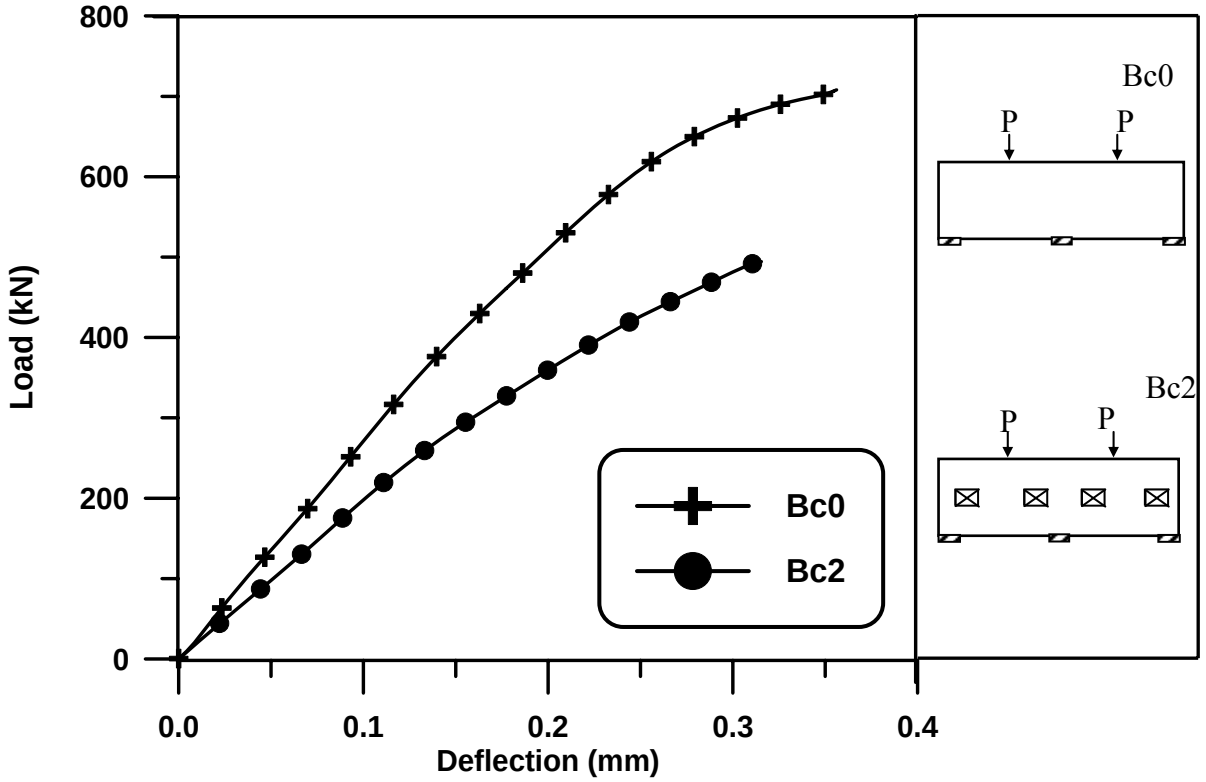

Figure (5. 32): Load -Deflection Curve at Mid-Span for Bc0 and Bc2

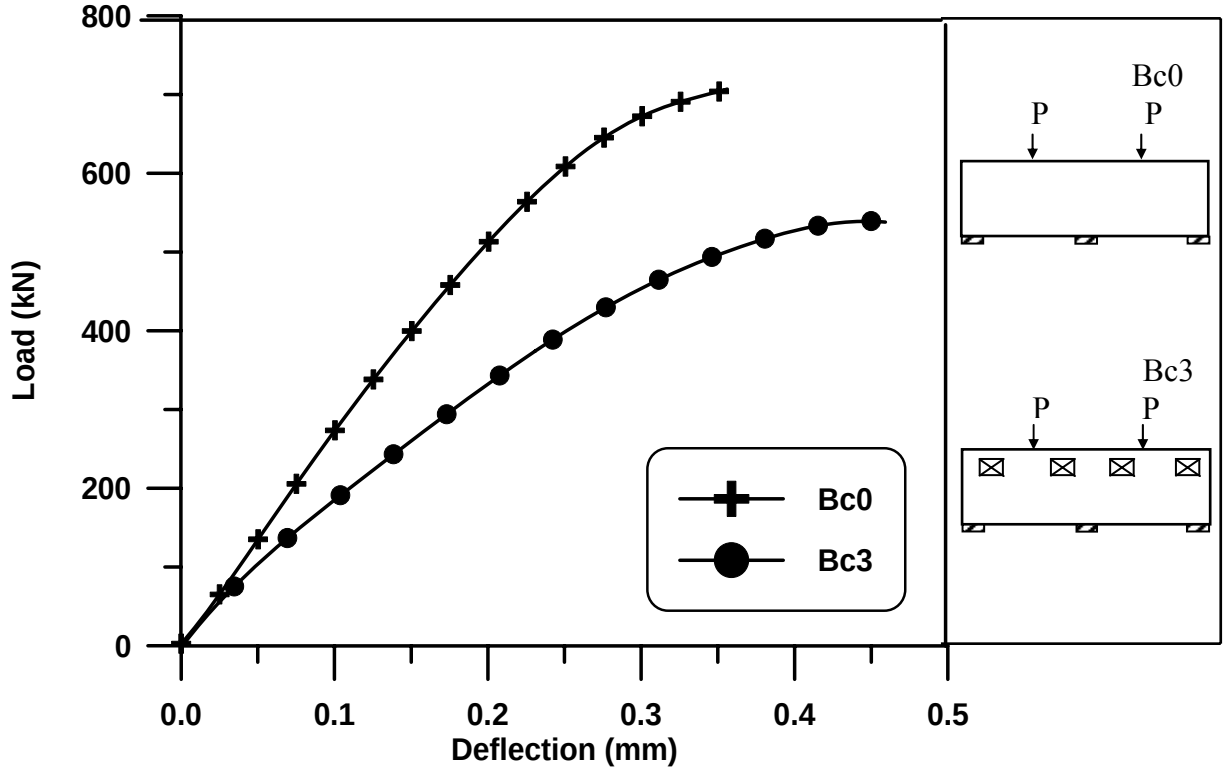

Figure (5.33): Load -Deflection Curve at Mid-Span for Bc0 and Bc3

5.7 Estimation of Shear Strength of Continuous Reinforced Concrete Deep Beams by Various Methods

Several methods exist in the literature for prediction of the shear strength of reinforced concrete deep beams. These methods are used in this study for the comparison of the results with the finite element method and they are :

5.7.1 ACI-Code Method

The recommended formula in the code consists of a set of empirical rules based on large amount of test data. For shear design of continuous deep beams, the formula given in section (11-8) of ACI-Code (2002) for the nominal shear strength of reinforced concrete deep beams with web reinforcement is:

$V_u = \emptyset (V_c + V_s)$ ……..*(5.4)*

in which the V_c is computed by

$$V_c = \frac{\sqrt{f'}\, b_w d}{6} \qquad \text{(SI units)}$$

and

$$V_s = \frac{A_v}{s} fy\, d$$

and where:

V_u = ultimate shear strength of deep beam (N)

V_c and V_s = shear strength provided by concrete and shear reinforcements respectively (N)

Ø = reduction factor equal to 0.85

d = effective depth of the section (mm)

bw = width of section (mm)

f'_c = cylinder compressive strength of concrete (N/mm^2)

Av = area of shear reinforcement in distance (s)

f_y = yield strength of shear reinforcement (N/mm^2)

5.7.2 Strut-and-Tie Method

The strut and tie method was used by Siao (1995). He assumed that no difference exists in shear strength between a simply supported deep beam or a continuous deep beam, therefore; he used Eq.(5.5) to analyze single and double-span deep beams. Fig. (5.34) shows the conventional load path in a deep beam.

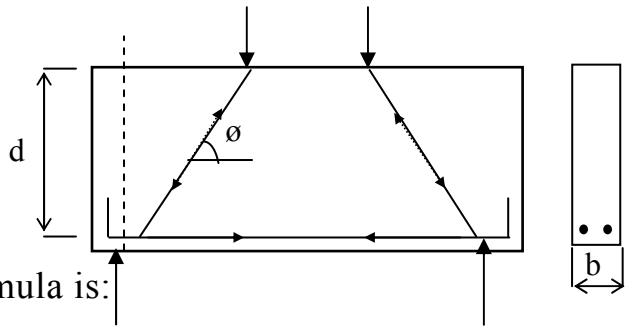

The proposed formula is:

Figure (5.34): Deep Beam

$$V_u = 0.69 \sqrt{f'} \; b\, d \, \{1+n (\rho_h \sin^2 ø + \rho_v \cos^2 ø)\} \qquad \ldots. (5.5)$$

where:

V_u = ultimate shear strength of deep beam (N)

b_w and d = width and effective depth of the beam (mm)

f′c = compressive strength (N/mm^2)

n = modular ratio of steel reinforcement to concrete $n = \frac{E_s}{E_c}$

ρ_h and ρ_v = steel ratio of horizontal and vertical steel reinforcement.

ø = angle with horizontal made by the line joining the edges of the loading plates and supports.

5.7.3 Finite Element Method

The three-dimensional finite element method is utilized to predict the shear capacity of continuous deep beams. Fig. (5.35) shows the beam geometry, loading arrangement, reinforcement detail, and finite element idealization. Due to symmetry of the beams, one-half of each beam was considered in the finite element analysis. The steel reinforcement was represented by embedded bars through the element of concrete with perfect bond between them. Thirty 20-node brick element were used to represent the concrete. Material properties and additional parameters of the continuous deep beam are given in Table (5.11).

The shear capacity of the continuous deep beams predicted by the finite element method is listed in Table (5.12) together with the values of two methods, ACI-Code and the Strut-tie model, respectively.

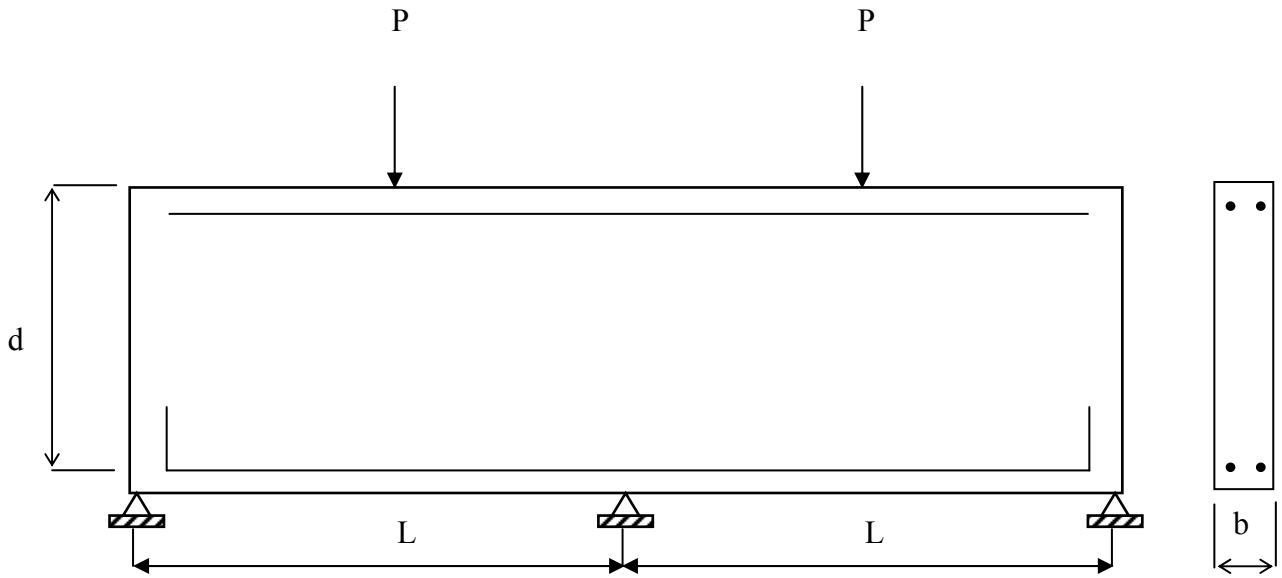

(a): Beam geometry and reinforcement detailes

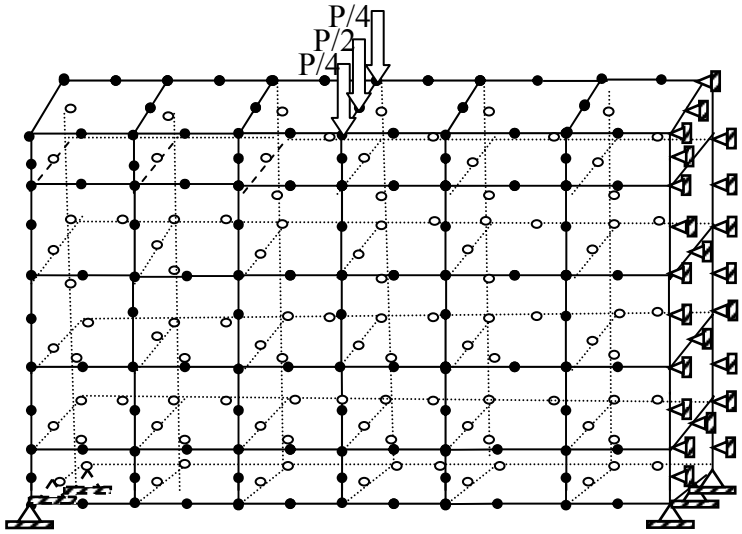

(b): Finite Element idelization of one span

Figure(5.35): Continuous Deep Beam

Table (5.11): Material Properties and Additional Parameters of Continuous Deep Beam

	Material properties and material parameters	**Symbol**	value
Steel	Young's modulus	Es(N/mm^2)	200000
	Yield stress	f_y(N/mm^2)	350
	Hardening parameter	H	0.0
Tension stiffening parameters	Rate of stress release	α_1	20.0
	Sudden loss of tension stiffness at the instant of cracking	α_2	0.5
Shear retention parameters	Rate of decay of shear stiffness	γ_1	10.0
	Sudden loss of shear stiffness at the instant of cracking	γ_2	0.5
	Residual shear stiffness due to the dowel action	γ_3	0.1

Table(5. 12): Predicted and Actual Ultimate Shear Strength in Continuous Deep Beams with Single Point Load per Span

No.	**Beams Reference No.**	**f'_c N/mm^2**	**ρ_v %**	**ρ_h %**	**V_u Exp. kN**	**V_u kN ACI**		**V_u kN Strut-tie**	**V_u kN F.E.**
						Shallow	**Deep**		
1	Bm3/1.0 (T1)	28.9	0.15	0	685	287	618	704	716
2	Bm4/1.0 (T1)	28.5	0	0.094	663	162	493	699	682
3	Bm5/1.0 (T1)	36.9	0.3	0	875	418	767	795	898
4	Bm7/1.0 (T1)	34.5	0	0	695	185	529	769	756
5	VW	49.5	0.87	0	363	288	299	393	403
6	HW	51.6	0	0.98	414	76	139	401	392

Specimens no. 1-4 (b=200, d=950, L=2000) (Choo and Lim,(1993)).
5-6 (b=100, d=640, L=1300) (Rogowsky et al,(1986)).

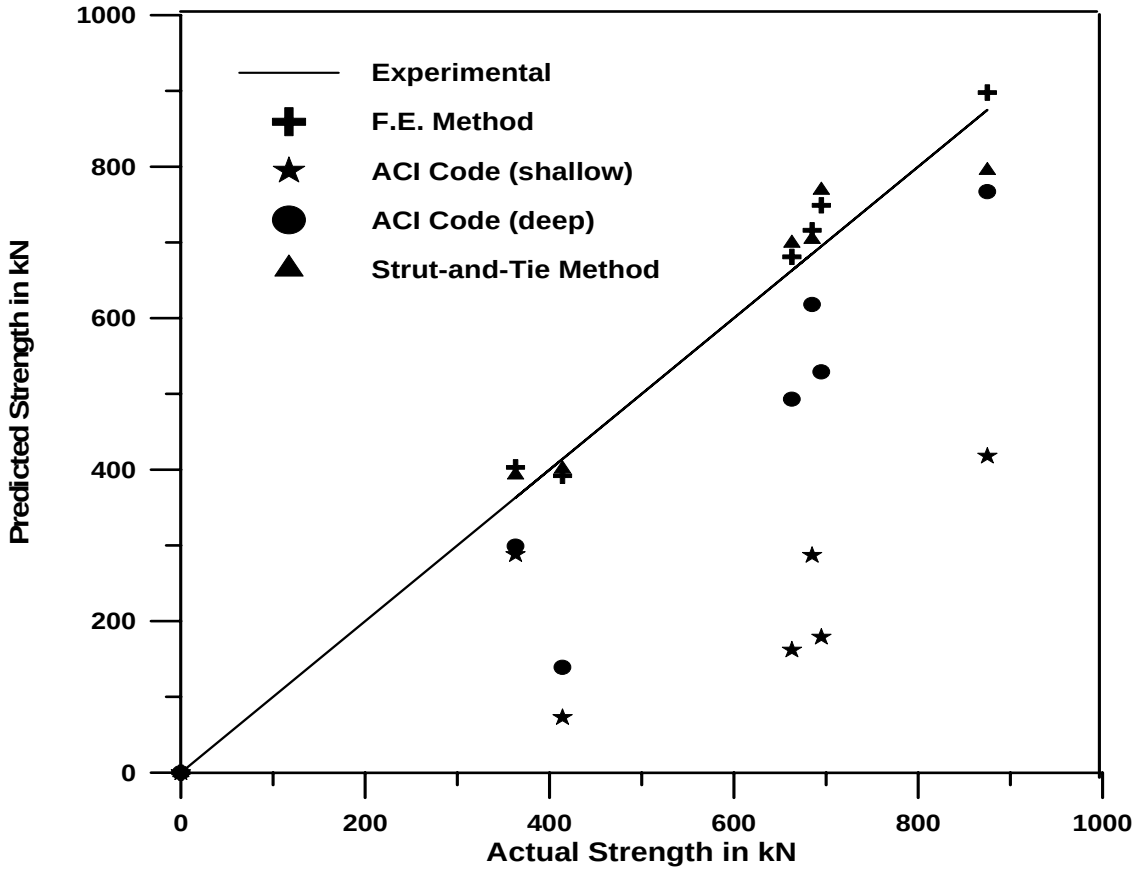

5.7.4 Discussion of the Result

It is clear from the results obtained from Fig. (5.36) and Table (5.12) that the ACI formula predicts the shear strength of continuous deep beams on the conservative side with very large safety margin whereas the strut-and-tie method over-estimates in most of specimens. Also it is found that the strength values obtained from the finite element method are much more accurate than those determined from ACI-Code or strut and tie methods when compared to experimental values.

On the other hand, from ACI-Code formula for shallow and deep beams, it can be concluded that the tied-arch action is present in continuous deep beams as in simply supported deep beams, while the ACI-Code provision does not recommend this concept.

Chapter Six

CONCLUSIONS AND RECOMMENDATIONS

6.1 Conclusions

On the basis of the analysis carried out by using three-dimensional nonlinear finite element method with **P3DNFEA** computer program as described in the previous chapters, the following conclusions can be made:

1. The results obtained from the presented finite element analysis show that the computational models adopted in this study are suitable for prediction of overall behavior of the reinforced concrete deep beams with and without openings under static loads, such as load-deflection, cracking pattern, and ultimate load. The comparison between the present finite element and the available experimental results has shown good agreement with difference about (6%) in the prediction of ultimate loads and about (9%) in deflection as average.
2. The comparison between the present finite element and ACI-Code has a difference about (15%, 60%) of ultimate loads for a simply supported and a continuous deep beam, respectively.
3. The effect of opening on the ultimate load of deep beams depend primarily on the extent to which it intercepts the ‘load path’ and on

the location at which this interception occurs. Therefore, if the designer has to provide an opening in a deep beam, he should keep it far away from the load path.

4. Providing an opening at the shear zone causes sharp decrease in the ultimate load by about (31%-56%) for simply supported deep beams and about (8%-30%) for continuous deep beams.
5. Mechanism of tied-arch action is present in continuous deep beams as in simply supported deep beams and no difference exists between the shear strength calculation of simply supported and continuous deep beams, while the ACI-Code provision does not recommend this concept.
6. Finite element method is more fitting than that of ACI-Code method and strut-tie model for the analysis of reinforced concrete deep beams.
7. Presence of openings in the critical shear zones of deep beams leads to reduce considerably the ultimate load more than that in flexural zone by about (34%).
8. The overall behavior of beams with fixed edges is better than for fixed-simply edges and simply supported reinforced concrete deep beams.

6.2 Recommendations

The following topics are suggested as an extension for the present work:

1. Investigating the behavior of curved deep beams with openings.
2. The dynamic behavior of deep beams needs to be investigated.
3. Extension of the material models to include long term effects on concrete behavior(creep and shrinkage) as well as cyclic loading.
4. Investigating the behavior of fibrous deep beams with openings.

REFERENCES

1. Abdul-Kareem, I. M., (2003), ***"NonLinear Analysis of R.C Thick Plates Foundation on Soil"***, M.Sc. Thesis, University of Babylon.
2. American Concrete Institute, (1995), "***Building Code Requirements for Reinforced Concrete***", Detroit, ACI-381-95.
3. American Concrete Institute, (2002), "***Building Code Requirements for Reinforced Concrete***", Detroit, ACI-381-02.
4. AL-Taan, S.A. and Ali, T.Q., (1998), "***Nonlinear Finite Element Analysis of Fibrous Concrete Deep Beams***" Engineering and Technology, Vol. 17, No. 9, pp. 862-876.
5. AL-Shaarbaf, I.A.S., (1990),"***Three-Dimensional Nonlinear Finite Element Analysis of Reinforced Concrete Beams inTorsion***", Ph.D. Thesis, University of Bradford, England.
6. AL-Shaarbaf, I.A.S., and Mohammed, A.Z., (1999), "***Nonlinear Analysis of Reinforced Concrete Cylindrical Shell Using Two and Three-Dimentional Finite Element Methods***", Engineering and Technology, Iraq,Vol. 21, No. 8, pp. 1-10.
7. Ashour, A.F., (2000), "***Shear Capacity of Reinforced Concrete Deep Beams***", Journal of Structural Engineering, ASCE, Vol. 126, No. 9, September, pp. 1045-1052.
8. Bathe, K.I. and Ramaswamy, S., (1979), "***On Three-Dimentional Nonlinear Analysis of Concrete Structure***" Nuclear Engineering and Design, Vol. 52, pp. 385-409.
9. Besser, I.I, and Cusens, A.R., (1984), "***Reinforced Concrete Deep Beam Panels with High Depth / Span Ratios***" Proceedings of the Institute of Civil Engineers, Vol. 77, Part2, June, pp. 265-278.

10. Cervenka, V., and Gerstle, K.H., (1971), ***"Inelastic Analysis of Reinforced Concrete Panels, Theory, Experimental Verification and Application"***, IABSE Publication, Vol. 31-II, pp.32-45 and Vol. 32-II (1972), pp.26-39
11. Cervenka, V., (1985), "***Constitutive Model for Cracked Reinforced Concrete***" ACI Journal, November-December, pp. 877-882.
12. Cervera, M., Hinton, E., and Hassan, O., (1987), "***Nonlinear Analysis of Reinforced Concrete Plate and Shell Structures Using 20-Noded Isoparametric Brick Element***" Computers and Structures, Vol. 25, No. 6, pp. 845-869.
13. Chen, W.F., (1982), "***Plasticity in Rinforced Concrete***", McGraw-Hill, Inc, New York.
14. Choo,Q.L., and Lim, H.L., (1993) ***"Design and Behavior of Continuous Concrete Deep Beams"***, B. Eng. Final Year Project Report, Nanyang Technological University. (as cited in Siao 1995)
15. Coenen, J.H., (1980) "***3-D limit Load Analysis of Reinforced Concrete Shells of Arbitrary Shape***", Computers and Structures, Vol.12, No.1.
16. Cook, R.D., (1974), "***Concept and Application of Finite Element Analysis***", John Wiley and Sons, Inc., New York.
17. Damjanic, F., and Owen, D.R.J., (1984), "***Practical Considerations for Modeling and Analysis of Reinforced Concrete Structures***", Invited paper at Int. Conf. Computer-Aided Analysis and Design of Concrete Structures, Split, Yugoslavia, September.
18. Daniel, A., and Patrick, B., (1999) "***Shear Desgin of Reinforced Concrete Deep Beam:Numerical Approach",*** Journal of Structural Engineering, ASCE, Vol. 125, No. 3, March, pp. 309-318.
19. El-Hashimy. H., Naser. M., and Farahat. A., (1990), ***"Cracking Load of Reinforced Concrete Deep Beams with Openings",*** Convention paper.
20. Hinton, E, (1988), ***"Numerical Methods and Software for Dynamic Analysis of Plate and Shell"***, Pineridge press limited.

21. Hu, H., and Schnobrich, W.C., (1990), "***Nonlinear Analysis of Cracked Reinforced Concrete***", Journal of ACI, Vol 87., No.2., March-April, pp. 199-207.
22. Husain, H.M, and AL-Jubori, A.A., (1995), "***Numerical Solution of Deep Beams under Generalized Loadings***", Journal of Engineering at Technology, Iraq, Vol.15., No. 10, pp. 31-45.
23. Irons, B.M., (1971), "***Quadrature Rules for Brick Based Finite Elements***", International Journal of Numerical Methods in Engineering, Vol. 3, pp. 293-294
24. Khalaf, I.M., (1986), "***Nonlinear Finite Elements Analysis of Reinforced Concrete Deep Beam",*** M.Sc. Thesis, University of Mosul.
25. Kong, F.K., and Sharp, (1973), "***Shear Strength of lightweight Reinforced Concrete Deep Beams with web openings***", Structural Engineer, Vol. 51, No. 8, August, pp. 267-274.
26. Kupfer, H.B., Hilsdrof, H.K., and Rusch, H., (1969), "***Behavior of Concrete under Biaxial Stresses***", J. Am. Concr. Inst, Vol. 66, No. 8, August, pp. 656-666.
27. Mahmoud, M.N., (1992) "***Nonlinear Finite Element Analysis of Reinforced Concrete Deep Beam",*** M.Sc. Thesis, University of Mosul.
28. Mansur, M.A., and Ong, K.C.G., (1991), "***Behavior of Reinforced Concrete Deep Beams in Shear***", ACI Structural Journal, Vol. 88, No. 1, January-February , pp. 98-105.
29. Metha, R.P., (1986),"***Concrete Structure:Purposes and Material***", Prentice-Hill, Inc., New Jersey.
30. Moaveni, S., (1999), "***Finite Element Analysis Theory and Application with ANSYS***", Prentice-Hall, Inc., New Jersey.
31. Nam, C.H. and Salmon, C.G, (1974), "***Finite Element Analysis of Reinforced Concrete Beam***", Journal of Structural Division, ASCE, Vol. 100, No. St12, December, pp. 2419-2432.

32. Oran, C. and Kassimali, A., (1976), "Large Deformation of Framed Structures under Static and Dynamic Loads", International Journal of Computers and Structures, Vol. 6, Dec., pp. 539-547.
33. Owen, D.R. J. and Hinton, E., (1980), ***"Finit Element in Plasticity: Theory and Practice"***, Pineridge Press limited, Swansea, U.K.
34. Phillips, D.V., and Zienkiewcz,O.C., (1976), "***Finite Element Analysis of Concrete Structures***", ", Proccedings of the Institute of Civil Engineer, Vol. 61, patr 2, March, pp. 59-88.
35. Ramakrishan, V., and Anathanarayana, Y., (1968), "***Ultimate Strength of Deep Beams in Shear***", Journal of ACI, Vol. 65, pp. 87-98.
36. Roberto, F.P., Pietro, G.G., and Semiglia, M., (1999), "***Residual Capacity of HSC Thermally Damaged Deep Beams***", Journal of Structural Engineering, ASCE, Vol. 125, No. 3, March, pp. 319-327.
37. Rogowsky, D., Macgregor, J.G, and Ong, S.Y., (1986), ***"Tests of Reinforced Concrete Deep Beams"***, ACI Journal, Proceedings, Vol. 83, No. 4, July-Aug, pp. 6114-623. (as cited in Siao 1995)
38. Sanad, A., and Saka, M.B., (2001), "***Prediction of Ultimate Shear Strength of Reinforced Concrete Deep Beams using Neural Networks***", Journal of Structural Engineering, ASCE, Vol. 127, No. 7, July, pp. 818-828.
39. Siao, W.B., (1995), "***Deep Beams Revisited***", ", ACI Structural Journal, Vol. 92, No. 1, January-February , pp. 95-102.
40. Suidan, M., and Schnobrich, W.C., (1973), "***Finite Element Analysis of Reinforced Concrete***", Journal of Structural Division, ASCE, Vol. 99, No. St10, October, pp. 2019-2122.
41. Tan, K.H., Tong,K., and Tang, C.Y., (2001), "***Direct Strut-and-Tie Model for Prestressed Deep Beams***", Journal of Structural Engineering, ASCE, Vol. 127, No. 9, September, pp. 1076-1084.

42. Valliappan, S., and Doolan, T.F., (1972), "***Nonlinear Stress Analysis of Reinforced Concrete***", Journal of Structural Division, ASCE, Vol. 98, No. St4, April, pp. 885-897.
43. Van Mier, J.G.M., (1987), "***Examples of Nonlinear Analysis of Reinforced Concrete Structures with DIANA***", HERON, Vol. 32, No.3.(as cited by Mahmoud (1992)).
44. Wanchoo, M.K., and May, G.W., (1975), "***Cracking Analysis of Reinforced Concrete Plates***", Journal of Structural Division, ASCE, Vol. 101, No. St12, January, pp. 201-215.
45. Winter, G., and Nilson, A.H., (1978), "***Design of Concrete Structures***", 9th Edition.
46. Zeinkiewcz, O.C., (1977), "***The Finite Element Method***", 3rd Edition, McGraw-Hill Book Company, New York.

APPENDIX A

Table (A-1) Weights and Locations of Sampling Points in The 27 and 15 Integration Rules

Points	27 Integration Rule				15a,15b, 14 Integration Rule			
	ξ	η	ζ	Weight	ξ	η	ζ	Weight
1	+A	–A	–A	W1	0.0	0.0	0.0	W1
2	0.0	–A	–A	W2	0.0	–B	0.0	W2
3	–A	–A	–A	W1	0.0	+B	0.0	W2
4	–A	0	–A	W2	0.0	0.0	–B	W2
5	–A	+A	–A	W1	0.0	0.0	+B	W2
6	0	+A	–A	W2	1.0	0.0	0.0	W2
7	+A	+A	–A	W1	–B	0.0	0.0	W2
8	+A	0.0	–A	W2	+C	-C	-C	W3
9	0.0	0.0	-A	W3	+C	+C	-C	W3
10	+A	-A	0.0	W2	+C	-C	+C	W3
11	0.0	-A	0.0	W3	+C	+C	+C	W3
12	-A	-A	0.0	W2	-C	-C	-C	W3
13	-A	0.0	0.0	W3	-C	+C	-C	W3
14	-A	+A	0.0	W2	-C	-C	+C	W3
15	0.0	A	0.0	W3	-C	+C	+C	W3
16	+A	+A	0.0	W2				
17	+A	0.0	0.0	W3				
18	0.0	0.0	0.0	W4				
19	+A	-A	+A	W1				
20	0.0	-A	+A	W2				
21	-A	-A	+A	W1				
22	-A	0.0	+A	W2				
23	-A	+A	+A	W1				
24	0.0	+A	+A	W2				
25	+A	+A	+A	W1				
26	+A	0.0	+A	W2				
27	0.0	0.0	+A	W3				

where

Symbol	Integration Rule			
	27	15a	15b	14
A	0.77459	-	-	-
B		1.0	0.84842	0.79582
C		0.6741	0.72766	0.75878
W1	0.171468	1.5644	0.712137	0
W2	0.27435	0.3556	0.686227	0.886427
W3	0.4389575	0.53778	0.396312	0.33518
W4	0.702332	-	-	-

APPENDIX B

Evaluation of the Flow Vector

The flow vector {a}, is defined as the derivative of the yield function with respect to the stress components, and given by:

$$\{a\} = \left[\frac{\partial f}{\partial \sigma_x}, \frac{\partial f}{\partial \sigma_y}, \frac{\partial f}{\partial \sigma_z}, \frac{\partial f}{\partial \tau_{xy}}, \frac{\partial f}{\partial \tau_{yz}}, \frac{\partial f}{\partial \tau_{zx}} \right] \tag{B-1}$$

where,

$$\left.\begin{aligned}
a_1 &= \frac{\partial f}{\partial \sigma_x} = c + \left[2\left(c^2 + \beta\right)\sigma_x + \left(2c^2 - \beta\right)\left(\sigma_y - \sigma_z\right) \right] / Q \\
a_2 &= \frac{\partial f}{\partial \sigma_y} = c + \left[2\left(c^2 + \beta\right)\sigma_y + \left(2c^2 - \beta\right)\left(\sigma_x - \sigma_z\right) \right] / Q \\
a_3 &= \frac{\partial f}{\partial \sigma_z} = c + \left[2\left(c^2 + \beta\right)\sigma_z + \left(2c^2 - \beta\right)\left(\sigma_x - \sigma_z\right) \right] / Q \\
a_4 &= \frac{\partial f}{\partial \sigma_x} = 6.\beta.\tau_{xy} / Q \\
a_5 &= \frac{\partial f}{\partial \sigma_y} = 6.\beta.\tau_{yz} / Q \\
a_6 &= \frac{\partial f}{\partial \sigma_z} = 6.\beta.\tau_{zx} / Q
\end{aligned}\right\} \tag{B-2}$$

where c and β, are the material constants, and Q is given by:

$$Q = 2\left[\begin{matrix} \left(c^2 + \beta\right)\left(\sigma_x^2 + \sigma_y^2 + \sigma_z^2\right) + \left(2c^2 - \beta\right)\left(\sigma_x\sigma_y + \sigma_y\sigma_z + \sigma_z\sigma_x\right) \\ 3\beta\left(\tau_{xy}^2 + \tau_{yz}^2 + \tau_{zx}^2\right) \end{matrix} \right]^{1/2}$$

الخلاصة

البحث يتناول التحليل اللاخطي للعتبات العميقة المحتوية علىفتحات و المصنوعة من الخرسانة المسلحة تحت تأثير الأحمال الساكنة باستعمال طريقة العناصر المحددة . تم اخذ اللاخطية لتصرف المادة بنظر الاعتبار عند تمثيل الخرسانة. تم عرض العلاقات الرياضية التي تمثل السلوك غير الخطي للمواد مثل علاقة الإجهاد و الانفعال للخرسانة,التشقق,خضوع حديد التسليح .العنصر الطابوقي ذو عشرين عقده و ستين درجة حرية تم توضيفه لتمثيل الخرسانة. قضبان حديد التسليح مثلت كعناصر محورية مطمورة ضمن العناصر الطابوقية مع ترابط تام بينهما.

المقارنة بين نتائج العناصر المحددة و النتائج النظرية و العملية المتوفرة للعتبات العميقة و العتبات العميقة المحتوية علىفتحات أظهرت توافقا جيدا. النسبة المئوية للفرق لم تتجاوز (6%) للحمل الأقصى و (9%) للهبوط.

نظمت دراسة عوامل لاختبار تأثير بعض المتغيرات مثل موقع الفتحة, حديد التسليح الغشائي, مقاومة الانضغاط ولظروف الحدود على تصرف العتبات العميقة. تم التوصل إلى إن موقع الفتحة هو من أهم العوامل التي يجب آن تؤخذ بنضر الاعتبار عند التصميم, فعندما تكون الفتحة في منطقة القص فأنها سوف تحدث انخفاظا كبيرا بقيمة الحمل الأقصى بمقدار (31%-56%) للعتبات المسندة إسناد بسيطا، وبمقدار (8%-30%) للعتبات العميقة المستمرة.

ومن جانب آخر فلقد تم أجراء مقارنة لتحليل العتبات العميقة المستمرة بعدة طرق هي : طريقة العناصر المحددة، الكود الأمريكي، وطريقة أضلاع (شد-عمود) ولقد تم التوصل إلى إن تأثيرا(الشد-القوس) يؤخذ بنظر الاعتبار في العتبات العميقة المستمرة وليس كما جاء في توصيات الكود الأميركي.

التحليل اللاخطي بالعناصر المحددة للعتبات الخرسانية المسلحة العميقة ذات فتحات

رسالة

مقدمة الى كلية الهندسة في جامعة بابل كجزء
من متطلبات نيل شهادة ماجستير علوم في الهندسة المدنية

من قبل
خمائل عبد المهدي مشير

بإشراف
أ.م.د. عمارياسر علي
أ.م.د. نمير عبد الامير علوش

2005م
1425 هـ